NASA TN D-1633

TECHNICAL NOTE

D-1633

INVESTIGATION OF BUFFET PRESSURES ON MODELS OF LARGE MANNED LAUNCH VEHICLE CONFIGURATIONS

By George W. Jones, Jr., and Jerome T. Foughner, Jr.

Langley Research Center
Langley Station, Hampton, Va.

NATIONAL AERONAUTICS AND SPACE ADMINISTRATION
WASHINGTON

May 1963

NATIONAL AERONAUTICS AND SPACE ADMINISTRATION

TECHNICAL NOTE D-1633

INVESTIGATION OF BUFFET PRESSURES ON MODELS OF LARGE MANNED LAUNCH VEHICLE CONFIGURATIONS

By George W. Jones, Jr., and Jerome T. Foughner, Jr.

SUMMARY

An exploratory wind-tunnel investigation of the buffet characteristics of a vehicle representative of the launch vehicle for the manned lunar mission has been made. The investigation was made to define buffet problem areas on the vehicle and to study whether buffet pressures measured on space vehicle models follow scaling relationships based on simple dimensional considerations. To obtain these data, fluctuating pressures were measured in the Langley transonic dynamics tunnel on two rigid models of a large manned launch vehicle differing in size by a factor of 5. The models were tested over a Mach number range from 0.4 to 1.2, a Reynolds number range from 0.4×10^6 to 9.0×10^6 (based on the second-stage diameter), and at angles of attack from 0° to $\pm 4^\circ$.

The results of the investigation show that, for the configurations tested, the wake from the escape tower under certain flow conditions produced relatively high noise levels (about 168 decibels) on the nose cone and on the area just aft of the cone-cylinder shoulders on the vehicle upper stages. In addition, independently of the presence or absence of the escape tower, large pressure fluctuations occur on the vehicle just aft of the two cone-cylinder shoulders in a narrow band of Mach numbers just below 1.0. These pressure fluctuations present a design problem in venting unpressurized portions of the vehicle but do not present a structural response problem in the free-free bending or rigid-body pitch modes. These pressure fluctuations have a time-history wave form which resembles "square waves." However, only one such pressure fluctuation is expected to occur during the exit trajectory of the vehicle. An evaluation of buffet scaling relationships derived from simple dimensional considerations lends confidence to the use of suitably scaled models in determining the buffet pressure characteristics of large launch vehicles.

INTRODUCTION

Several space vehicles have failed during the transonic and low supersonic range of their exit trajectories. Usually, the local aerodynamic loads on the vehicle are a maximum at transonic speeds and the presence of unsteady shock—boundary-layer interactions in the flow around the vehicles has led to the

suggestion that buffeting loads may have contributed to some of the failures. Several wind-tunnel investigations (refs. 1 to 4) have been undertaken to examine the nature of these buffeting flows. Generally, it has been found that the characteristics of buffet pressure fluctuations on launch vehicles are very strongly configuration dependent. Therefore, as part of the work of the Langley Research Center in support of the manned lunar mission, a wind-tunnel investigation of the buffet characteristics of a vehicle representative of the launch vehicle for the manned lunar mission has been made.

Some very early buffet pressure characteristics from a preliminary investigation of a representative launch vehicle were published in reference 5. These early data indicated that, under certain conditions, root-mean-square buffet pressures as high as one-fourth the free-stream dynamic pressure might be obtained behind the first shoulder of the configuration. The magnitude of these buffet loads and peculiarities of the fluctuating pressures were such as to cast doubt on the validity of the usual laws for scaling buffet pressure characteristics from model to full scale. The present more detailed investigation was then undertaken with emphasis on attacking the problems raised by the preliminary investigation.

The twofold purpose of the investigation was: (1) to define any buffet problem areas on the large manned launch vehicle, and (2) to study whether buffet pressure characteristics measured on models of space vehicle configurations can be scaled with confidence to the full-size vehicle by using normal scaling relationships.

To obtain the required data, fluctuating aerodynamic pressures were measured on two rigid models representative of the large manned launch vehicle which were sized, respectively, 8 percent and 1.6 percent of the full-size vehicle. In addition, limited response studies were made on a dynamically and elastically scaled model of a similar vehicle modified to have the same nose shape as the large manned launch vehicle. Various escape-tower configurations were investigated on the models which were tested in the Langley transonic dynamics tunnel with both air and Freon-12 as test mediums. The investigation covered a Reynolds number range from 0.4×10^6 to 9.0×10^6 (based on second-stage diameter), a Mach number range from 0.4 to 1.2, and an angle-of-attack range from 0° to $\pm 4^\circ$.

SYMBOLS

C_p time-average pressure coefficient, $\dfrac{p_{l,s} - p}{q}$

$\left(\Delta C_p\right)_{rms}$ coefficient of root-mean-square fluctuations of pressure about mean, $\dfrac{1}{q}\left[\dfrac{1}{T}\displaystyle\int_0^T \left(p_{l,u} - p_{l,s}\right)^2 dt\right]^{1/2}$

$(\Delta C_p)_{peak}$	coefficient of maximum fluctuation of peak pressure, $\frac{\text{Maximum peak-to-peak pressure fluctuation}}{2q}$
D	diameter of second stage, in.
f	frequency, cps
M	free-stream Mach number
p	free-stream static pressure, lb/sq ft
$p_{l,s}$	time-average local pressure on model surface, $\frac{1}{T}\int_0^T p_{l,u}\,dt$
$p_{l,u}$	unsteady local pressure on model surface
q	free-stream dynamic pressure, lb/sq ft
R	Reynolds number based on second-stage diameter, $\frac{\rho VD}{\mu}$
r	radius measurement on nose cone
t	time, sec
T	specific period of time, sec
V	velocity, ft/sec
x	axial distance along vehicle measured rearward from nose, in.
α	vehicle angle of attack, deg
θ	angular distance around circumference of vehicle, positive clockwise when viewed from rear, origin at 12 o'clock, deg
μ	viscosity of test medium, $\frac{\text{lb-sec}}{\text{ft}^2}$
ρ	density, slugs/cu ft
Φ	power spectral density of fluctuating pressure, $\frac{(\text{lb/sq in.})^2}{\text{cps}}$

Subscripts:

fs	full scale
m	model

APPARATUS AND TESTS

Test Facility

The Langley transonic dynamics tunnel which was used for the investigation is a single-return-flow, variable-pressure, slotted-throat wind tunnel having a test section 16 feet square (with cropped corners). The tunnel can operate at stagnation pressures from near vacuum to slightly above atmospheric at Mach numbers from 0 to 1.2, and either air or Freon-12 may be used as a test medium. This facility is particularly suited for general dynamics testing because Mach number and dynamic pressure can be varied independently and are continuously controllable. A quick operating bypass valve is available as a "flutter stopper"; thus, a rapid reduction or increase of test-section Mach number and dynamic pressure may be made. The flow in the tunnel test section is such that the maximum deviation from the average free-stream Mach number is on the order of 0.011 to 0.018 at the highest test Mach numbers and less than 0.003 at the lower test Mach numbers.

Models

The principal models for the investigation were two rigid models of a large manned launch vehicle which are 8.035-percent full size and 1.607-percent full size. These models were identical in exterior shape, but differed in size by a factor of 5. Pertinent model dimensions scaled to full size are shown in figure 1(a).

Various escape-tower configurations were tested on the rigid models and these are illustrated with full-scale vehicle dimensions in figure 2. Two different escape tower designs with a skirt or shroud around the rocket nozzles and two designs without skirts were investigated. The two designs without skirts are tower configurations 1 and 3 as shown in figure 2. Both escape towers were similar in that each had a conical nose, cylindrical body, three rocket nozzles, and tripod mounting legs. The escape towers differed principally in that the tower of configuration 3 had a larger length-to-diameter ratio, larger rocket nozzles, and a greater length from tower base to vehicle nose cone. Configuration 2 consisted of tower configuration 1 with a conical skirt around the rocket nozzles and configuration 4 consisted of tower 3 with a skirt which was similar to that of configuration 2 except this skirt had an annular inlet between the shroud leading edge and the cylindrical tower body. (See fig. 2.) Photographs of the models are presented in figure 3.

The 1.6-percent and 8-percent models were rigidly attached to the tunnel sting mount. Shake tests of the model support system with the 8-percent model attached gave resonant frequencies of 6.9, 45.5, 104.3, and 162 cycles per second in a vertical direction and 5.4, 38.1, 171.0, and 197.0 cycles per second in a horizontal direction. The structural damping coefficient in the first vertical mode as determined from a decrement was 0.028. The natural frequencies and structural damping were not measured on the 1.6-percent model.

In addition, limited response studies were made of a 2-percent-size dynamically and elastically scaled model of a similar vehicle modified to have the same nose shape as the large manned vehicle. Pertinent model dimensions scaled to full size are illustrated in figure 1(b). With the removable sleeve installed on the 2-percent model, as shown in figure 1(b), that portion of the model from the nose to the rear of the sleeve becomes a 1.427-percent model, whereas the booster becomes oversize to this scale. The 1.427-percent elastic model was attached to the sting by two pairs of soft springs located so that restraint to model response in the free-free bending modes was minimized. The model first free-free bending and rigid-body pitching frequencies scaled to within about 20 percent of the corresponding frequencies on the full-size vehicle.

Instrumentation

The rigid pressure models were equipped with six pressure transducers which measured the fluctuating aerodynamic pressures on the upper stages along a streamwise ray and the 8-percent model also had a seventh transducer on the forward cone-cylinder shoulder, 180° around the circumference from transducer 3. (See fig. 1.) In addition, the 8-percent model was equipped with 22 static-pressure orifices which gave the time-average local pressure distribution along a streamwise ray over the same length of the vehicle as covered by the fluctuating pressure transducers. The locations of the pressure transducers and the static-pressure orifices are shown in figure 1.

The pressure transducers were an electrical, variable-air-gap, inductance type known as the NACA miniature electrical pressure gage model 49. A detailed description and performance analysis of this transducer is presented in reference 6. The range of the pressure transducers used was ±2 psi and the maximum nonlinearity in this range is about 1 percent. Each pressure transducer was installed as a unit by using a special mounting bracket. A transducer unit and mounting bracket are shown in figure 4(a). One side of the transducer is connected through its pressure opening to the pressure to be measured, and the other side is connected to a reference pressure. In the present installation the reference pressure was measured at an orifice adjacent to the fluctuating pressure orifice. The reference pressure orifice was connected to the reference side of the transducer by about 50 feet of small-diameter tubing which smoothed transient fluctuating pressures and gave a time-average local pressure. Thus, each pressure transducer measured, at one model station, the fluctuations of pressure about the mean.

A block diagram of the instrumentation used in measuring and recording the fluctuating pressures is presented in figure 4(b). The output from the pressure

transducer was fed through a 3-kilocycle carrier amplifier and a low-pass filter which had a cutoff frequency of approximately 2,800 cycles per second. The signal then passed through a 16-microfarad blocking condenser which removed any d-c components without perceptible attenuation and was recorded by an FM tape recorder which had a center frequency of 6.75 kilocycles and a recording speed of 7.5 inches per second. The low-pass filter prevented any interaction between the carrier and tape recorder.

In addition to the tape record of pressure fluctuations, the mean squares of the pressure fluctuations from four selected transducers were obtained by sending the outputs from each of these four transducers through a vacuum-bulb thermocouple. The output of each thermocouple is proportional to the mean square of the input signal voltage, and these thermocouple outputs were each simultaneously displayed on a microammeter and recorded on a recording oscillograph. These mean-square fluctuating pressure data were used to compute quickly the root-mean-square values of the fluctuating pressures.

Power-spectral-density data presented were obtained through the use of the FM tape recorder. The taped data were analyzed for the frequency range of 0 to 600 cycles per second. The $\left(\Delta C_p\right)_{rms}$ values obtained from the area under the power-spectral-density curves were compared with the $\left(\Delta C_p\right)_{rms}$ values computed from the mean-square values as measured by vacuum-bulb thermocouples. Although some differences existed for the two sets of $\left(\Delta C_p\right)_{rms}$ values, the agreement was generally fair even though the thermocouple signals were not cut off at 600 cycles per second. No frequency-response curve for the entire instrumentation system was made. However, frequency responses were obtained for important segments of the system - a pressure transducer, 3-kilocycle carrier amplifier, and 2,800-cycle-per-second low-pass filter - and these frequency responses are presented in figure 5. Examination of figure 5 shows the preceding units to have a constant frequency response within $\pm 2\frac{1}{2}$ percent at frequencies up to approximately 600 cycles per second. Above 600 cycles per second the frequency response drops off rather slowly so that attenuated signals at frequencies above 600 cycles per second could have passed through the thermocouple mean-square circuits. In view of the generally fair agreement observed between the two sets of $\left(\Delta C_p\right)_{rms}$ values, it is believed that there was no significant power input at frequencies above 600 cycles per second.

Each of the 22 static-pressure orifices on the 8-percent model was connected by tubing to a multiple-glass-tube manometer filled with butylthiolate liquid and referenced to the free-stream static pressure in the tunnel plenum chamber. A photograph of the manometer board for each test data sample recorded the distribution of the difference between local time-average and free-stream static pressures for each data point.

Tests

For both the 8-percent and 1.6-percent models, the test procedure was as follows: With the model installed in the tunnel and all instrumentation set up for the tests, a static-pressure calibration was made of the output of the fluctuating pressure transducers. For the calibration, known static pressures at several pressure levels were applied to each pressure transducer and the corresponding output in millivolts was measured. The tape recorder and thermocouples were calibrated with 100-cycle-per-second and 225-cycle-per-second sine waves of known root-mean-square voltage. The tunnel was then started and the tunnel stagnation pressure, temperature, and speed were set to give a desired Mach number and Reynolds number. The Mach number and Reynolds number were held constant and data points were taken for each angle of attack desired. For each data point, a 45-second data sample record was taken of the fluctuating pressures by using the tape recorder and for the 8-percent model a photograph was taken of the static-pressure manometer board. For the four transducers connected to thermocouples, the thermocouple outputs on the microammeters were recorded and also an oscilloscope was used to check visually the output of any desired pressure transducer. Tunnel stagnation temperature and pressure and static pressure were also tabulated for each data point.

The tests covered Reynolds numbers from 0.4×10^6 to 9.0×10^6 (based on the second-stage diameter), Mach numbers from 0.4 to 1.2, and angles of attack from -4° to 4°. Most of the data consisted of root-mean-square fluctuating pressures taken at two Reynolds numbers, 1×10^6 and 4.5×10^6, throughout the Mach number and angle-of-attack ranges. The static-pressure distributions were measured only on the 8-percent model with tower configuration 1 in Freon at Reynolds number 4.5×10^6, angles of attack of -4°, 0°, and 4°, and Mach numbers from 0.6 to 1.2.

REDUCTION OF DATA

The differences between the local time-average static pressure and the free-stream static pressure were reduced to the form of a time-average pressure coefficient C_p. This C_p is the measured difference between the local time-average static pressure and the free-stream static pressure (obtained from a photograph of the manometer board) divided by the free-stream dynamic pressure.

Since random fluctuations of pressure about the mean were measured by the electrical pressure transducers, conventional characteristics of a continuous random process such as root-mean-square values and power spectral densities are used to describe these random pressure fluctuations. All the measured fluctuating pressure transducer outputs presented in this report were reduced to the form of a root-mean-square fluctuating pressure coefficient $\left(\Delta C_p\right)_{rms}$. This coefficient is the square root of the time average of the square of the fluctuating pressure about a mean divided by the free-stream dynamic pressure.

Visual time histories of some data samples were obtained by playing back the magnetic tape recordings of the fluctuating pressures into a recording oscillograph. Some selected samples of the randomly fluctuating data as recorded on

magnetic tape were reduced to power spectral densities by use of an electronic analog analyzer. The data were analyzed in the frequency range from 0 to 600 cycles per second by using a 13.5-cycle-per-second band-pass filter and a 15-second tape loop. It should be pointed out that the power spectral densities thus obtained are questionable at very low frequencies (that is, within one or two band widths of zero frequency). The model power spectral densities were converted to full-scale power spectral densities by using the following scaling relationships developed from simple dimensional considerations (ref. 7):

$$\Phi_{fs} = \Phi_m \left(\frac{q_{fs}}{q_m}\right)^2 \frac{D_{fs}}{D_m} \frac{V_m}{V_{fs}}$$

$$f_{fs} = f_m \frac{D_m}{D_{fs}} \frac{V_{fs}}{V_m}$$

The full-scale dynamic pressures used in the scaling of the power spectral densities and in the scaling of the acoustic environment for this paper were obtained from the curves of dynamic pressure and Mach number against time from lift-off for a large launch vehicle which are presented in figure 6.

As mentioned in the section on "Test Facility," the Langley transonic dynamics tunnel can use either Freon-12 or air as a test medium. In order to obtain Reynolds numbers of 4.5×10^6 or higher on the 8-percent model or 1×10^6 or higher on the 1.6-percent model, Freon had to be used as a test medium. Since the ratio of specific heats for Freon-12 is approximately 1.13 as compared with 1.4 for air, some differences exist between the data obtained in Freon and the data obtained in air. Methods for predicting aerodynamic characteristics of bodies in air from data obtained in Freon-12 have been developed for steady flows and are presented in reference 8. No correction for unsteady flow data such as the fluctuating pressures of the present investigation has been developed. Figure 7 shows for typical root-mean-square fluctuating pressure coefficients on the 8-percent model a comparison of data taken in air and Freon (at the same Mach number, Reynolds number, and angle of attack) with the Freon data corrected by the method of reference 8. Although the correction of reference 8, when applied to the data, is in the direction which would reduce the difference between the Freon and air data, the amount of the correction is small compared with the amount of correction needed. As will be indicated subsequently in the section entitled "Buffet Pressure Scaling," there are other reasons why $\left(\Delta C_p\right)_{rms}$ values obtained in air and Freon might differ. Because of these other reasons for differences and in view of the uncertainty of applicability of the correction of reference 8, the remainder of the data taken in Freon are presented as uncorrected Freon data.

PRESENTATION OF DATA

The results of the investigation are presented in the following tables and figures:

The objective of figures 20 to 24 which cover several combinations of flow conditions, model sizes, and test mediums is to show how well buffet pressures measured on models of a space vehicle can be scaled to the full-size vehicle.

In the presentation of the fluctuating pressure data, little or no data are presented for some of the transducers. The maximum root-mean-square pressure fluctuations on the 8-percent model were measured by transducers 1, 3, 5, and 7. (See fig. 1.) Transducer 2 fluctuating pressures were about the same as those of transducer 1 and both transducers were on the 30° nose cone. The fluctuating

pressures from transducers 4 and 6 were considerably less than those from transducers 3, 5, and 7. Consequently, for the 8-percent model, only limited data from transducers 2, 4, and 6 are given and these data are found in the axial distribution plot of figure 12. The maximum root-mean-square pressure fluctuations on the 1.6-percent model were measured by transducers 1, 3, 4, and 5. The 1.6-percent model had no transducer location corresponding to the transducer 7 location on the 8-percent model. Again the pressures from transducers 1 and 2 were about equal and the pressures from transducer 6 were very small. Therefore, no data from transducers 2 and 6 are presented for the 1.6-percent model.

RESULTS AND DISCUSSION

Buffet Problem Areas

The flow about the vehicle is characterized by a turbulent wake behind the escape tower, unsteady shock—boundary-layer interactions at the cone-cylinder shoulders of the vehicle, and flow separation around the 30° nose-cone shoulder at subsonic speeds. These phenomena present possible buffet problem areas which will be discussed in some detail. A visual presentation of the flow about the vehicle is given by the spark-shadowgraph of figure 8 obtained at the Marshall Space Flight Center on a 0.0068-size model which had a slightly different escape tower than the models of this investigation.

The fluctuating pressures measured on the models are presented in the form of root-mean-square fluctuating pressure coefficients and power spectral densities which are conventional methods of describing a continuous random process. However, it is of interest to indicate the magnitude of the maximum peak fluctuations of pressure in relation to the root-mean-square values of these pressure fluctuations. Such an indication is given in figure 14 in which the maximum peak values of fluctuating pressures for each of several data samples are compared with the root-mean-square values for the same data samples. Comparisons are presented for two configurations, namely, the 8-percent model without escape tower at the transducer 3 location and the 1.6-percent model with tower configuration 1 at the transducer 1 location.

The alinement or nonalinement of the pressure transducers on the models with the escape-tower rocket nozzles in some cases affected the fluctuating pressures measured by the transducers. For all tests with an escape tower on the models, the escape tower was installed so that each pressure transducer was either directly downstream of an escape-tower rocket nozzle or directly downstream of the midpoint of the valley between two escape rocket nozzles.

Turbulent-flow effects.- The escape-rocket and tower combination create a turbulent wake that bathes the vehicle behind it in a turbulent flow. Also at subsonic Mach numbers around 0.6 there is flow separation around the shoulder of the 30° payload nose cone. This separation creates a turbulence in the vicinity of the nose-cone shoulder which adds to the effect of the turbulent escape-tower wake. The turbulent flow from subsonic separation around this shoulder is present even without an escape tower on the model.

The primary effect of installing an escape tower on the model is an increase in the level of the measured buffet pressures on the nose cone and (at supersonic speeds) on the cone-cylinder shoulder behind the nose cone. Figures 9, 11, and 13, which present tower-off and tower-on $(\Delta C_p)_{rms}$ data, show the increases that are due to the presence of the tower.

The maximum $(\Delta C_p)_{rms}$ value on the nose cone (transducer 1) with a tower-on configuration is 0.141 as shown in figure 9(c) for tower configuration 2 at $\alpha = 4^\circ$ and $M = 0.6$. An average tower-on value of $(\Delta C_p)_{rms}$ on the nose would be about 0.08. For the tower-off configurations, a $(\Delta C_p)_{rms}$ level of less than 0.01 was measured on the nose cone throughout the Mach number range at angles of attack from -4° to 4°. This level is about that expected for turbulent boundary-layer flow over a smooth surface.

The increase in $(\Delta C_p)_{rms}$ at supersonic Mach numbers on the forward cone-cylinder shoulder is shown by a comparison of the $(\Delta C_p)_{rms}$ values from transducers 3 and 7 for the tower-off and tower-on configurations. (See figs. 9 and 11.) Although large differences exist in the level of $(\Delta C_p)_{rms}$ for the various tower configurations, it is seen that the tower-on supersonic $(\Delta C_p)_{rms}$ values behind the cone-cylinder shoulder are always higher than the tower-off values.

Examination of figure 9 shows some values of fluctuating pressure coefficients as high as 0.17 to 0.19 measured by transducers 3 and 7 at subsonic Mach numbers from 0.4 to 0.6. As figure 1 shows, transducers 3 and 7 are located 180° apart around the circumference of the vehicle at a station just rearward of the 30° nose-cone shoulder. These high fluctuating pressures are attributed to turbulence created by flow separation around this cone-cylinder shoulder as the flow tries to turn this corner at these subsonic Mach numbers. The flow separation on this shoulder appears to be present either with or without an escape tower on the model. The resulting turbulence is a noise source which extends the possible buffet problem area to Mach numbers as low as 0.6.

Power-spectral-density analyses were made of a number of data samples of fluctuating pressures associated with the wake of the escape tower and subsonic flow separation. Some of these analyses are shown in figure 15 in the form of full-scale power spectral densities. Examination of figure 15 reveals that two distinct types of spectra occur in the wake of the escape tower. One type is characterized by a "white noise" spectrum (no predominant peaks) such as shown in the lower two curves of figure 15(b). The other type is characterized by a broad peak at full-scale vehicle frequencies ranging from 20 to 60 cycles per second, the most definite of these peaks occurring on the nose cone between 35 and 40 cycles per second. These peaks do not appear to represent resonant model natural frequencies and differences in magnitude and frequency between different peaks are thought to be functions of different tower configurations, angle of attack, and Mach number.

The distinction between the broad peaks and white noise spectra are thought to be associated with the circumferential distribution of the tower wake buffeting over the vehicle which has not been well defined with the limited number of pressure transducers used. Each transducer was either directly downstream of one of the escape-tower rocket nozzles or directly downstream of a valley between two rocket nozzles. This transducer-tower orientation is denoted in figure 15 by the notation "valley" or "rocket" in the key of the figure. Examination of figures 15(a) and 15(b) shows that the power spectral densities which are of the "broad peak" type were measured by transducers downstream of an escape-tower rocket nozzle, and the "white noise" power spectral densities were measured by transducers downstream of a valley between two rocket nozzles. This localized circumferential variation of buffet pressure with tower rocket nozzle orientation is also shown by the supersonic fluctuating pressure coefficients in figures 9(b) and 9(d). Transducers 3 and 7 were located at the same station just aft of the first cone-cylinder shoulder but were 180° apart around the circumference with transducer 3 downstream of a rocket nozzle and transducer 7 downstream of a valley between rocket nozzles. The $(\Delta C_p)_{rms}$ buffet pressures at supersonic Mach numbers are definitely higher downstream of a rocket nozzle (transducer 3) than downstream of a valley between rocket nozzles (transducer 7).

The use of skirts around the escape-tower rocket nozzles eliminated the differences between $(\Delta C_p)_{rms}$ values downstream of a tower rocket nozzle and those downstream of a valley between tower rocket nozzles as is shown by the similarity of the data from transducers 3 and 7 in figures 9(c) and 9(e). Unfortunately, as shown by these same figures, there is a much larger variation in the supersonic buffet levels behind the cone-cylinder shoulders with changes in angle of attack than is found on the two towers without skirts. For this reason the towers with skirts appear to be less desirable from a buffet standpoint than the towers without skirts.

Figure 15(c) presents power spectral densities of fluctuating pressures at subsonic Mach numbers on the shoulder of the 30° nose cone of the models with escape towers. The turbulence from separated flow around this corner at subsonic Mach numbers apparently has combined with the turbulent escape-tower wake as shown by the differences between "valley" and "rocket" power spectral densities.

Flow fluctuations at shoulders.- The flow over the cone-cylinder shoulders of the vehicle is characterized by unsteady shock—boundary-layer interactions just rearward of the cone-cylinder junctions. In these localities the flow undergoes intermittent transition between supersonic attached flow and subsonic detached flow as the shock wave oscillates fore and aft. Figures 8(a) and 8(b) show visually the subsonic and supersonic flow regimes. The alternate separation and reattachment of the flow creates large pressure fluctuations which are shown by the high values of $(\Delta C_p)_{rms}$ in figure 9 for transducers 3, 7, and 5, occurring over a narrow range of Mach numbers just below 1.0. A comparison of these transducer outputs in figure 9(a) with those of figures 9(b) to (9e) show the large root-mean-square fluctuating pressures are present either with or without an escape tower on the model at Reynolds number 4.5×10^6. Indications of a similar peak in root-mean-square fluctuating pressures behind the forward cone-cylinder shoulder of a reentry body on a missile are presented in reference 3.

Somewhat lower peaks in root-mean-square fluctuating pressure coefficients occur behind the cone-cylinder shoulders of model 5 of reference 4. The fluctuating pressure peaks of these references are at slightly different Mach numbers than those of this investigation.

There is an interesting phenomenon in figure 13 which shows the effects of Reynolds number on the $(\Delta C_p)_{rms}$ values on the nose and first cone-cylinder shoulder of the model with and without escape tower. At a Reynolds number of 4.5×10^6 the high fluctuating pressures at $M \approx 0.95$ are shown to occur either with or without the tower. However, at a Reynolds number of 1×10^6, the fluctuating pressure coefficients on the model with tower are considerably greater at a Mach number of 0.95 than on the model without tower. It is conjectured that the effect of the tower is to act as a turbulence generator which changed the flow from laminar to turbulent at a lower Reynolds number than would occur without the tower; and this turbulent flow may be necessary to obtain the high root-mean-square fluctuating pressure peaks. Also of general interest in figure 13 is the fact that the data obtained show little or no Reynolds number effects at values greater than 4.5×10^6. Therefore the data obtained at $R \approx 4.5 \times 10^6$ may be valid design data even though full-scale Reynolds numbers are as high as 60×10^6. (See fig. 6.)

The explanation of the high fluctuating pressures on the vehicle shoulders is corroborated by a cross plot of the static-pressure-coefficient data of figure 12. This cross plot which is presented in figure 16 gives the variation of the static pressures on the cone-cylinder shoulders with Mach number. A step increase in static pressure is seen to occur on both shoulders at Mach numbers between 0.93 and 0.96. The magnitude of these static-pressure increases is directly comparable to the measured fluctuating pressure increases in which pressure changes as high as 80 percent of the dynamic pressure occurred in a few milliseconds. A sudden pressure change of this magnitude may present a design problem in the venting of unpressurized portions of the vehicle in these areas.

Time histories of fluctuating pressures behind the first cone-cylinder shoulder at Mach number 0.95 where the pressure is jumping back and forth between the two levels are presented in figure 17. These are typical oscillograph time histories of the peak fluctuating pressures measured behind the shoulder of both the 1.6-percent and 8-percent models and recorded at the same paper speed. The wave form of the pressure pulses resembles a square wave (particularly for the 1.6-percent model) except the square tops tend to "bleed off" with time because the instrumentation did not have zero frequency response. Similar time histories are found in reference 3. The two time histories are not identical in appearance as the duration of a pressure pulse and the time interval between pressure pulses, although random, are generally less for the small model than for the large model. This difference is in agreement with scaling effects based on simple dimensional considerations. Equivalent full-scale times are indicated in figure 15. The power spectral density of a "square-wave" data sample at a peak value of $(\Delta C_p)_{rms}$ is presented in figure 18. This power spectral density which has been scaled to the full-scale vehicle is typical of all power spectral densities of these peaks in root-mean-square fluctuating pressures in that the power input is great at very low frequencies but rapidly drops off to near zero at higher frequencies.

In considering the effects of these large pressure pulses on the full-scale vehicle, it is important to consider the length of time the full-scale vehicle will be subjected to this type of flow. Examination of the typical launch trajectory information for vehicles of this type such as that in figure 6 shows the vehicle will accelerate through the narrow Mach number range (0.05 Mach number) in which this type of flow occurs in approximately 1.5 seconds. These 1.5 seconds, when scaled to the models, give the time intervals of 0.24 second for the large model and 0.048 second for the small model since

$$\Delta T_m = \Delta T_{fs} \frac{D_m}{D_{fs}} \frac{V_{fs}}{V_m}$$

These time intervals are marked off in brackets in figure 17. These bracketed time intervals show that it is improbable that more than one such pressure pulse will occur in a given 1.5-second time period. Furthermore, these time histories are for flow conditions at constant Mach number, dynamic pressure, and angle of attack. For the accelerated flow conditions of the full-scale vehicle, it seems even less likely that more than a single pressure pulse would occur as the vehicle passes through the Mach number range for this type of flow.

Consequently, the type of flow that would probably occur in accelerated flight should be considered as a transient phenomenon. Conventional characteristics of a continuous random process such as the root-mean-square value or power spectral density would not have their usual significance and are not the proper quantities for representing a transient phenomenon. An attempt was made to obtain pressure time histories more descriptive of the transient case by testing the 8-percent model in accelerated flow obtained by closing a fast acting bypass valve in the tunnel circuit. Unfortunately, instrumentation difficulties and the relatively slow rate of change of Mach number produced inconclusive results.

In order to obtain an indication of the effects of the increases in pressure on the response of the vehicle, some tests were made of a 1.427-percent aeroelastic model which had an oversized booster. (See fig. 1.) These tests were made with no escape tower and also with tower configuration 1. It was felt that, even though the nose was of a different scale from the booster, any significant vehicle response to these flow conditions would be indicated by this model. The model showed no significant response to these flow conditions even though a pressure transducer behind the first cone-cylinder shoulder showed typical "square-wave" time histories. Apparently, the distribution and frequency content of these pressure pulses is such that they do not lead to significant bending moments in the first free-free elastic bending mode or pitching moments in the rigid-body pitching mode.

Buffet Pressure Scaling

All wind-tunnel buffet studies such as these are dependent upon scaling relationships which have been developed from simple dimensional considerations

(see, for example, ref. 7) and are presented in the section on "Reduction of Data." These relationships have not been fully evaluated for buffeting of launch-vehicle—spacecraft configurations. An objective of the present investigation was to make such an evaluation.

One indication of the applicability of the scaling relationships to the data has been previously mentioned, namely, the fact that the differences in the time histories of figure 17 were in agreement with the scaling laws. Another indication of the applicability to the full-scale vehicle of fluctuating pressure data measured on a model is to compare the root-mean-square fluctuating pressure coefficients measured at the same Mach number, Reynolds number, and angle of attack on the same model configurations for the two rigid models which differed in size by a factor of 5. Such a comparison is presented in figure 19 which shows the variation with Mach number of the fluctuating pressure coefficients measured by transducers 1, 3, and 5 on the 8-percent and 1.6-percent models. The agreement between these data is considered to be fair. One limitation to this type of comparison is that the same instrumentation was used to measure the fluctuating pressures on both size models and this instrumentation had flat response up to 600 cycles per second. Both models were tested in Freon where the velocity at a given Mach number is approximately one-half that in air at the same Mach number. Thus, if the frequency of pressure fluctuations on the models is scaled to full scale by the following scaling relationship:

$$f_{fs} = f_m \frac{D_m}{D_{fs}} \frac{V_{fs}}{V_m}$$

the 600 cycles per second on the 1.6-percent model is equivalent to about 20 cycles per second full scale and the same 600 cycles per second on the 8-percent model is equivalent to about 100 cycles per second full scale. If a substantial portion of the buffeting pressures occurred at frequencies between 20 cycles per second and 100 cycles per second full scale, the instrumentation on the 1.6-percent model would not accurately record it and a discrepancy would be expected in the correlation of the data between the two models. A more rigorous method of ascertaining the degree of confidence with which model buffet data can be scaled to full scale by application of the usual buffet scaling relationships is to make comparisons on the basis of spectral analysis of selected data samples. The power spectral densities selected are presented in figures 20 to 24. In these figures comparisons are made between the power spectral densities measured on the 8-percent model and 1.6-percent model both in Freon, the 8-percent model in Freon and in air, and the 8-percent model in Freon, and the 1.6-percent model in air. For each such comparison the transducer location, Reynolds number, Mach number, angle of attack, and tower configuration were the same for the power spectral densities being compared. The first such comparison is presented in figure 20 which shows in two forms, comparison of the power spectral densities of buffet pressures measured at the forward cone-cylinder shoulder (transducer 3) of the large and small models, both in Freon. In figure 20(a) the power spectra are essentially raw data except that the model power-spectral-density ordinate has been divided by the square of the dynamic pressure to put the two curves on a

comparable basis. In order to obtain the same Reynolds number and Mach number on both models, it was necessary to test them at different dynamic pressures. On the basis of figure 20(a) the power spectral densities for the two models are two distinctly separated curves. If these separate curves are scaled to the full-size vehicle by application of the scaling relationships, the power spectral densities are seen to be in good agreement (fig. 20(b)). The $(\Delta C_p)_{rms}$ values presented in part (a) of figures 20 to 24 were obtained from the area under the respective power-spectral-density curves. As discussed under the section entitled "Instrumentation," these $(\Delta C_p)_{rms}$ values differ somewhat from the $(\Delta C_p)_{rms}$ values obtained from the root-mean-square instrumentation readout circuits because the power spectral densities were cut off at 600 cycles per second whereas the root-mean-square circuits could have received signals at frequencies greater than 600 cycles per second. (See fig. 5.) For most of the power spectral densities presented in this paper, fair agreement was obtained between the two sets of $(\Delta C_p)_{rms}$ values so that significant power inputs above 600 cycles per second are believed to occur only for a minority of cases, principally on the 1.6-percent model.

Two similar comparisons of power spectral densities of fluctuating pressures on the first cone-cylinder shoulder of the two different size models are presented in figures 21 and 22. The power spectral densities compared in figure 21 are for tower configuration 1, transducer 1, at $M = 0.8$. Although the values of $(\Delta C_p)_{rms}$ are low in respect to the $(\Delta C_p)_{rms}$ values of the other comparisons, scaling the data of figure 21(a) to that for the full-scale vehicle (fig. 21(b)) gives a fair correlation of data from the two models. Figure 22 presents a similar comparison for tower configuration 2, transducer 3, at $M = 1.01$, but the correlation in figure 22(b) is not as good as that in figure 21. Again the $(\Delta C_p)_{rms}$ values are so low, 0.0279 and 0.0165, for the two models that it is readily possible that the buffet pressure is affected by the level of residual tunnel turbulence which could adversely affect the correlation of the scaling.

Another power-spectral-density comparison is given in figure 23 in which power spectral densities measured on the 8-percent model in the two different test mediums, air and Freon-12, are compared. This comparison shows good agreement between the two spectra when scaled to the full-size vehicle.

Figure 24 presents one further comparison in which power spectral densities of fluctuating pressures on the 8-percent model in air and on the 1.6-percent model in Freon are compared. Again the use of the scaling relationships results in good agreement between the two curves.

The results obtained from the preceding evaluation of buffet scaling relationships derived from simple dimensional considerations lend confidence to the use of suitably scaled models in determining the buffet pressure characteristics of large launch vehicles, provided the instrumentation on the model covers the frequency range of interest on the full-scale vehicle.

Acoustical Environment of Large Manned Launch Vehicle

Examination of the power spectra scaled to the full-size vehicle such as presented in figures 15, 22, and 23 shows that a substantial part of the power input is at frequencies greater than the first several structural frequencies of the full-scale vehicle and thus might be considered as aerodynamic noise. Since such spectra are typical of a large portion of the measured fluctuating pressure data, the $(\Delta C_p)_{rms}$ data have been used to make an engineering estimate of the maximum acoustic environment of the large manned launch vehicle. This estimate is presented in figure 25 in which the noise levels in decibels from engines or aerodynamic sources are presented as functions of time from lift-off in seconds. The procedure used in converting the aerodynamic root-mean-square fluctuating pressure coefficients $(\Delta C_p)_{rms}$ into a noise level in decibels was as follows. The $(\Delta C_p)_{rms}$ values were multiplied by the dynamic pressure for the full-scale vehicle (see fig. 6) at the Mach number at which the $(\Delta C_p)_{rms}$ was measured. Thus $(\Delta C_p)_{rms} \times q = p$ where p is a root-mean-square pressure level. The reference root-mean-square intensity level p_0 (defined by ASA Tentative Standard, 1940 for a plane progressive sound wave in air as 4.18×10^{-7} pounds per square foot) was used to form the ratio p/p_0. The noise level in decibels is then defined as:

$$\text{Noise level in decibels} = 20 \log_{10} \frac{p}{p_0}$$

The engine noise levels are those of figure 8 of reference 5, and are based on measured data from static firings and launch tests. The engine noise is highest at lift-off because of flow impingement and ground reflections, but decreases after lift-off because of the vehicle's forward velocity. The aerodynamic noise levels then begin to dominate as the dynamic pressure increases. It should be noted that the estimates of the overall aerodynamic noise level cover a frequency range up to only 100 cycles per second. The inclusion of higher frequency components generally considered in acoustic environments would be expected to increase the values presented. The solid portions of the maximum aerodynamic noise level curves are based on the maximum values of $(\Delta C_p)_{rms}$ at each Mach number throughout the Mach number range at any transducer location or angle of attack on the 8-percent model with either configuration 1 or 2 or configuration 3 or 4 at a Reynolds number of 4.5×10^6. Thus, these curves represent the maximum (worst) noise levels that are predicted. The dashed extrapolations to these curves are based on wind-tunnel measurements on the Mercury-Atlas configuration which had similar buffeting pressures. The data for the large root-mean-square pressure fluctuations at the cone-cylinder shoulders were excluded from this estimate because these fluctuations are too low in frequency to be considered as noise. The lower 0.006q curve represents a minimum expected noise level such as might be caused by turbulent boundary-layer flow over a smooth surface. Such values were measured on the nose cone with tower removed. Thus the difference

between the 0.006q curve and the maximum aerodynamic noise curves is a measure of the buffeting effects of the tower and other separated-flow sources.

It should be noted that the estimated noise levels of figure 25 are those for the vicinity of the nose of the vehicle. For regions near the engine nozzles, noise levels of about 15 decibels higher would be expected during static firing and lift-off. However, model measurements indicate that the aerodynamic noise on the aft portion of the vehicle second stage will be appreciably less than that in the vicinity of the nose.

CONCLUSIONS

A wind-tunnel investigation of the transonic buffet characteristics of a large manned launch vehicle involving the measurement of fluctuating and time-average pressures on two different size rigid models has shown the following:

1. For the large manned launch vehicle, the wake from the escape tower under certain conditions produces relatively high noise levels (about 168 decibels) on the nose and cone-cylinder shoulders of the upper stages of the vehicle; the addition of two skirt designs over the tower rocket nozzles generally increased rather than decreased these noise levels.

2. Independently of the presence or absence of the escape tower, large pressure fluctuations occur on the vehicle just aft of the two cone-cylinder shoulders in a narrow band of Mach numbers just below 1.0. These pressure fluctuations present a design problem in venting unpressurized portions of the vehicle but do not present a structural response problem in the free-free bending or rigid body pitch modes.

3. An evaluation of buffet scaling relationships derived from simple dimensional considerations lends confidence to the use of suitably scaled models in determining the buffet pressure characteristics of large launch vehicles.

Langley Research Center,
National Aeronautics and Space Administration,
Langley Station, Hampton, Va., January 24, 1963.

REFERENCES

1. Goldberg, Arthur P., and Adams, Richard H.: Mercury-Atlas Buffeting Loads at Transonic and Low Supersonic Speeds. STL/TR-60-0000-AS431, Space Tech. Labs., Inc., Nov. 28, 1960.

2. Coe, Charles F.: Steady and Fluctuating Pressures at Transonic Speeds on Two Space-Vehicle Payload Shapes. NASA TM X-503, 1961.

3. Austin, R. F., and Prunty, C. C.: Investigation of Buffet Phenomena on a 0.24-Scale Model of the Forward Portion of the Titan B Missile With the Mark 4 and Mark 6 Re-Entry Bodies. AEDC-TN-61-78 (Revised) (Contract No. AF 40(600)-800 S/A 24(61-73), Arnold Eng. Dev. Center, Sept., 1961.

4. Coe, Charles F.: The Effects of Some Variations in Launch-Vehicle Nose Shape on Steady and Fluctuating Pressures at Transonic Speeds. NASA TM X-646, 1962.

5. Runyan, Harry L., Jr., and Rainey, A. Gerald: Launch-Vehicle Dynamics. NASA TM X-607, 1961.

6. Patterson, John L.: A Miniature Electrical Pressure Gage Utilizing a Stretched Flat Diaphragm. NACA TN 2659, 1952.

7. Liepmann, H. W.: Parameters for Use in Buffeting Flight Tests. Rep. No. SM-14631, Douglas Aircraft Co., Inc., Jan. 3, 1953.

8. Von Doenhoff, Albert E., Braslow, Albert L., and Schwartzberg, Milton A.: Studies of the Use of Freon-12 as a Wind-Tunnel Testing Medium. NACA TN 3000, 1953.

TABLE I.- FLUCTUATING PRESSURE COEFFICIENTS MEASURED ON 8-PERCENT RIGID MODEL

Mach number	Reynolds number	q, lb/sq ft	α, deg	$(\Delta C_p)_{rms}$ for transducer -			
				1	3	5	7
Model without tower in Freon							
0.400	4.31×10^6	87.9	0	0.004	0.108	0.008	0.172
.503	4.30	110.6	0	.005	.138	.015	.122
.603	4.31	132.7	0	.006	.091	.015	.111
.700	4.27	151.9	0	.007	.101	.022	.111
.803	4.34	173.5	0	.007	.113	.031	.124
.900	4.29	191.5	0	.005	.108	.040	.123
.929	4.25	195.2	0	.004	.121	.039	.143
.951	4.28	201.3	0	.004	.197	.097	.160
.960	4.23	201.1	0	.004	.236	.147	.116
.963	4.30	204.6	0	.004	.164	.130	.051
.977	4.25	205.0	0	.003	.006	.056	.006
1.003	4.27	210.0	0	.003	.002	.013	.002
1.050	4.27	218.8	0	.003	.001	.009	.002
1.102	4.32	228.2	0	.004	.001	.011	.002
1.203	4.26	244.4	0	.006	.001	.006	.002
.802	4.33	173.0	-1	.007	.106	.028	.131
.902	4.30	191.9	-1	.005	.114	.037	.128
.960	4.27	202.9	-1	.003	.090	.096	.189
.801	4.34	172.8	1	.007	.129	.033	.117
.904	4.31	192.6	1	.005	.097	.044	.107
.961	4.28	203.9	1	.004	.247	.093	.036
.959	4.27	203.0	-2	.003	.017	.064	.244
.960	4.29	203.4	2	.004	.143	.050	-----
.803	4.33	173.3	-4	.006	.058	.022	.177
.961	4.28	203.6	-4	.003	.002	.004	.071
1.102	4.32	228.9	-4	.003	0	.004	.005
.801	4.34	172.9	4	.008	.082	.040	.104
.960	4.29	203.5	4	.003	.074	.051	-----
1.102	4.32	229.7	4	.004	.001	.028	.002
Model without tower in Freon; repeat run							
0.608	4.65×10^6	134.0	-4	0.004	0.079	0.016	0.152
.909	4.46	192.9	-4	.003	.068	.044	.106
.933	4.47	197.3	-4	.002	.158	.140	.106
.962	4.47	202.4	-4	.002	.002	.005	.115
.607	4.65	133.4	4	.006	.107	.026	.096
.908	4.48	193.0	4	.003	.058	.068	.128
.932	4.45	196.5	4	.003	.059	.067	.026
.963	4.47	202.9	4	.002	.066	.065	.002

TABLE I.- FLUCTUATING PRESSURE COEFFICIENTS MEASURED ON 8-PERCENT RIGID MODEL - Continued

Mach number	Reynolds number	q, lb/sq ft	α, deg	$(\Delta C_p)_{rms}$ for transducer -			
				1	3	5	7
Model with tower configuration 1 in air							
0.794	0.97 × 10^6	105.8	0	0.021	0.068	0.029	0.069
.842	.97	110.2	0	.022	.068	.032	.070
.856	.97	111.2	0	.022	.069	.033	.070
.866	.97	112.4	0	.023	.068	.033	.070
.870	.96	111.8	0	.023	.069	.034	.069
.876	.97	117.9	0	.022	.067	.033	.068
.899	.97	115.2	0	.023	.068	.034	.071
.913	.99	119.0	0	.023	.068	.035	.071
.936	.99	118.8	0	.024	.071	.034	.068
.959	1.01	125.2	0	.025	.013	.098	.075
.962	1.01	125.4	0	.024	.042	.088	.060
.964	1.01	125.6	0	.024	.093	.159	.162
.965	1.02	126.3	0	.024	.013	.138	.112
.984	1.02	128.6	0	.024	.012	.024	.054
1.034	1.05	135.4	0	.026	.012	.014	.052
Model with tower configuration 1 in Freon							
0.815	0.98 × 10^6	39.1	0	0.030	0.072	0.032	0.085
.917	.97	43.2	0	.030	.086	.038	.084
.945	.96	44.4	0	.031	.160	.125	.102
.946	.98	44.9	0	.030	.116	.128	.108
.966	.94	44.5	0	.031	.015	.024	.077
.992	.95	45.9	0	.030	.017	.015	.076
1.016	.95	47.2	0	.028	.013	.012	.075
1.113	.98	52.0	0	.029	.013	.013	.074
Model with tower configuration 1 Freon data corrected to air by method of reference 8							
0.806	0.98 × 10^6	39.1	0	0.028	0.070	0.031	0.082
.913	.97	43.2	0	.029	.082	.036	.080
.942	.96	44.4	0	.029	.152	.118	.099
.943	.98	44.9	0	.028	.110	.122	.103
.964	.94	44.5	0	.030	.014	.023	.074
.992	.95	45.9	0	.029	.016	.014	.073
1.017	.95	47.2	0	.026	.012	.011	.072
1.122	.98	52.0	0	.027	.012	.011	.069

TABLE I.- FLUCTUATING PRESSURE COEFFICIENTS MEASURED ON

8-PERCENT RIGID MODEL - Continued

Mach number	Reynolds number	q, lb/sq ft	α, deg	$(\Delta C_p)_{rms}$ for transducer -			
				1	3	5	7
Model with tower configuration 1 in Freon							
0.610	4.40×10^6	135.0	0	0.039	0.124	0.018	0.104
.706	4.36	153.4	0	.038	.089	.045	.064
.802	4.36	172.6	0	.038	.075	.061	.061
.860	4.38	184.6	0	.038	.074	.070	.064
.898	4.46	190.6	0	.038	.080	.059	.067
.930	4.48	196.7	0	.039	.097	.080	.073
.957	4.48	201.5	0	.039	.069	.091	.067
1.002	4.45	209.4	0	.032	.053	.015	.014
1.053	4.46	218.6	0	.031	.049	.010	.013
1.102	4.42	227.3	0	.033	.046	.010	.014
.609	4.40	134.7	-4	.075	.167	.018	.118
.706	4.35	153.4	-4	.079	.139	.042	.078
.806	4.38	173.7	-4	.082	.114	.068	.077
.855	4.38	183.4	-4	.084	.101	.079	.076
.893	4.37	189.5	-4	.084	.071	.062	.075
.929	4.46	196.2	-4	.087	.064	.065	.103
.954	4.47	200.8	-4	.088	.063	.021	.097
1.006	4.44	210.4	-4	.084	.060	.020	.027
1.055	4.46	219.1	-4	.079	.056	.018	.026
1.099	4.44	227.0	-4	.080	.056	.014	.022
.605	4.37	133.3	4	.029	.101	.019	.081
.702	4.34	152.5	4	.028	.077	.051	.042
.801	4.34	171.9	4	.026	.075	.066	.040
.855	4.39	183.3	4	.025	.074	.075	.045
.900	4.46	190.7	4	.026	.075	.082	.063
.929	4.48	196.7	4	.023	.074	.058	.110
.956	4.46	201.5	4	.023	.123	.047	.005
1.008	4.46	210.8	4	.021	.035	.017	.006
1.050	4.42	218.1	4	.021	.033	.010	.006
1.101	4.45	227.6	4	.021	.031	.011	.008
.610	.98	29.9	0	.037	.091	.018	.081
.603	8.49	254.6	0	.039	.124	.018	.106
.809	6.82	270.9	0	.039	.077	.032	.088
Model with tower configuration 1 in Freon; repeat run							
0.866	4.40×10^6	185.6	0	0.030	0.101	0.042	0.085
.918	4.39	194.9	0	.030	.097	.044	.102
.924	4.32	192.8	0	.032	.100	.044	.122
.935	4.34	195.7	0	.031	.134	.051	.059
.941	4.35	197.2	0	.031	.145	.058	.059
.956	4.37	201.0	0	.025	.147	.128	.072
.960	4.39	202.9	0	.026	.093	.106	.041

TABLE I.- FLUCTUATING PRESSURE COEFFICIENTS MEASURED ON

8-PERCENT RIGID MODEL - Continued

Mach number	Reynolds number	q, lb/sq ft	α, deg	$(\Delta C_p)_{rms}$ for transducer -			
				1	3	5	7
Model with tower configuration 1 in Freon; repeat run							
0.967	4.39×10^6	204.0	0	0.025	0.082	0.070	0.013
.973	4.35	203.2	0	.025	.078	.040	.013
.991	4.39	208.1	0	.025	.079	.018	.012
1.017	4.39	212.2	0	.024	.077	.013	.012
1.111	4.39	229.1	0	.027	.076	.012	.012
Model with tower configuration 2 in Freon							
0.606	4.29×10^6	133.6	0	0.057	0.134	0.016	0.144
.703	4.23	152.7	0	.052	.111	.022	.115
.855	4.24	183.3	0	.047	.083	.037	.098
.906	4.35	192.7	0	.082	.081	.032	.066
.932	4.33	196.9	0	.080	.046	.061	.053
.960	4.38	203.0	0	.046	.049	.016	.052
1.009	4.42	214.2	0	.003	.042	.016	.046
1.051	4.45	223.4	0	.003	.040	.015	.044
1.112	4.51	237.2	0	.003	.043	.016	.047
.603	4.27	132.6	-4	.034	.087	.015	.191
.706	4.25	154.1	-4	.044	.064	.022	.178
.855	4.24	183.8	-4	.108	.069	.039	.126
.904	4.35	192.2	-4	.119	.083	.032	.119
.932	4.32	196.5	-4	.122	.063	.072	.131
.954	4.38	201.6	-4	.120	.013	.006	.120
1.007	4.44	213.8	-4	.062	.013	.006	.119
.601	4.27	132.2	4	.142	.157	.020	.082
.701	4.23	152.3	4	.100	.160	.023	.062
.856	4.25	184.3	4	.046	.104	.031	.073
.906	4.35	192.6	4	.074	.098	.032	.120
.927	4.34	195.6	4	.070	.138	.041	.010
.963	4.38	203.2	4	.068	.090	.045	.009
1.003	4.45	213.3	4	.040	.096	.028	.009

TABLE I.- FLUCTUATING PRESSURE COEFFICIENTS MEASURED ON

8-PERCENT RIGID MODEL - Continued

Mach number	Reynolds number	q, lb/sq ft	α, deg	$(\Delta C_p)_{rms}$ for transducer -			
				1	3	5	7
Model with tower configuration 3 in Freon							
0.401	4.52 × 106	87.9	0	0.058	0.055	0.005	0.085
.457	4.59	101.9	0	.050	.080	.005	.126
.506	4.53	111.4	0	.057	.118	.011	.149
.552	4.55	122.1	0	.061	.145	.012	.126
.607	4.55	134.0	0	.057	.155	.015	.103
.705	4.49	152.6	0	.055	.138	.019	.094
.807	4.51	173.7	0	.054	.095	.025	.093
.856	4.54	183.7	0	.075	.101	.030	.099
.880	4.51	187.0	0	.081	.107	.030	.086
.904	4.50	191.4	0	.086	.097	.032	.107
.930	4.49	195.3	0	.081	.149	.034	.170
.942	4.51	198.7	0	.076	.114	.092	.192
.953	4.45	197.7	0	.087	.126	.096	.192
.958	4.52	202.2	0	.075	.129	.073	.148
.981	4.50	205.0	0	.059	.064	.025	.043
1.001	4.50	209.4	0	.079	.080	.028	.035
1.051	4.51	218.5	0	.072	.060	.018	.044
1.102	4.61	233.0	0	.065	.066	.027	.036
1.210	4.70	257.9	0	.093	.083	.035	.044
.403	4.54	88.4	-1	.046	.060	.004	.084
.805	4.51	173.2	-1	.047	.082	.025	.103
.882	4.52	187.8	-1	.062	.091	.031	.099
.905	4.51	191.9	-1	.063	.097	.033	.109
.929	4.49	195.3	-1	.071	.149	.044	.196
.955	4.52	201.5	-1	.084	.112	.060	.188
1.007	4.52	210.9	-1	.057	.061	.021	.041
1.103	4.61	233.5	-1	.092	.106	.031	.037
.407	4.58	90.0	1	.058	.052	.006	.084
.804	4.52	173.2	1	.061	.106	.025	.086
.878	4.51	186.8	1	.067	.100	.030	.094
.897	4.50	190.0	1	.078	.099	.030	.090
.929	4.49	195.4	1	.071	.133	.034	.131
.953	4.52	201.4	1	.040	.079	.068	.080
1.005	4.52	210.8	1	.071	.112	.035	.017
1.103	4.62	234.3	1	.089	.124	.035	.037
.953	4.51	201.1	-2	.069	.079	.030	.200
1.004	4.51	210.1	-2	.051	.044	.023	.041
1.106	4.62	234.2	-2	.104	.079	.030	.041
.955	4.52	201.7	2	.066	.130	.062	.036
1.004	4.52	210.4	2	.055	.093	.033	.015
1.102	4.62	234.2	2	.080	.096	.029	.029
.803	4.51	172.6	-4	.050	.083	.024	.102
.898	4.50	190.2	-4	.052	.049	.033	.101
.957	4.52	202.1	-4	.065	.035	.013	.254
1.004	4.52	210.5	-4	.051	.031	.011	.040
1.103	4.62	233.8	-4	.058	.049	.012	.052
.801	4.51	172.3	4	.046	.086	.025	.056
.905	4.52	192.3	4	.050	.091	.031	.086
.954	4.53	201.7	4	.049	.143	.034	.021
1.004	4.52	210.6	4	.055	.071	.024	.013
1.103	4.62	234.7	4	.063	.098	.032	.032

TABLE I.- FLUCTUATING PRESSURE COEFFICIENTS MEASURED ON

8-PERCENT RIGID MODEL - Concluded

Mach number	Reynolds number	q, lb/sq ft	α, deg	$(\Delta C_p)_{rms}$ for transducer -			
				1	3	5	7
Model with tower configuration 4 in Freon							
0.605	4.53×10^6	133.3	0	0.115	0.137	0.012	0.152
.704	4.48	152.7	0	.102	.155	.016	.130
.806	4.51	173.9	0	.089	.126	.022	.107
.865	4.46	183.5	0	.080	.110	.027	.102
.877	4.47	185.9	0	.079	.234	.025	.227
.883	4.47	187.6	0	.080	.136	.023	.157
.901	4.48	190.8	0	.075	.093	.027	.081
.952	4.48	200.1	0	.057	.071	.021	.058
1.007	4.48	210.6	0	.059	.076	.024	.064
1.051	4.47	217.2	0	.057	.075	.022	.061
1.106	4.49	228.2	0	.049	.076	.022	.064
1.200	4.49	243.0	0	.052	.066	.020	.059
.802	4.50	172.8	-1	.089	.108	.022	.127
.880	4.48	186.9	-1	.081	.246	.029	.225
.904	4.49	191.8	-1	.076	.069	.031	.100
1.004	4.48	209.8	-1	.065	.059	.017	.087
1.103	4.50	228.1	-1	.054	.059	.016	.083
.804	4.51	173.6	1	.092	.151	.022	.099
.879	4.49	187.0	1	.080	.144	.026	.144
.904	4.50	192.8	1	.074	.121	.027	.063
1.004	4.49	210.5	1	.065	.110	.036	.052
1.105	4.51	229.0	1	.052	.098	.033	.051
.878	4.48	186.4	-2	.092	.122	.031	.120
1.004	4.49	209.9	-2	.078	.048	.014	.112
1.105	4.50	228.4	-2	.064	.047	.013	.106
.879	4.49	187.1	2	.080	.127	.026	.094
1.005	4.50	211.0	2	.070	.131	.040	.043
1.105	4.51	229.2	2	.058	.120	.036	.045
.801	4.49	172.4	-4	.109	.084	.023	.156
.880	4.49	187.1	-4	.117	.094	.033	.124
.907	4.50	192.9	-4	.116	.199	.042	.125
1.004	4.49	210.1	-4	.109	.025	.007	.150
1.104	4.51	228.5	-4	.088	.029	.008	.139
.805	4.51	174.0	4	.090	.162	.023	.085
.878	4.49	187.1	4	.080	.137	.026	.089
.905	4.50	192.7	4	.075	.123	.025	.202
1.005	4.51	211.0	4	.076	.152	.049	.022
1.105	4.52	229.6	4	.065	.144	.046	.024

TABLE II.- FLUCTUATING PRESSURE COEFFICIENTS MEASURED ON

1.6-PERCENT RIGID MODEL IN FREON

Mach number	Reynolds number	q, lb/sq ft	α, deg	$(\Delta C_p)_{rms}$ for transducer -			
				1	3	4	5
Model without tower							
0.618	0.98×10^6	153.4	0	0.007	0.051	0.047	0.014
.718	.91	164.5	0	.008	.037	.070	.016
.816	.96	195.7	0	.009	.031	.078	.018
.868	.96	206.2	0	.008	.030	.073	.015
.916	.96	216.6	0	.007	.032	.063	.015
.941	.96	222.1	0	.006	.037	.055	.014
.956	.97	225.7	0	.005	.042	.053	.013
.962	.97	227.0	0	.005	.044	.053	.014
.965	.97	227.9	0	.005	.005	.007	.006
.995	.97	233.4	0	.004	.004	.006	.004
1.016	.96	235.8	0	.004	.004	.006	.004
1.065	.96	244.7	0	.004	.003	.005	.004
1.112	.96	253.4	0	.004	.002	.005	.004
.615	.98	152.4	-4	.006	.034	.010	.005
.960	.97	226.8	-4	.005	.063	.008	.007
.616	.98	153.0	4	.007	.099	.061	.020
.925	.97	226.2	4	.005	.074	.065	.020
Model with tower configuration 1							
0.616	0.94×10^6	152.6	0	0.024	0.072	0.020	0.008
.714	.87	163.6	0	.022	.070	.029	.011
.814	.93	195.6	0	.030	.044	.040	.015
.865	.93	205.7	0	.031	.044	.050	.018
.914	.93	216.2	0	.033	.045	.057	.019
.938	.94	221.8	0	.033	.105	.059	.035
.940	.93	222.1	0	.033	.129	.061	.044
.948	.94	224.1	0	.033	.136	.058	.151
.950	.94	224.9	0	.033	.088	.039	.107
.951	.94	225.2	0	.033	.075	.035	.112
.951	.94	224.8	0	.033	.043	.019	.040
.957	.94	226.4	0	.033	.006	.012	.015
.959	.93	225.1	0	.032	.009	.012	.016
.963	.94	227.8	0	.033	.006	.012	.013
1.005	.93	233.8	0	.032	.010	.010	.007
1.005	.92	242.2	0	.026	.008	.009	.006
1.100	.93	252.8	0	.027	.008	.008	.006
.815	1.50	311.7	0	.031	.070	.039	.016
.613	.93	151.8	-4	.034	.069	.011	.006
.815	.93	195.8	-4	.032	.044	.028	.014
.917	.93	215.7	-4	.031	.048	.044	.052
.935	.93	221.0	-4	.031	.061	.044	.096

TABLE II.- FLUCTUATING PRESSURE COEFFICIENTS MEASURED ON

1.6-PERCENT RIGID MODEL IN FREON - Concluded

Mach number	Reynolds number	q, lb/sq ft	α, deg	$(\Delta C_p)_{rms}$ for transducer -			
				1	3	4	5
Model with tower configuration 1							
0.957	0.94 × 10⁶	227.1	-4	0.030	0.053	0.014	0.026
1.102	.93	253.5	-4	.028	.006	.005	.002
.815	1.50	313.2	-4	.022	.077	.051	.018
.614	.93	151.9	4	.026	.073	.028	.009
.814	.93	195.6	4	.019	.044	.058	.019
.910	.93	215.2	4	.020	.047	.058	.023
.938	.93	222.0	4	.020	.051	.055	.024
.959	.94	227.3	4	.019	.144	.083	.057
1.102	.93	253.5	4	.021	.007	.014	.009
.812	1.50	310.1	4	.022	.077	.051	.018
Model with tower configuration 2							
0.614	0.99 × 10⁶	151.5	0	0.087	0.083	0.013	0.005
.720	.98	176.0	0	.071	.063	.017	.006
.815	.97	195.3	0	.063	.064	.049	.010
.866	.97	205.8	0	.060	.070	.034	.012
.904	.95	208.5	0	.055	.214	.031	.021
.909	.95	209.8	0	.056	.085	.016	.037
.922	.96	213.9	0	.056	.019	.009	.071
.936	.96	217.9	0	.055	.006	.009	.065
.939	.96	218.8	0	.055	.042	.009	.048
.945	.96	220.5	0	.055	.018	.010	.029
.955	.97	223.2	0	.054	.018	.010	.009
.960	.97	224.7	0	.056	.018	.010	.009
.962	.97	225.2	0	.055	.018	.010	.006
.968	.97	226.9	0	.055	.018	.010	.006
.971	.97	227.3	0	.056	.018	.010	.009
.988	.98	232.1	0	.056	.018	.010	.004
1.011	.97	234.6	0	.055	.018	.009	.004
1.068	.97	244.8	0	.035	.014	.008	.003
1.113	.97	254.6	0	.028	.015	.008	.003
.909	.95	209.9	-4	.076	.073	.040	.022
1.110	.98	254.6	-4	.069	.004	.005	.005
.906	.95	209.2	4	.057	.066	.040	.012
1.116	.98	255.5	4	.035	.043	.012	.009

TABLE III.- STATIC PRESSURE COEFFICIENTS C_p MEASURED ON 8-PERCENT MODEL (TOWER CONFIGURATION 1) IN FREON AT REYNOLDS NUMBER OF 4.5×10^6

(a) $\alpha = 0^\circ$

x/D	Static pressure coefficients for Mach numbers of -									
	0.610	0.706	0.802	0.860	0.898	0.930	0.956	1.002	1.053	1.102
0.21	0.399	0.383	0.355	0.381	0.421	0.449	0.475	0.524	0.588	0.742
.30	.290	.272	.250	.279	.323	.362	.386	.447	.510	.667
.39	.163	.148	.134	.167	.212	.256	.284	.353	.420	.578
.49	-.014	-.011	-.019	.028	.080	.125	.156	.233	.308	.470
.64	-.922	-.825	-.821	-.806	-.799	-.823	-1.453	-1.381	-1.231	-1.022
.75	-.699	-.811	-.863	-.859	-.853	-.869	-1.174	-1.166	-1.030	-.832
.86	-.325	-.607	-.773	-.802	-.793	-.794	-.695	-.998	-.871	-.686
.98	-.137	-.350	-.590	-.665	-.668	-.671	-.538	-.828	-.714	------
1.09	-.057	-.171	-.398	-.495	-.515	-.537	-.386	-.302	-.512	-.273
1.26	.026	-.045	-.194	-.279	-.311	-.350	-.129	-.062	.016	.166
1.48	.049	.000	-.085	-.121	-.134	-.167	.064	.167	.234	.397
1.58	-.026	-.065	-.120	-.128	-.123	-.131	.038	.131	.190	.369
1.68	-.114	-.148	-.192	-.181	-.159	-.151	-.037	.046	.110	.295
1.79	-.233	-.268	-.305	-.286	-.253	-.233	-.153	-.056	.019	.205
2.00	-.296	-.350	-.415	-.415	-.389	-.382	-.745	-.798	-.706	-.491
2.17	-.203	-.253	-.326	-.328	-.302	-.287	-.334	-.691	-.609	-.398
2.40	-.140	-.192	-.260	-.263	-.233	-.214	-.158	-.137	-.459	-.251
2.63	-.100	-.151	-.216	-.215	-.183	-.161	-.115	.002	-.368	-.174
2.85	-.048	-.097	-.156	-.153	-.120	-.095	-.050	.062	-.012	-.022
3.08	.014	-.031	-.088	-.083	-.048	-.024	.030	.141	.160	.290
3.30	.158	.113	.054	.056	.086	.103	.188	.309	.344	.490
3.55	.333	.283	.218	.218	.244	.252	.345	.452	.475	.628

TABLE III.- STATIC PRESSURE COEFFICIENTS C_p MEASURED ON 8-PERCENT MODEL (TOWER CONFIGURATION 1) IN FREON AT REYNOLDS NUMBER 4.5×10^6 - Continued

(b) $\alpha = 4^\circ$

x/D	Static pressure coefficients for Mach numbers of -									
	0.609	0.706	0.806	0.855	0.893	0.929	0.954	1.006	1.055	1.099
0.21	0.248	0.488	0.176	0.302	0.265	0.307	0.307	0.454	0.454	0.561
.30	.165	.413	.101	.235	.198	.245	.243	.397	.397	.505
.39	.051	.306	.000	.138	.106	.155	.157	.314	.316	.425
.49	-.119	.148	-.145	.000	-.028	.029	.034	.198	.208	.323
.64	-.950	-.584	-.855	-.732	-.785	-.821	-1.119	-1.330	-1.238	-1.118
.75	-.652	-.494	-.849	-.738	-.792	-.807	-.909	-1.161	-1.090	-.986
.86	-.357	-.302	-.737	-.649	-.711	-.710	-.753	-.997	-.934	-.825
.98	-.193	-.118	-.594	-.528	-.610	-.607	-.621	-.671	-.768	-.646
1.09	-.115	.016	-.463	-.406	-.505	-.512	-.503	-.265	-.288	-.160
1.26	-.035	.136	-.313	-.260	-.368	-.384	-.345	-.062	-.052	.043
1.48	-.015	.185	-.214	-.143	-.245	-.265	-.205	.107	.125	.233
1.58	-.081	.142	-.226	-.139	-.226	-.238	-.188	.091	.101	.218
1.68	-.156	.076	-.272	-.168	-.240	-.242	-.209	.029	.037	.158
1.79	-.259	-.021	-.355	-.238	-.294	-.283	-.282	-.077	-.061	.063
2.00	-.301	-.076	-.425	-.307	-.360	-.343	-.421	-.694	-.717	-.595
2.17	-.209	.006	-.350	-.238	-.295	-.275	-.303	-.576	-.570	-.438
2.40	-.148	.065	-.289	-.177	-.232	-.206	-.206	-.078	-.491	-.366
2.63	-.109	.106	-.246	-.132	-.185	-.155	-.148	.050	-.277	-.256
2.85	-.062	.154	-.196	-.080	-.132	-.101	-.089	.120	.002	.032
3.08	-.010	.206	-.144	-.030	-.082	-.052	-.032	.186	.137	.209
3.30	.101	.311	-.046	.062	.002	.021	.054	.285	.254	.348
3.55	.241	.444	.074	.167	.088	.093	.123	.334	.318	.445

TABLE III.- STATIC PRESSURE COEFFICIENTS C_p MEASURED ON 8-PERCENT MODEL (TOWER CONFIGURATION 1) IN FREON AT REYNOLDS NUMBER 4.5×10^6 - Concluded

(c) $\alpha = -4^\circ$

x/D	Static pressure coefficients for Mach numbers of -									
	0.605	0.702	0.801	0.855	0.900	0.929	0.956	1.008	1.051	1.101
0.21	0.730	0.442	0.539	0.462	0.529	0.544	0.620	0.629	0.748	0.765
.30	.629	.329	.443	.362	.433	.447	.528	.539	.661	.681
.39	.499	.206	.326	.249	.324	.341	.424	.439	.565	.587
.49	.308	.038	.167	.102	.184	.206	.292	.313	.442	.470
.64	-.744	-.908	-.727	-.806	-.853	-.919	-1.452	-1.335	-1.147	-1.057
.75	-.383	-.868	-.751	-.833	-.884	-.937	-1.152	-1.063	-.886	-.814
.86	.060	-.599	-.675	-.796	-.804	-.832	-.929	-.866	-.697	-.642
.98	.177	-.283	-.497	-.674	-.636	-.658	-.563	-.709	-.552	-.504
1.09	.220	-.109	-.270	-.499	-.437	-.474	-.050	-.615	-.462	-.419
1.26	.327	.005	.000	-.220	-.165	-.214	.203	.071	.163	.199
1.48	.365	.054	.146	.028	.069	.040	.265	.273	.389	.431
1.58	.279	-.034	.088	.010	.059	.052	.158	.170	.287	.337
1.68	.188	-.129	-.005	-.071	-.010	-.003	.072	.089	.213	.264
1.79	.057	-.265	-.146	-.209	-.134	-.119	-.023	.005	.135	.186
2.00	-.032	-.376	-.306	-.394	-.470	-.685	-.867	-.797	-.638	-.554
2.17	.071	-.274	-.210	-.311	-.248	-.256	-.636	-.634	-.495	-.411
2.40	.127	-.211	-.146	-.249	-.195	-.188	-.062	-.482	-.372	-.295
2.63	.165	-.171	-.103	-.203	-.150	-.145	-.037	-.008	-.299	-.235
2.85	.217	-.114	-.041	-.136	-.079	-.073	.021	.072	-.042	-.215
3.08	.288	-.041	.042	-.050	.014	.022	.109	.160	.232	.214
3.30	.454	.145	.232	.142	.211	.218	.325	.366	.462	.470
3.55	.690	.374	.460	.366	.439	.443	.563	.580	.663	.664

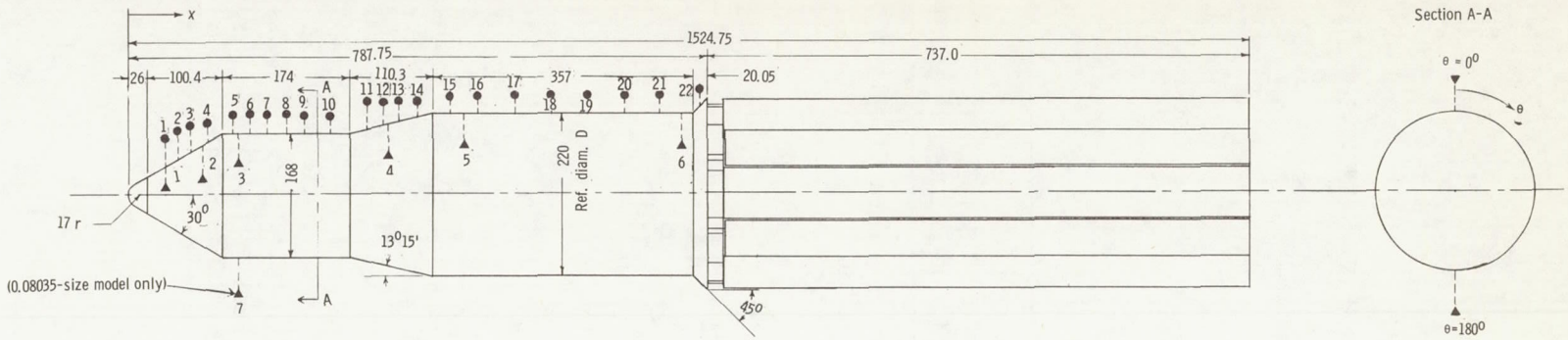

(a) 0.08035- and 0.01607-size models scaled to full scale.

Pressure transducer locations 0.08035- size rigid model ▲			
θ = 0°		θ = 180°	
No.	x/D	No.	x/D
1	0.21		
2	.44		
3	.68	7	0.68
4	1.59		
5	2.07		
6	3.42		

Pressure orifice locations 0.08035- size rigid model ●			
θ = 0°			
No.	x/D	No.	x/D
1	0.21	12	1.58
2	.30	13	1.68
3	.39	14	1.79
4	.49	15	2.00
5	.64	16	2.17
6	.75	17	2.40
7	.86	18	2.63
8	.98	19	2.85
9	1.09	20	3.08
10	1.26	21	3.30
11	1.48	22	3.55

Pressure transducer locations 0.01607- size rigid model ▲	
θ = 0°	
No.	x/D
1	0.21
2	.44
3	.68
4	1.59
5	2.07
6	3.42

Pressure transducer location 0.01427- size elastic model ▼	
θ = 0°	
No.	x/D
1	0.67

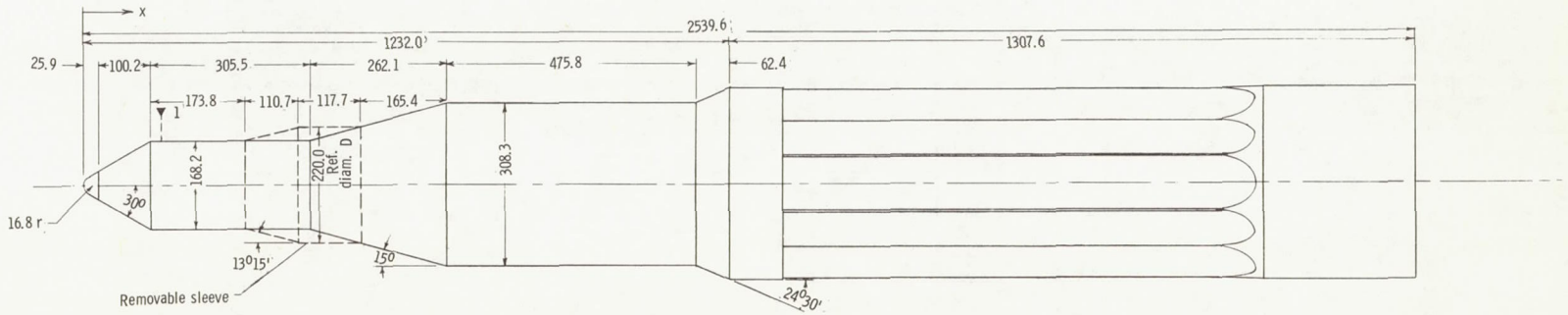

(b) Elastic model 0.01427 size (with oversize booster) scaled to full scale.

Figure 1.- Basic model configurations. All dimensions are model dimensions scaled to full size; inches (unless otherwise noted).

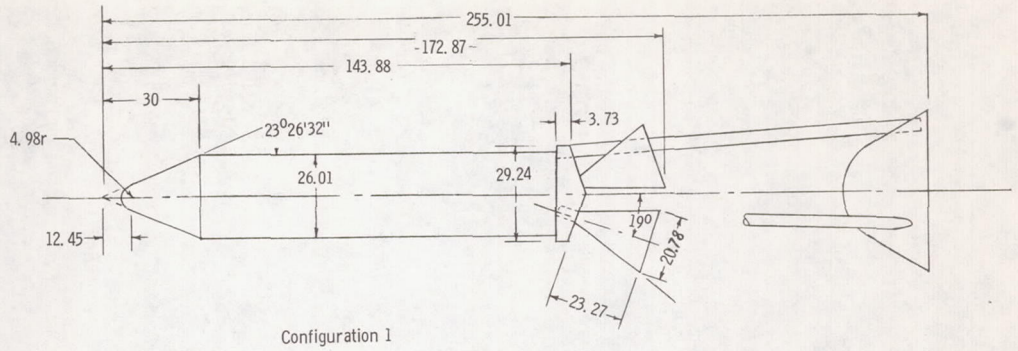

Configuration 1

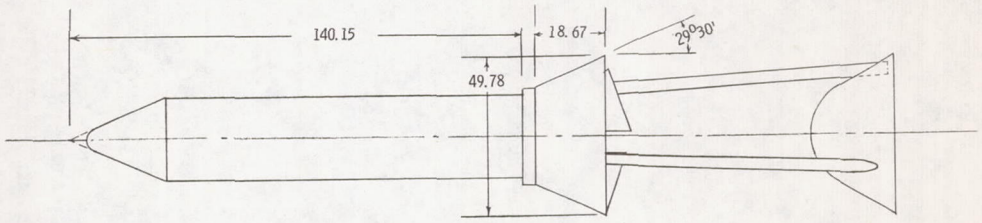

Configuration 2. (Configuration 1 with skirt)

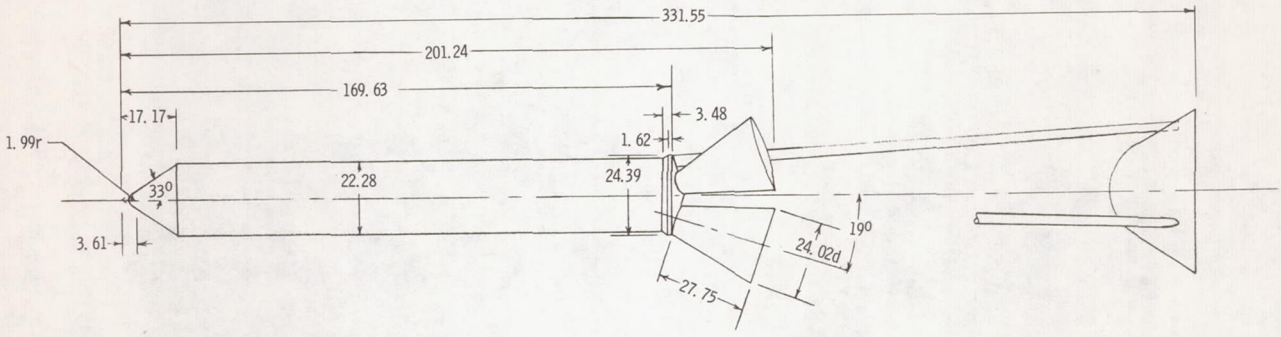

Configuration 3.

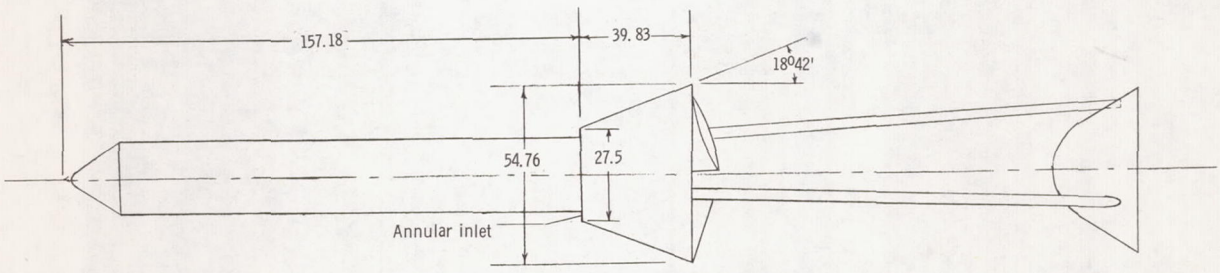

Configuration 4. (Configuration 3 with annular inlet skirt)

Note: All dimensions are model dimensions scaled to full size, inches (unless otherwise noted).

Figure 2.- Tower configurations. All dimensions are model dimensions scaled to full size; inches (unless otherwise noted).

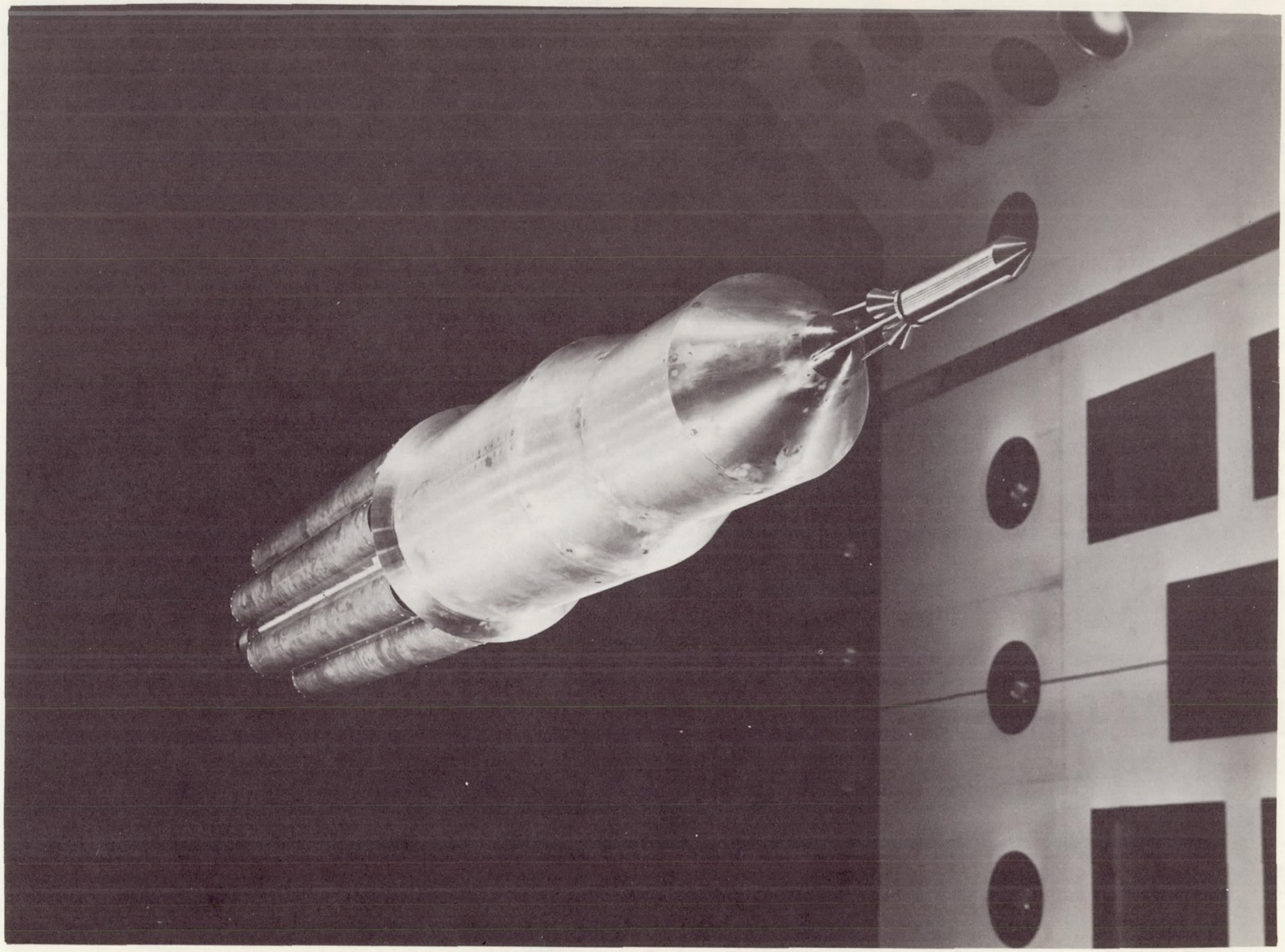

(a) 8-percent rigid model with tower configuration 1 mounted in tunnel. L-61-5987

Figure 3.- Photographs of models.

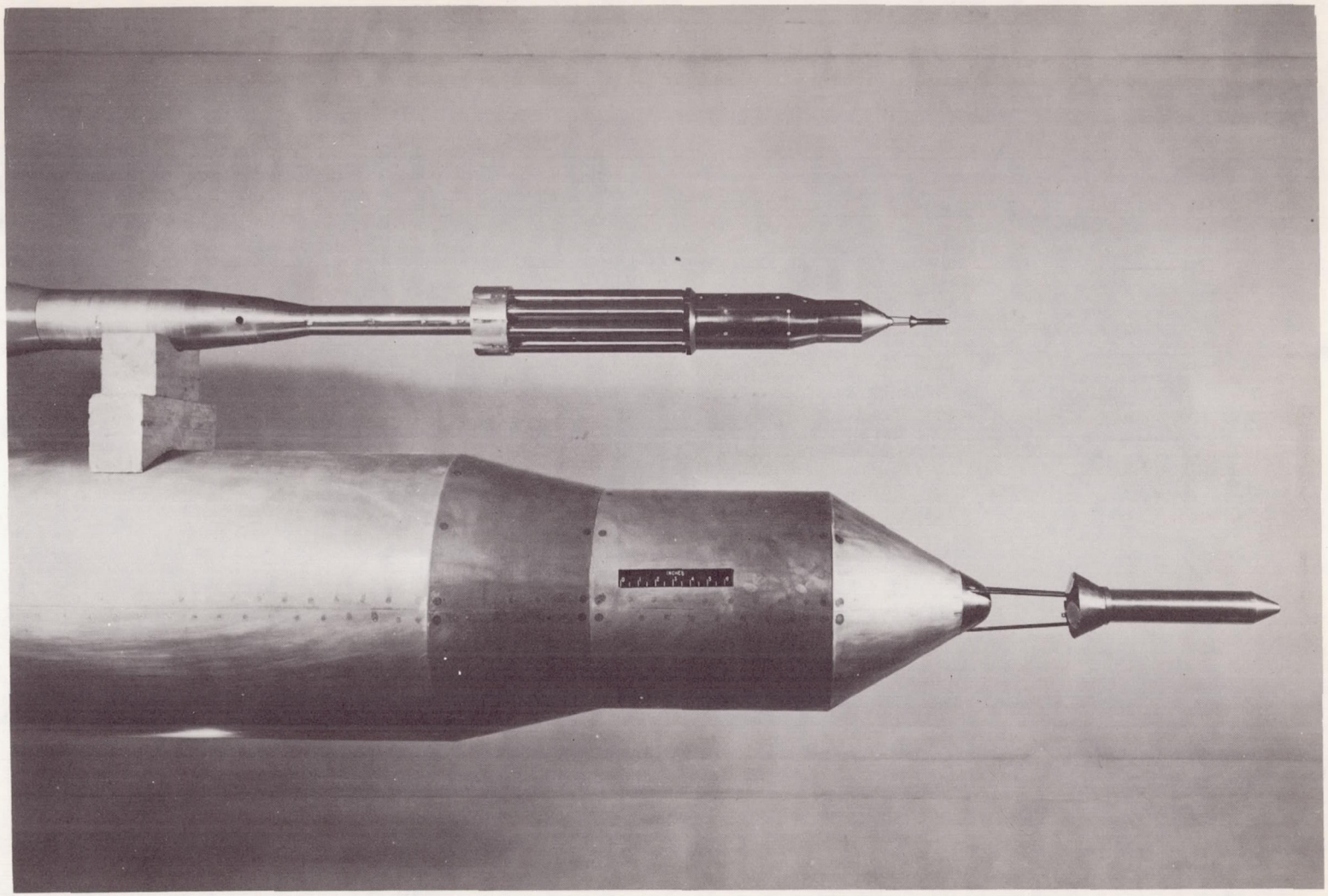

L-61-6339

(b) 1.6-percent rigid model on mounting sting and forebody of 8-percent model. Tower configuration 2.

Figure 3.- Concluded.

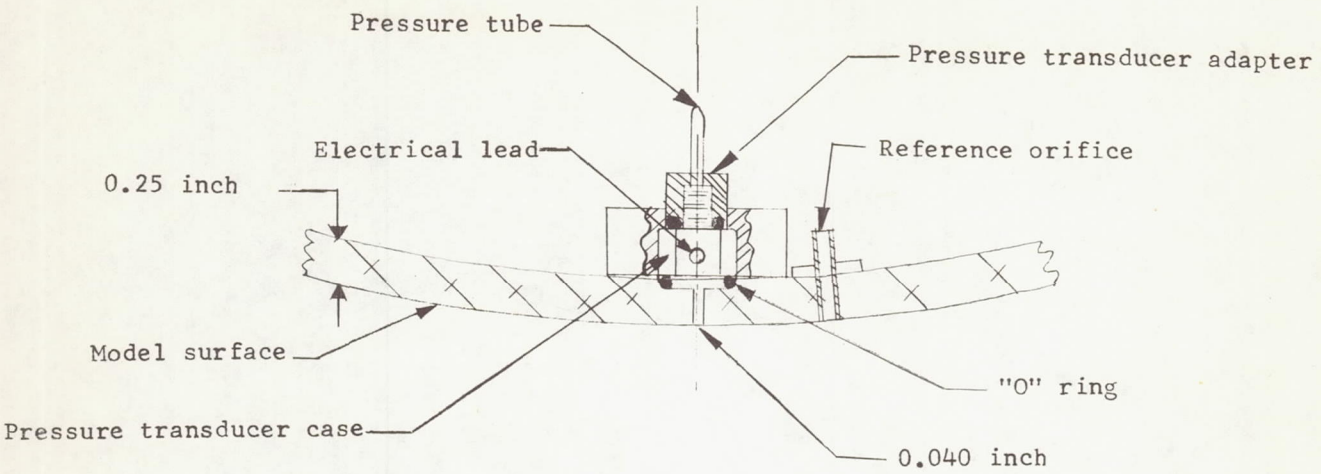

(a) Typical pressure transducer installation (full size).

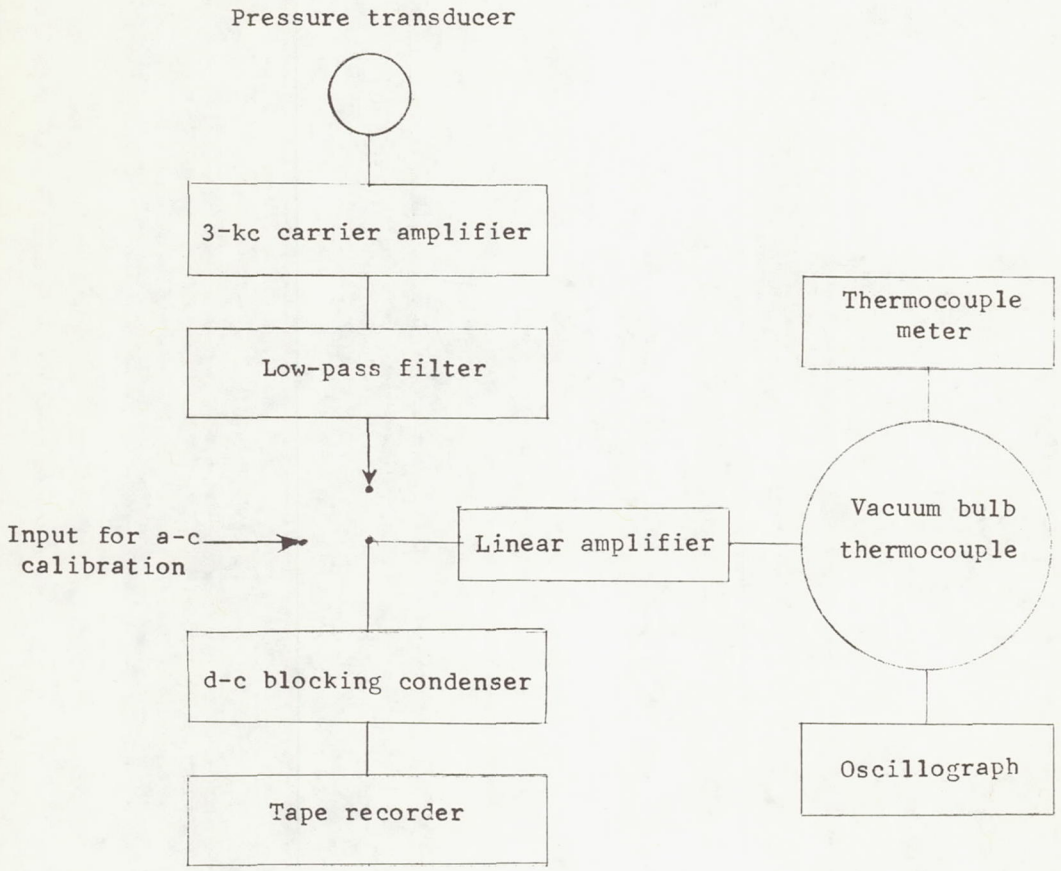

(b) Block diagram of instrumentation used.

Figure 4.- Transducer installation and instrumentation used to record buffet data.

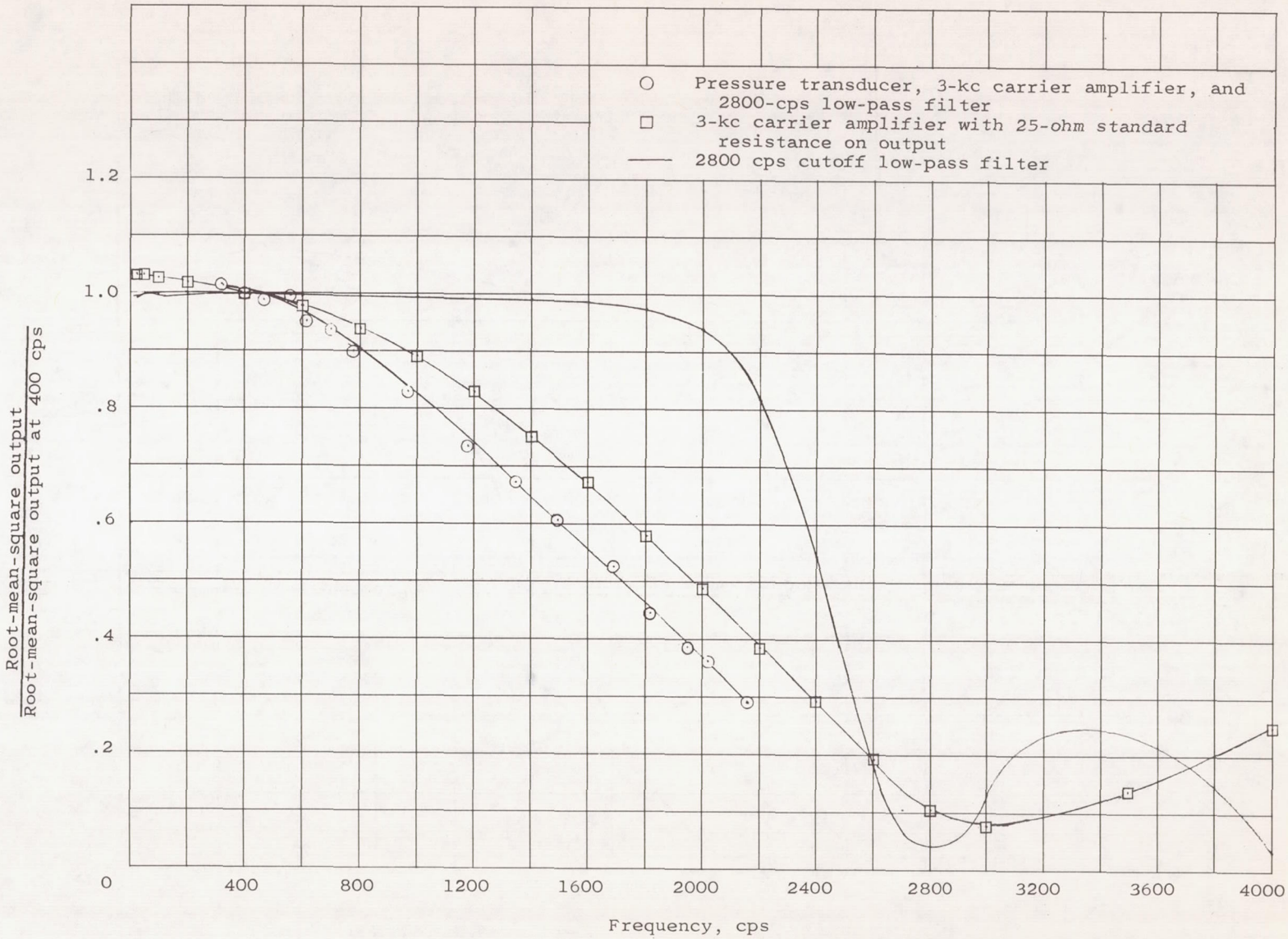

Figure 5.- Frequency response of components of the instrumentation used for measurement of fluctuating pressures.

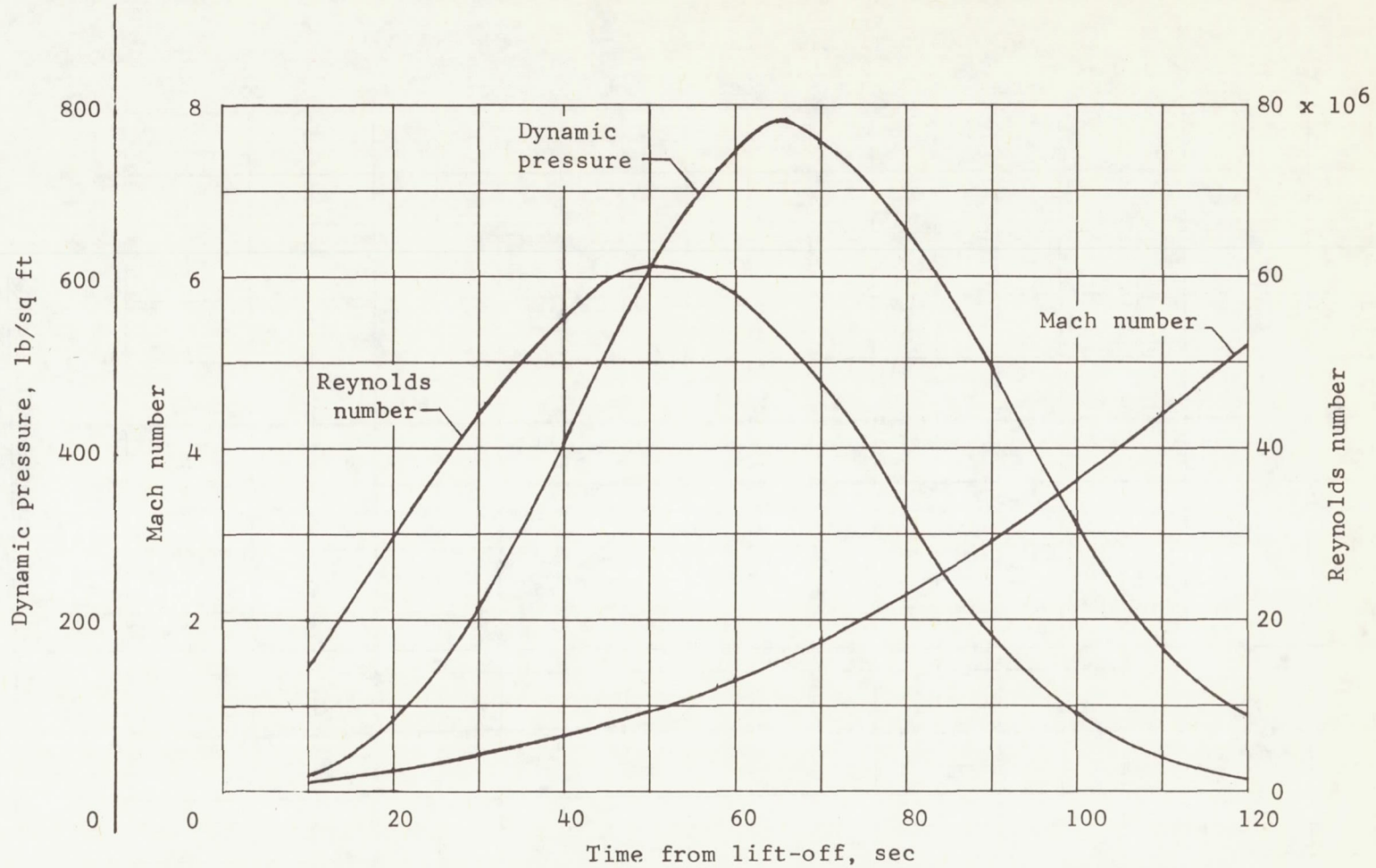

Figure 6.- Dynamic pressure, Reynolds number, and Mach number variation at lift-off for large launch vehicle configuration used in scaling model data to full-scale data and in computation of acoustic environment.

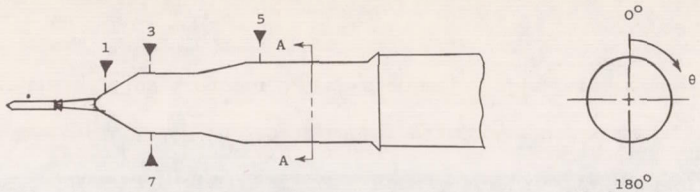

Pressure transducer locations

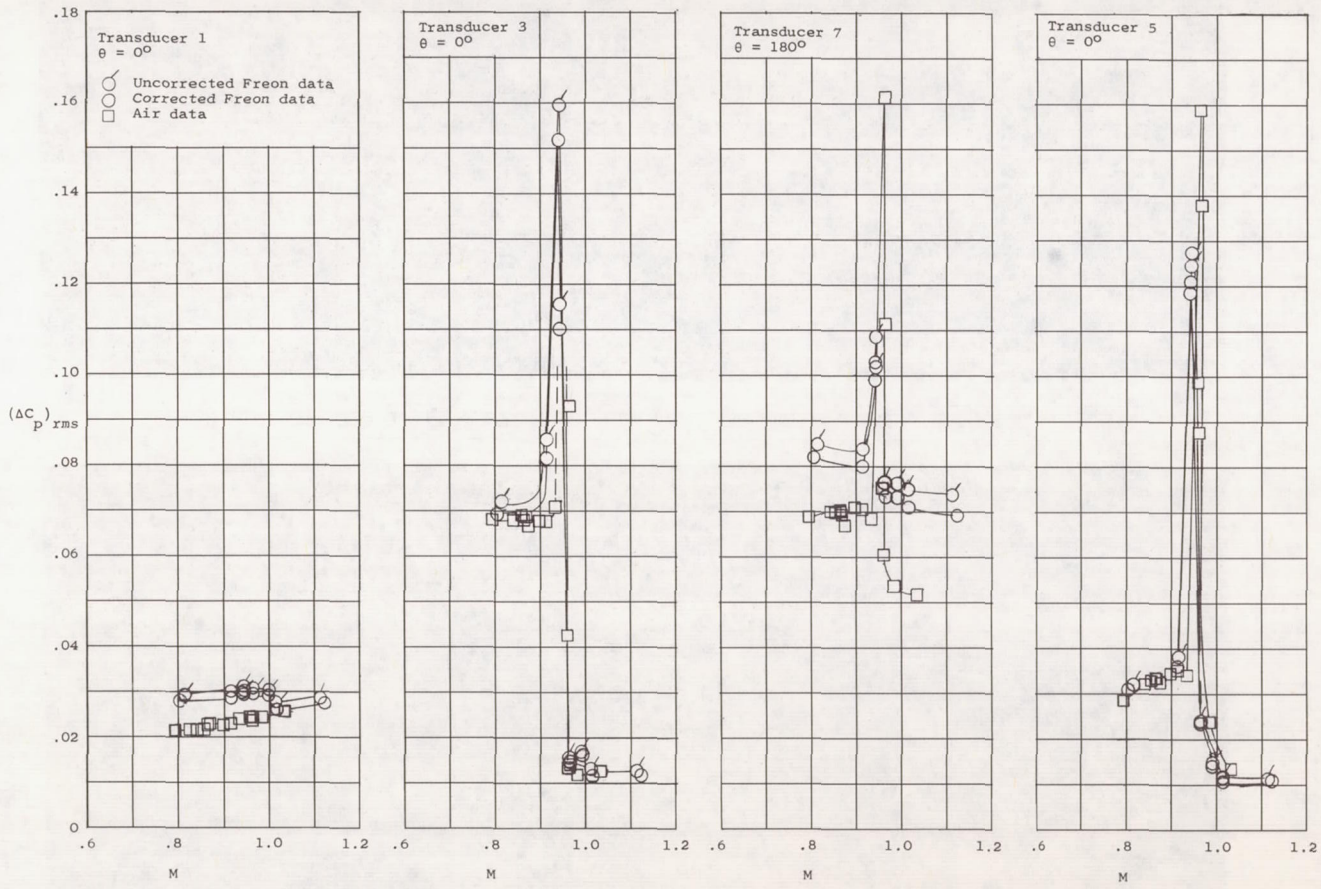

Figure 7.- Comparison of $\left(\Delta C_p\right)_{rms}$ data taken in air and Freon with Freon data corrected by reference 8. All data for 8-percent rigid model with tower configuration 1; $R \approx 1.0 \times 10^6$; and $\alpha = 0^\circ$.

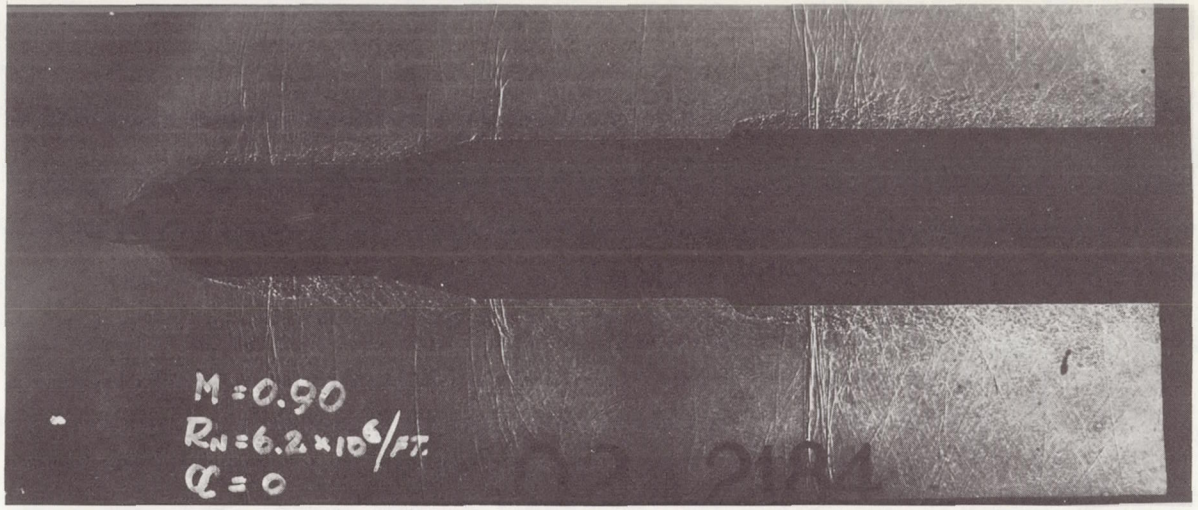

(a) M = 0.90, R ≈ 0.773 × 10^6 (Reynolds number per foot = 6.2 × 10^6), α = 0°.

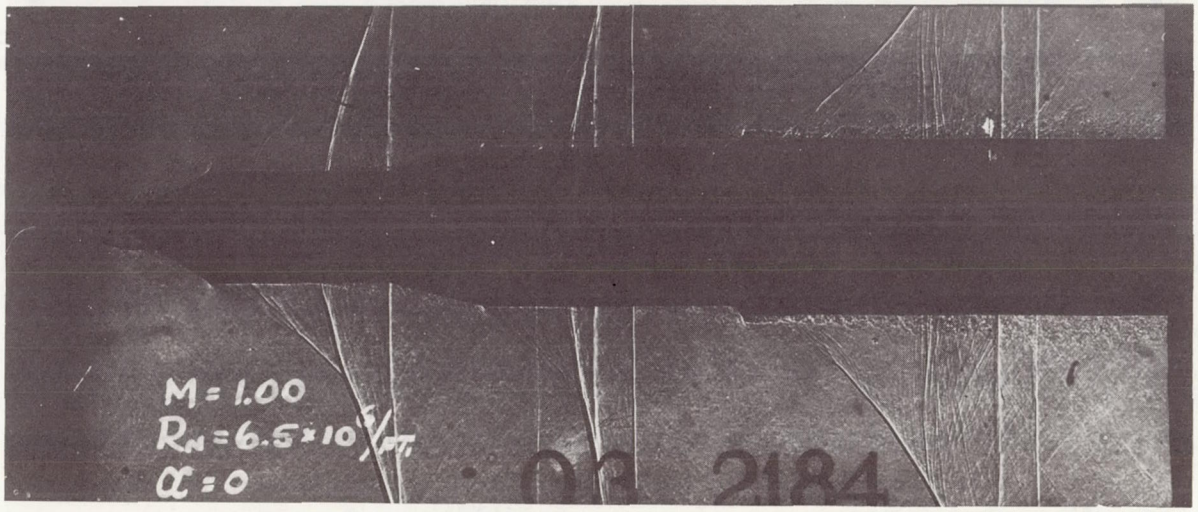

(b) M = 1.00, R ≈ 0.810 × 10^6 (Reynolds number per foot = 6.5 × 10^6), α = 0°.

L-63-30

Figure 8.- Spark shadowgraphs of flow around a 0.0068-size model of a large manned launch vehicle.

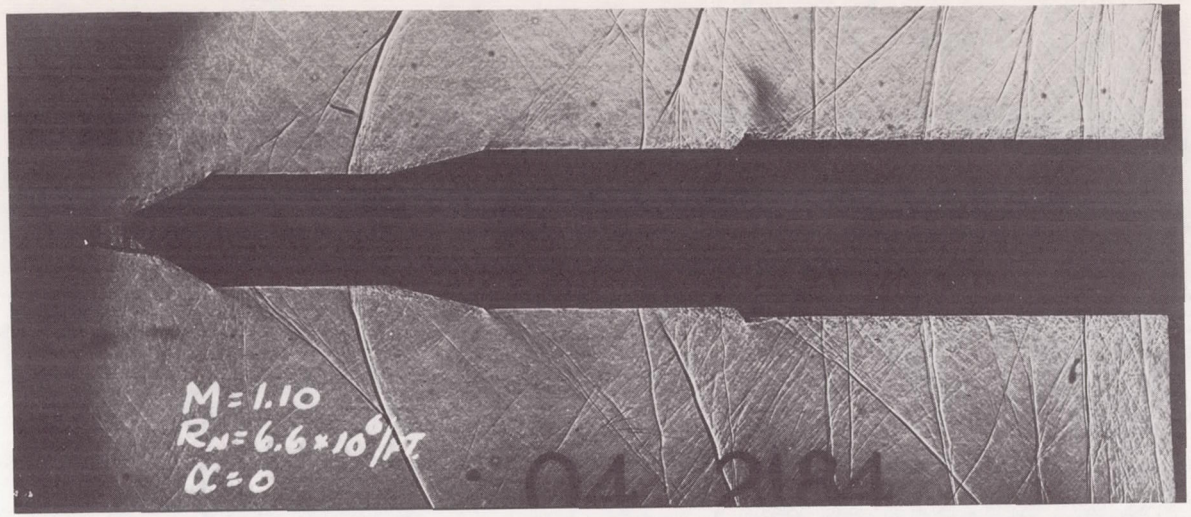

(c) M = 1.10, $R \approx 0.823 \times 10^6$ (Reynolds number per foot = 6.6×10^6), $\alpha = 0^\circ$.

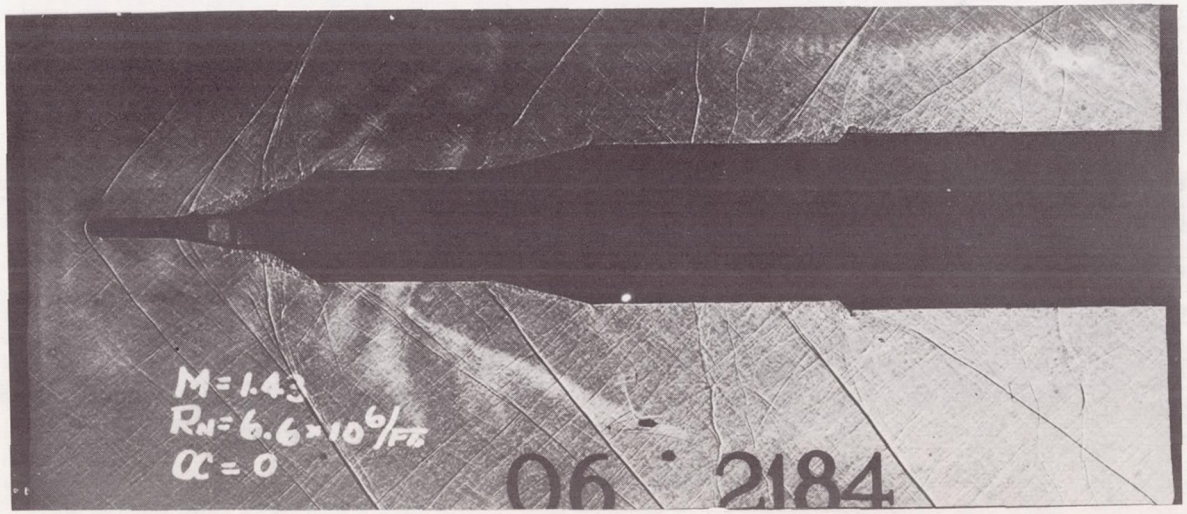

(d) M = 1.43, $R \approx 0.823 \times 10^6$ (Reynolds number per foot = 6.6×10^6), $\alpha = 0^\circ$. L-63-31

Figure 8.- Concluded.

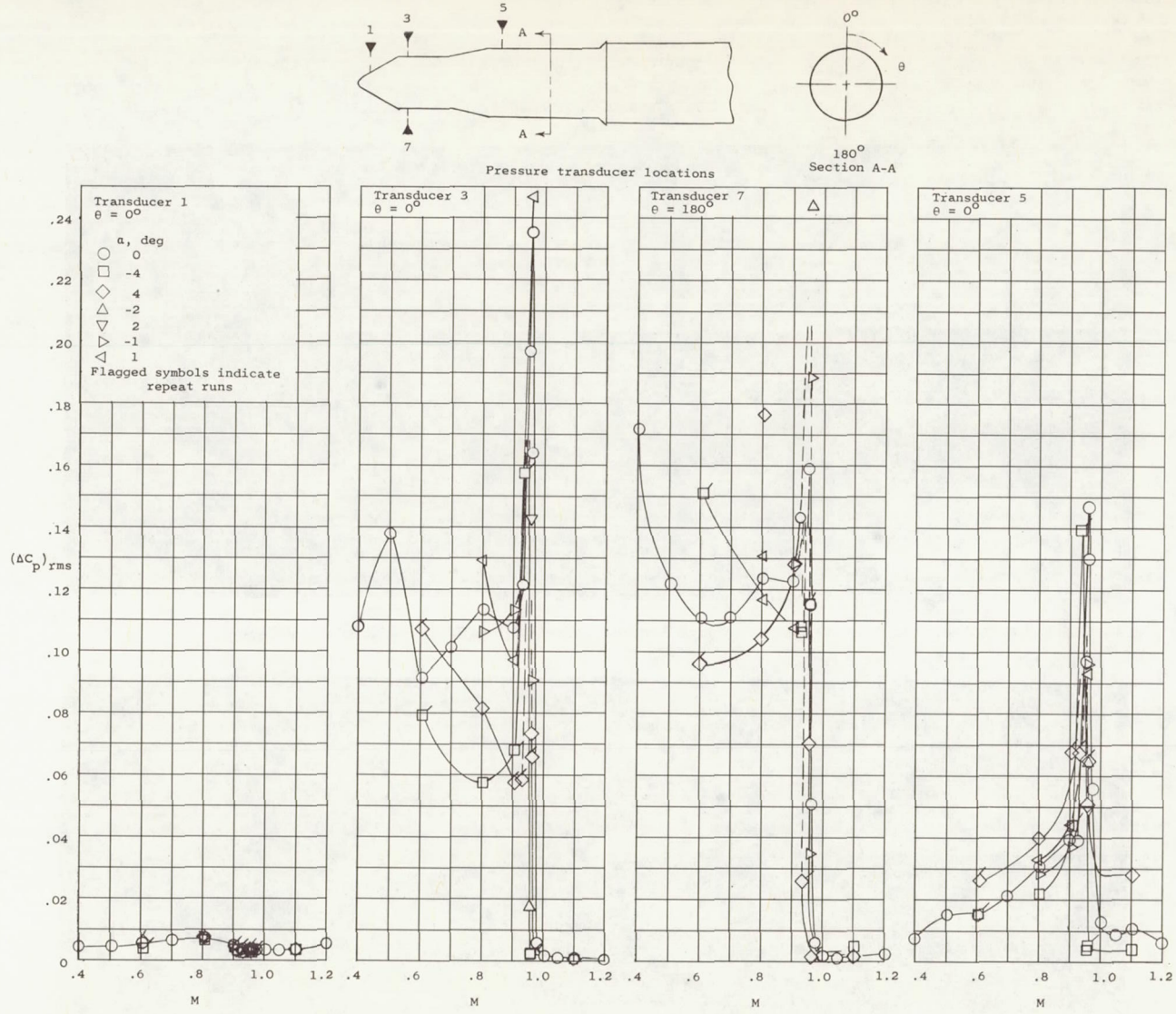

(a) Model without tower.

Figure 9.- Variation of fluctuating pressure coefficients with Mach number for several configurations and angles of attack on 8-percent rigid model in Freon at $R \approx 4.5 \times 10^6$.

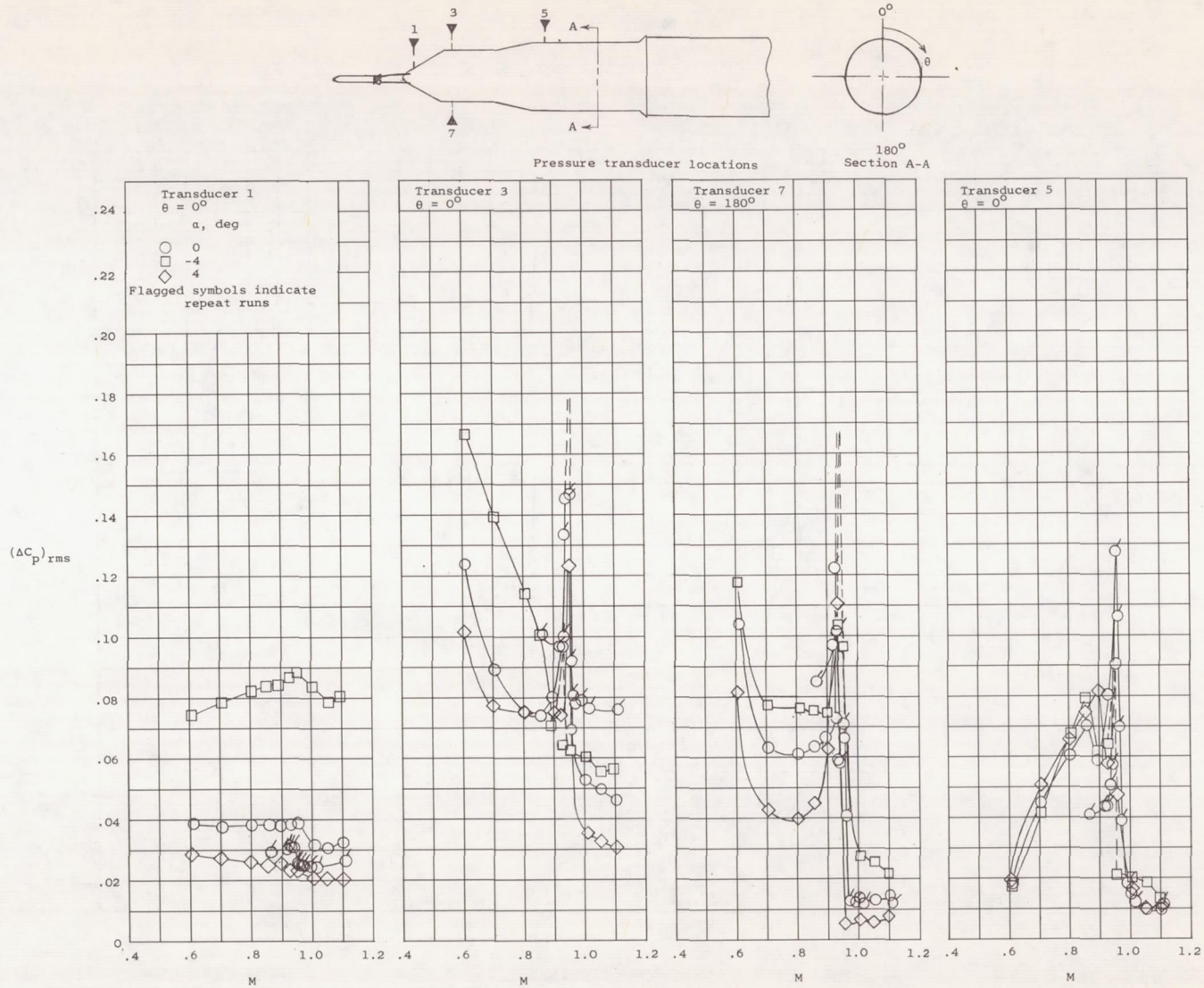

(b) Tower configuration 1.

Figure 9.- Continued.

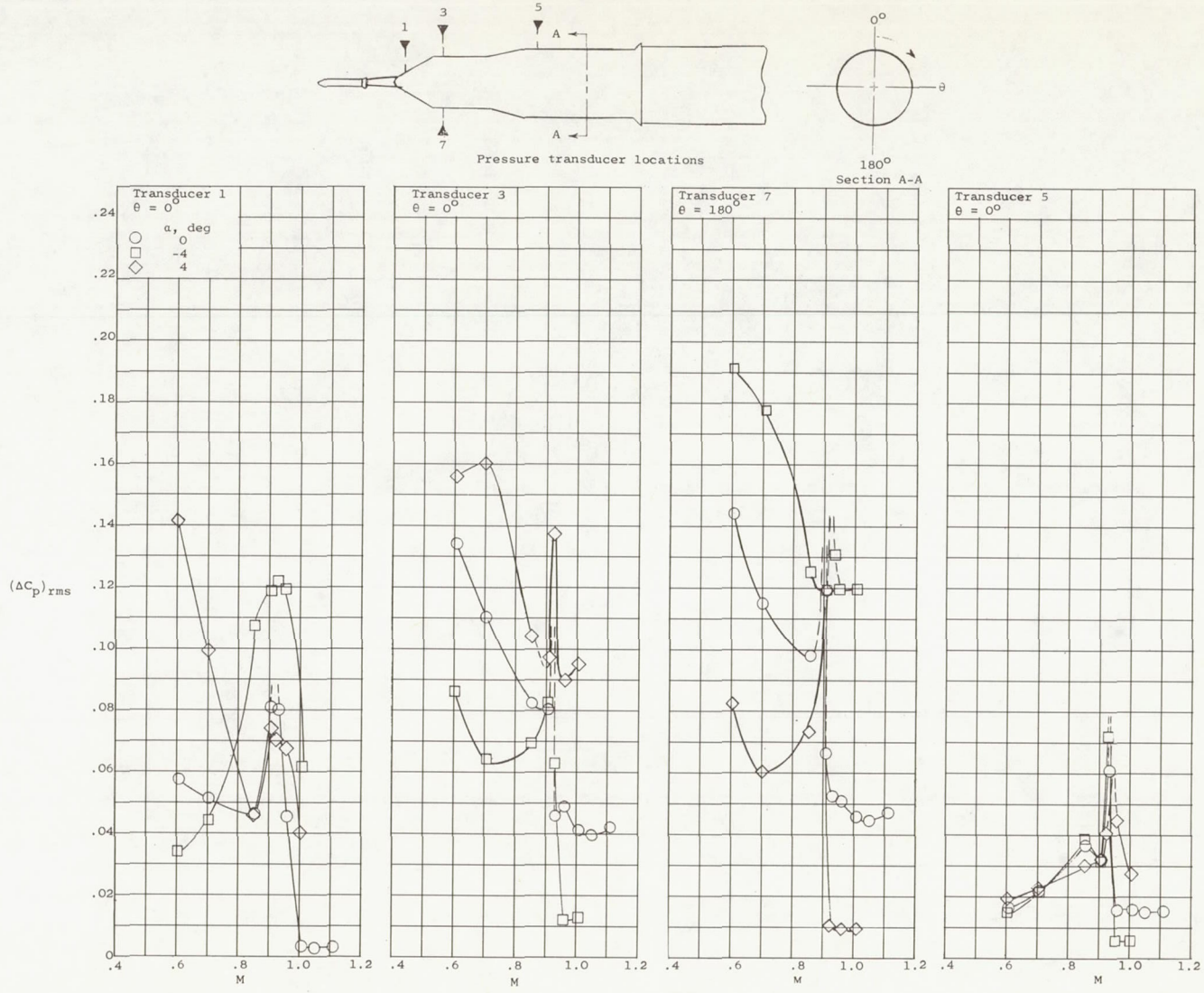

(c) Tower configuration 2.

Figure 9.- Continued.

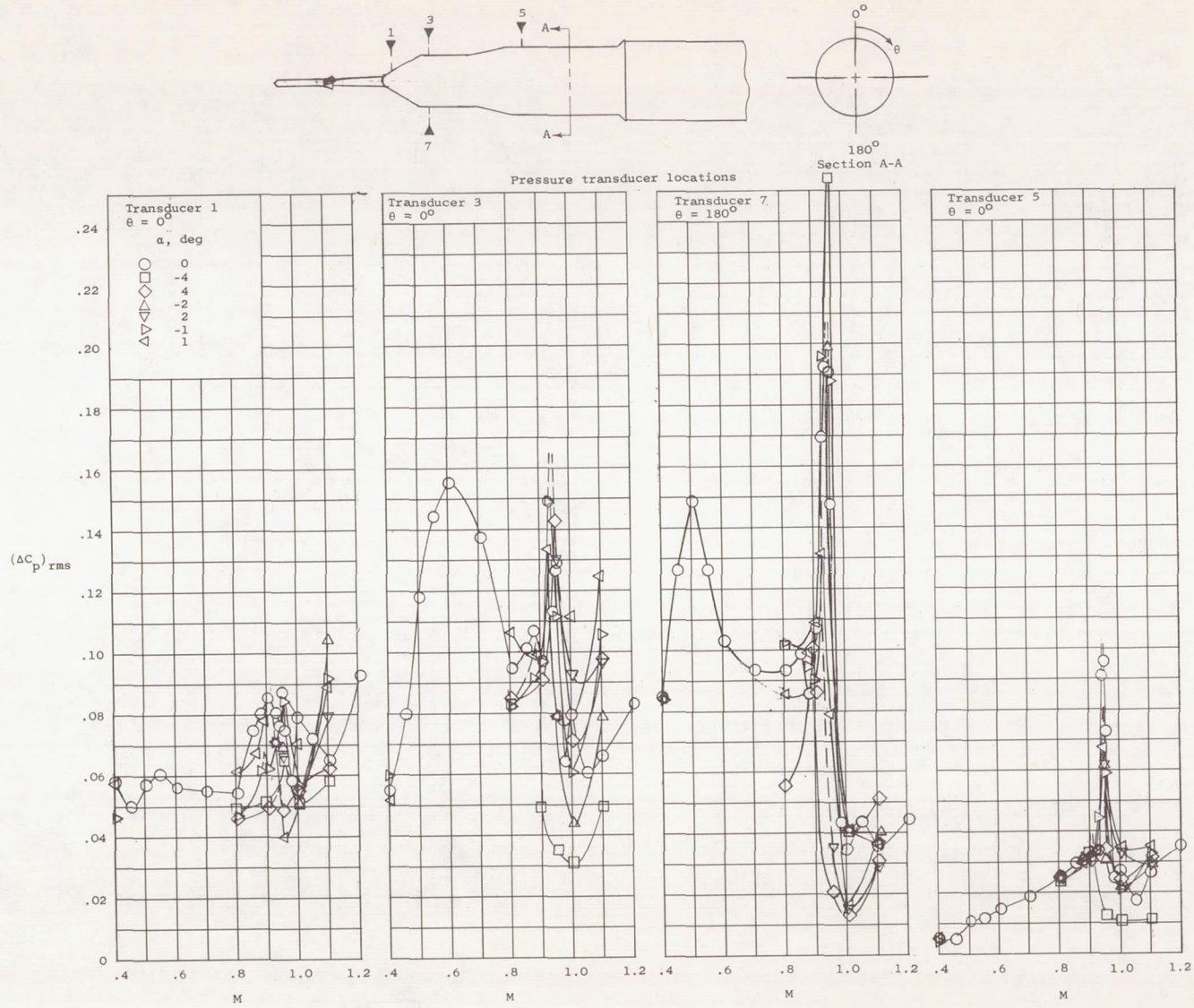

(d) Tower configuration 3.

Figure 9.- Continued.

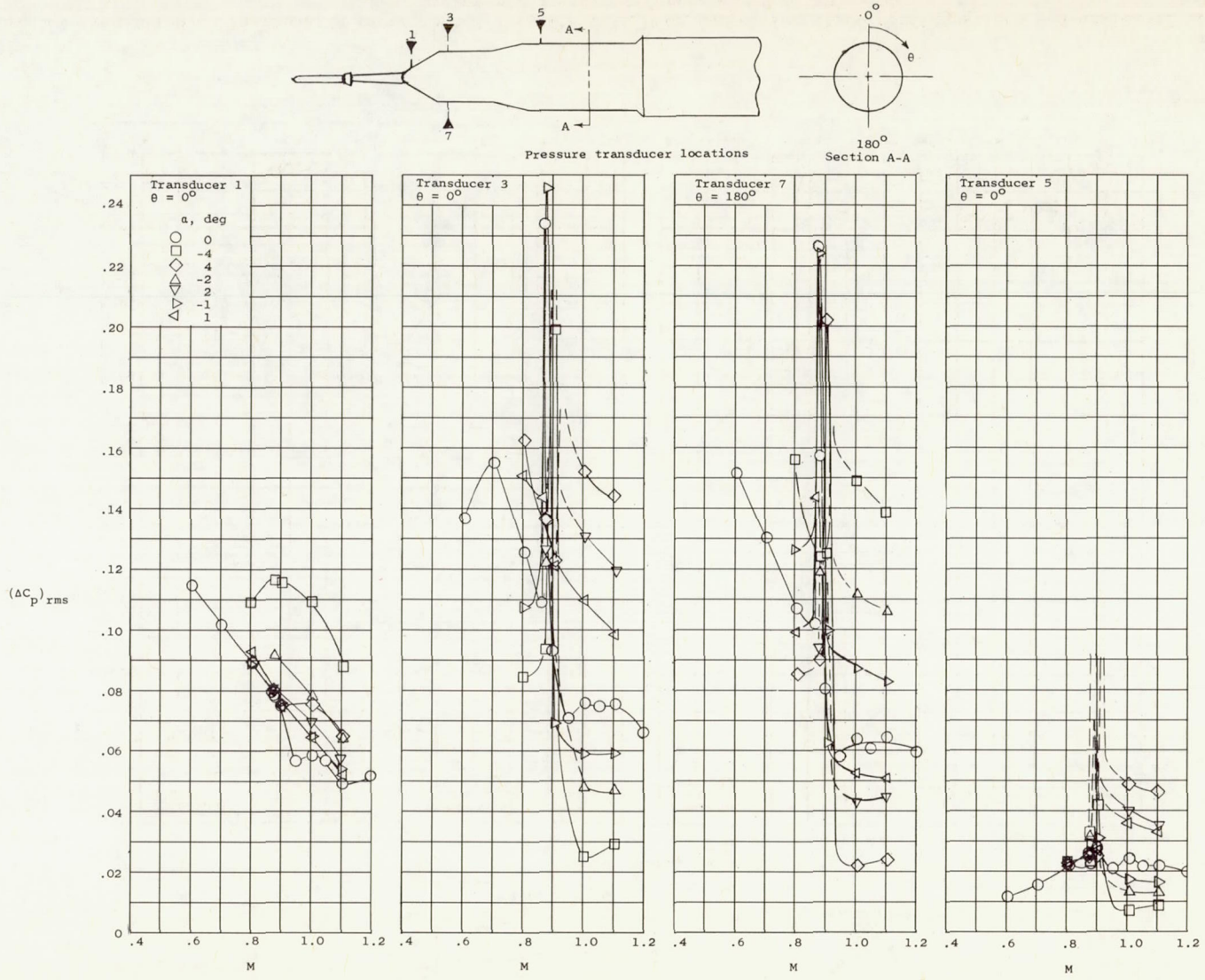

(e) Tower configuration 4.

Figure 9.- Concluded.

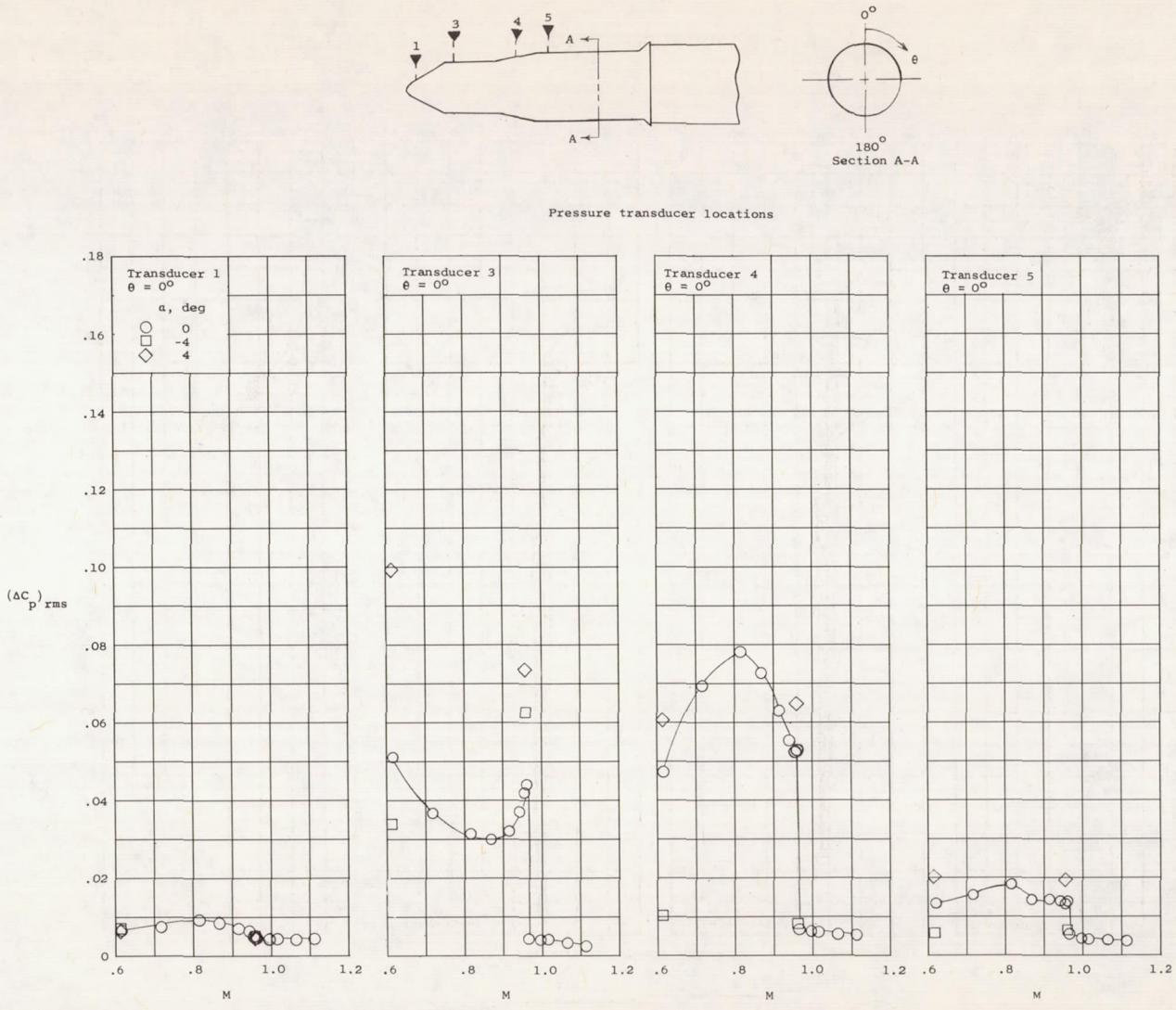

(a) Model without tower.

Figure 10.- Variation of fluctuating pressure coefficients with Mach number for three configurations and angles of attack on 1.6-percent rigid model in Freon at $R \approx 1.0 \times 10^6$.

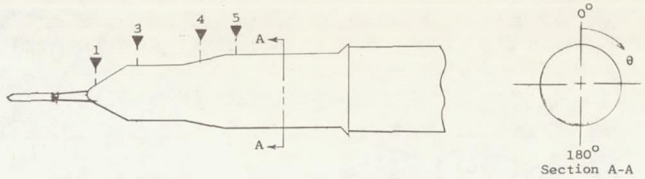

Pressure transducer locations

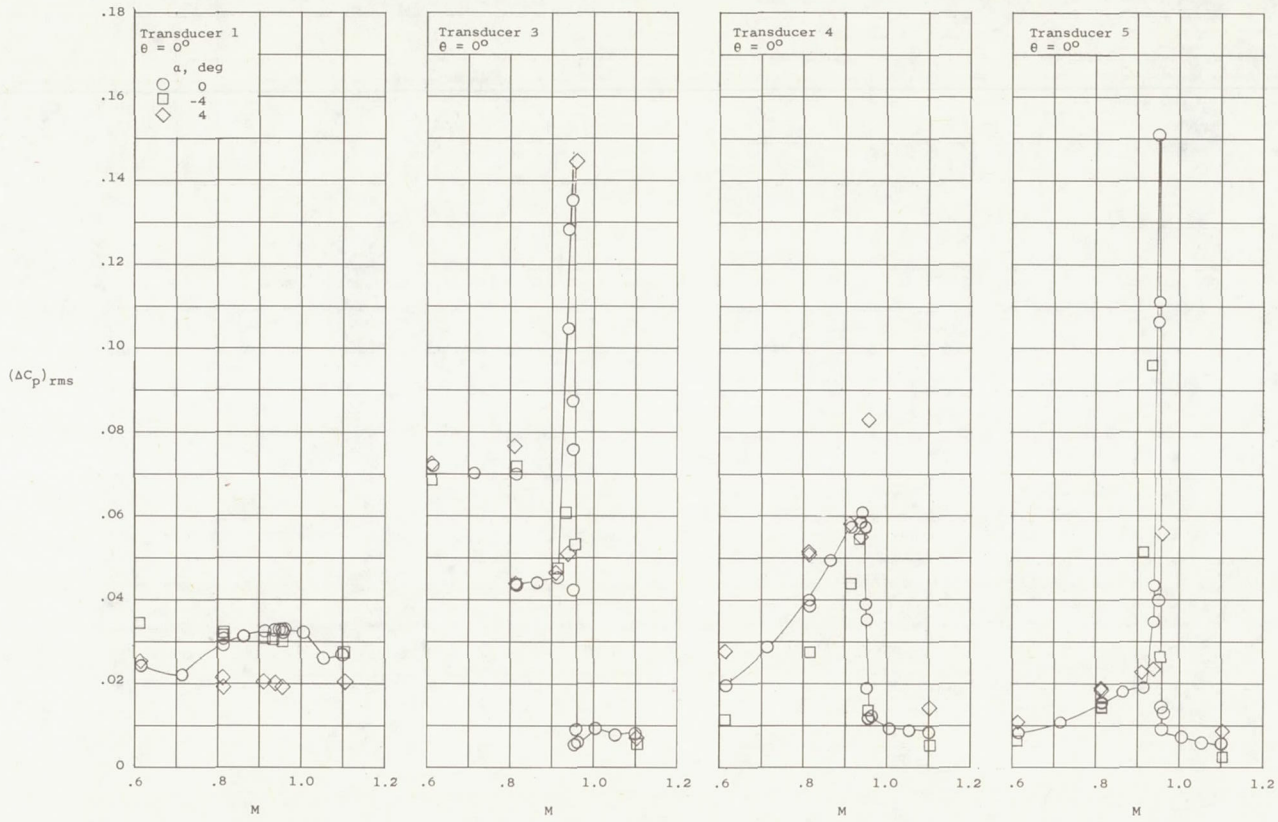

(b) Tower configuration 1.

Figure 10.- Continued.

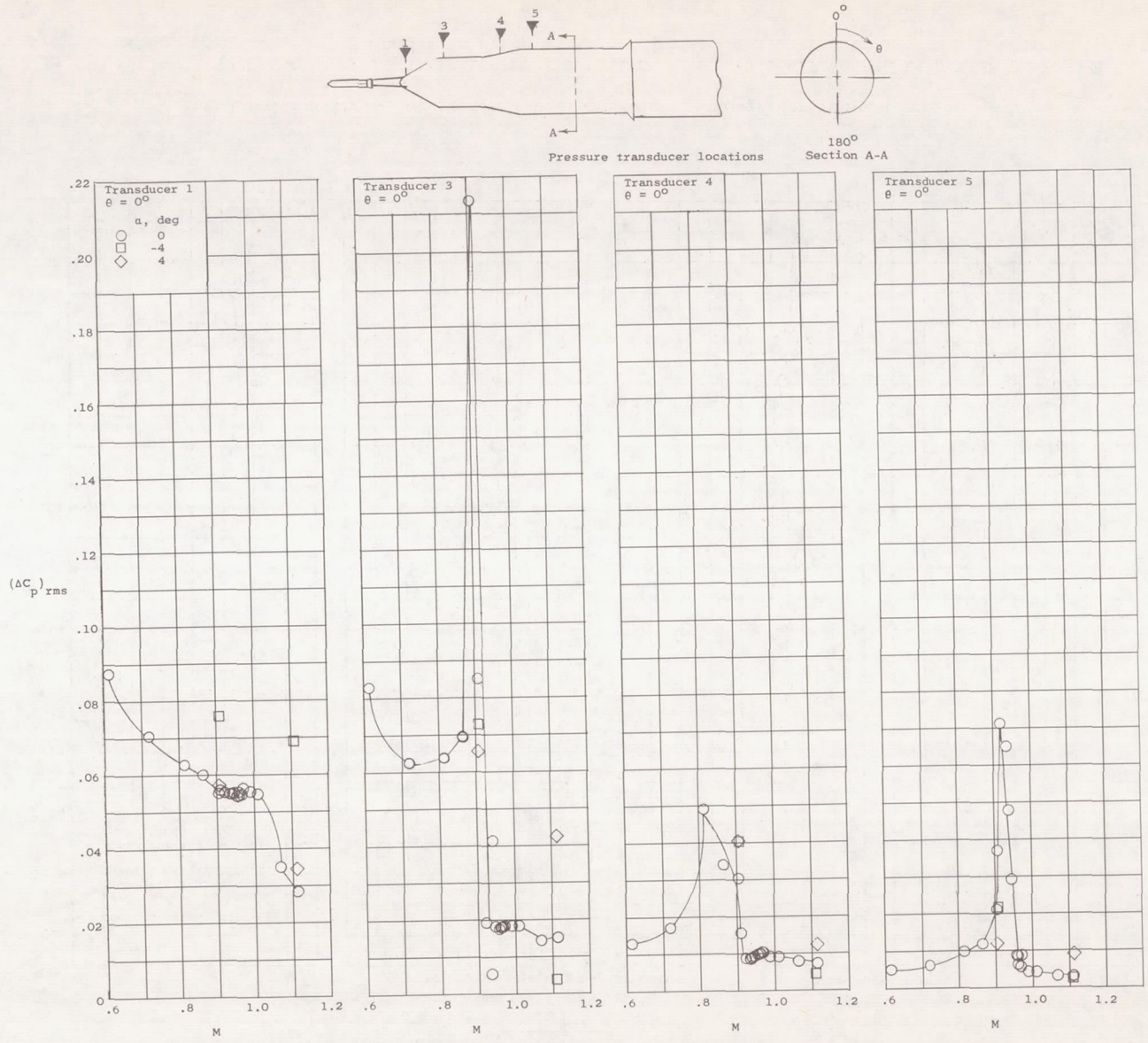

(c) Tower configuration 2.

Figure 10.- Concluded.

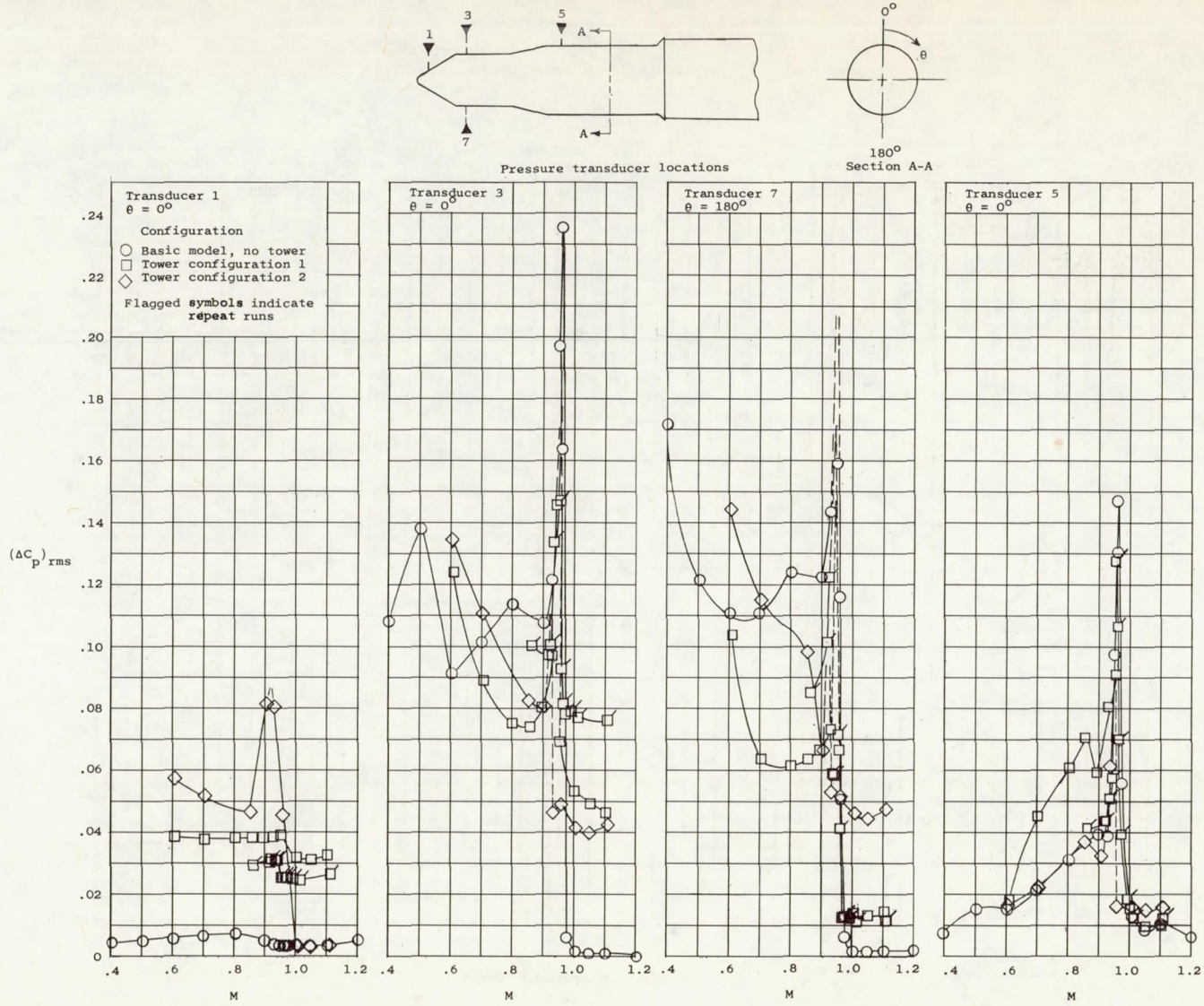

(a) Model without tower; tower configuration 1; tower configuration 2.

Figure 11.- Effect of tower configurations on variation of fluctuating pressure coefficients with Mach number on 8-percent rigid model in Freon at $\alpha = 0^{\circ}$; $R \approx 4.5 \times 10^{6}$.

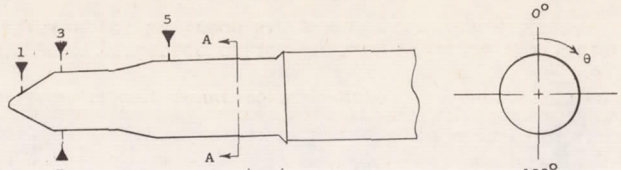

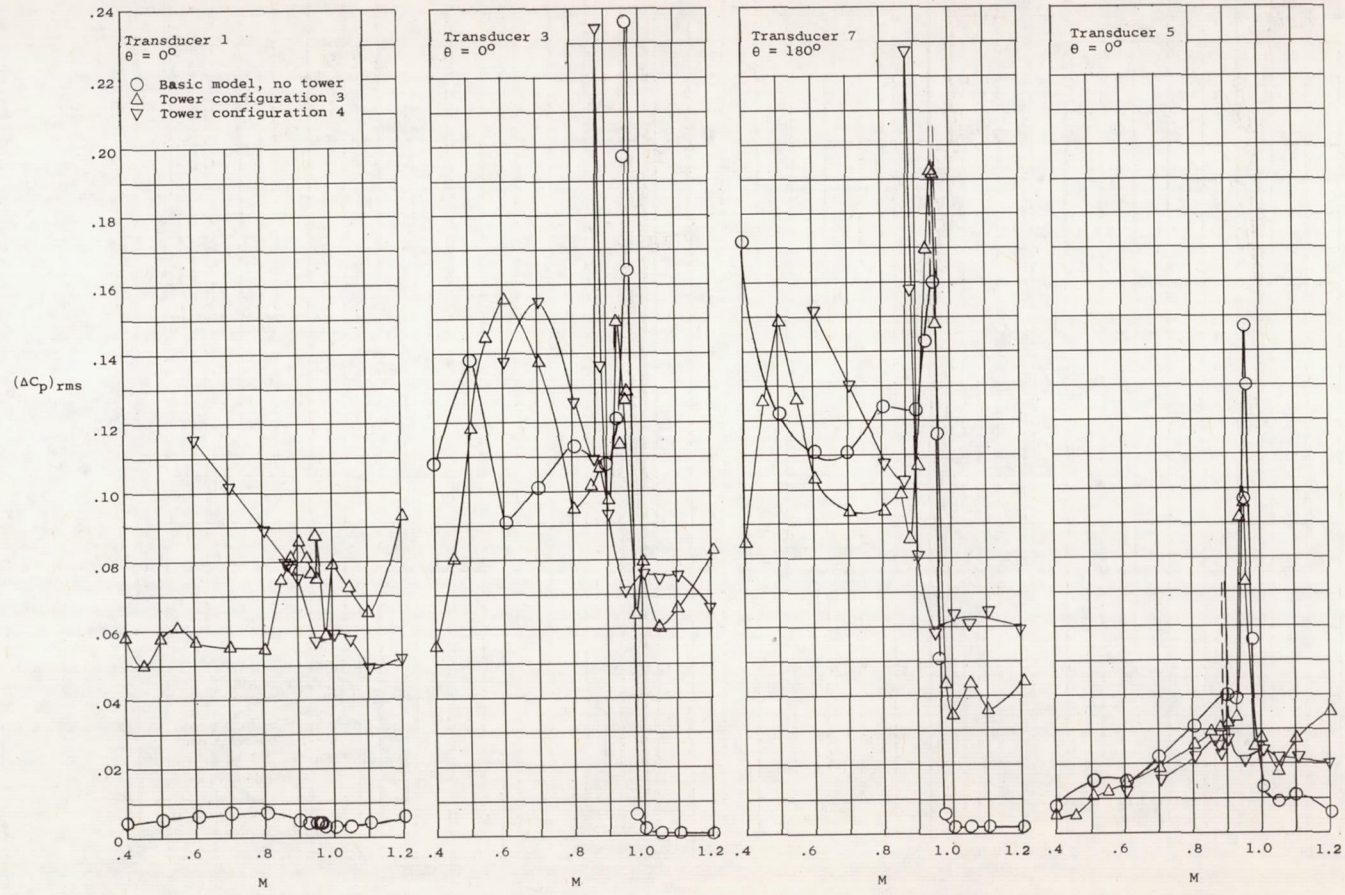

(b) Model without tower; tower configuration 3; tower configuration 4.

Figure 11.- Concluded.

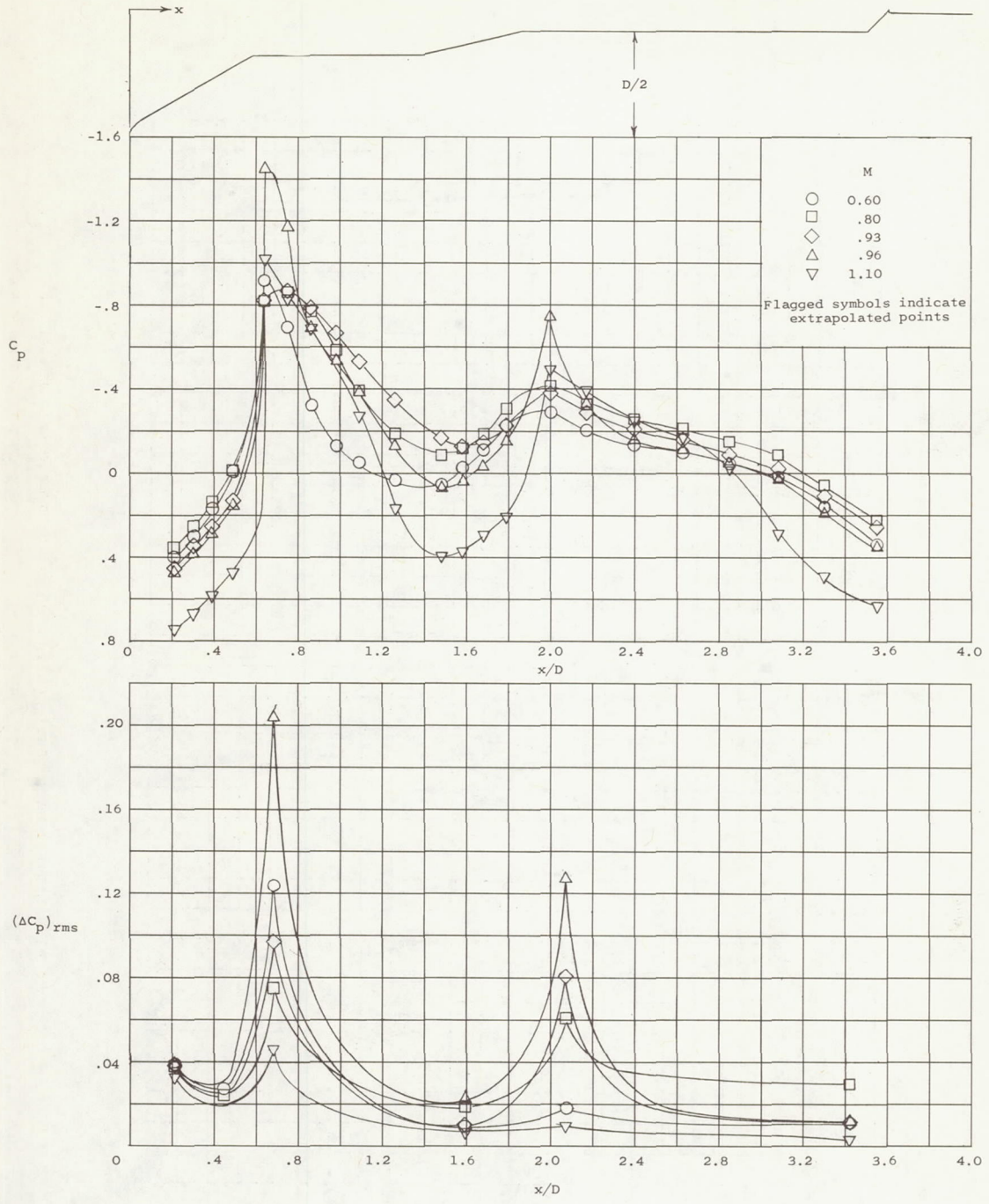

(a) $\alpha = 0^{\circ}$.

Figure 12.- Axial distributions of static and fluctuating pressure coefficients at several Mach numbers and angles of attack on 8-percent rigid model with tower configuration 1 in Freon at $R \approx 4.5 \times 10^6$.

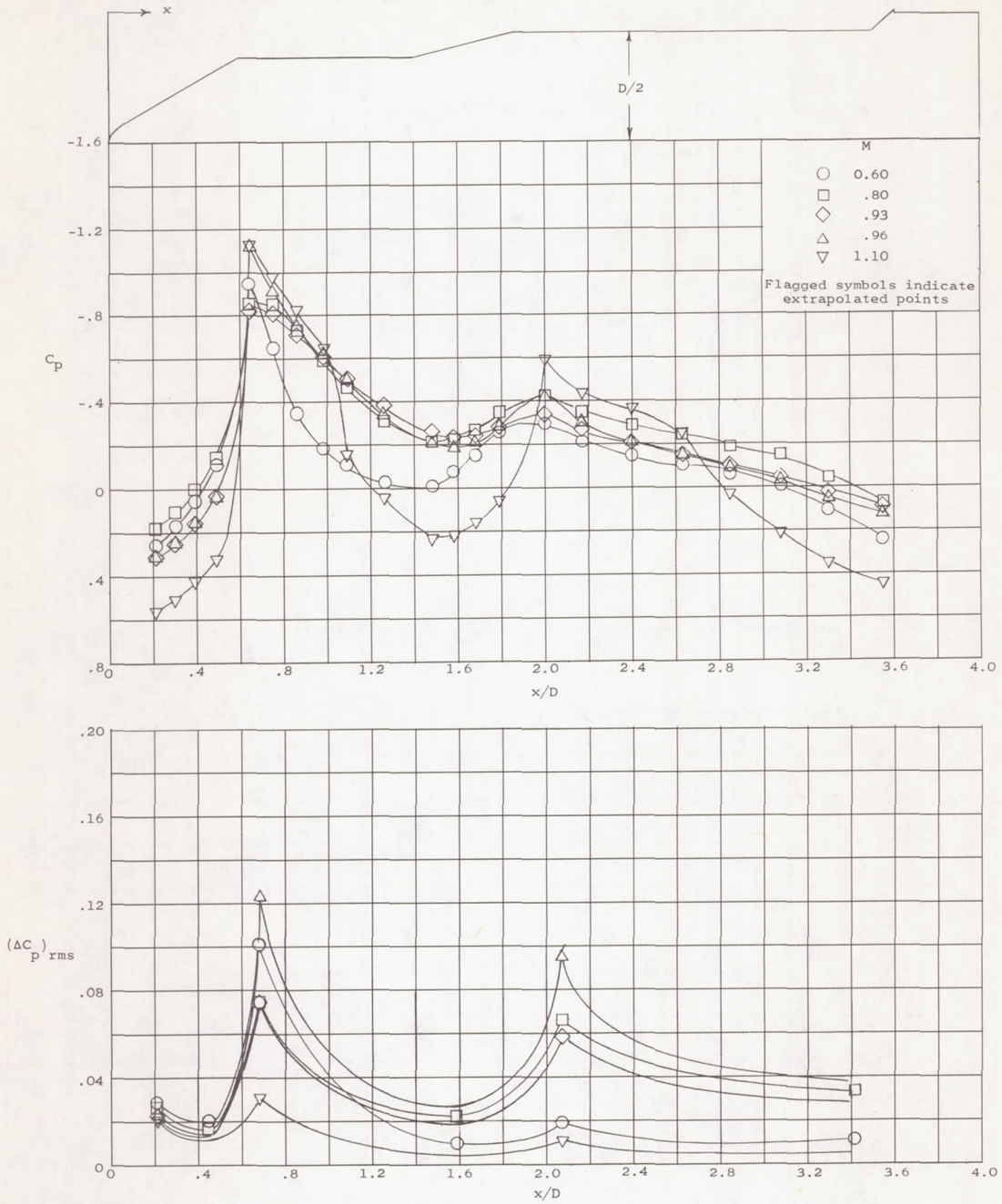

(b) $\alpha = -4^{\circ}$.

Figure 12.- Continued.

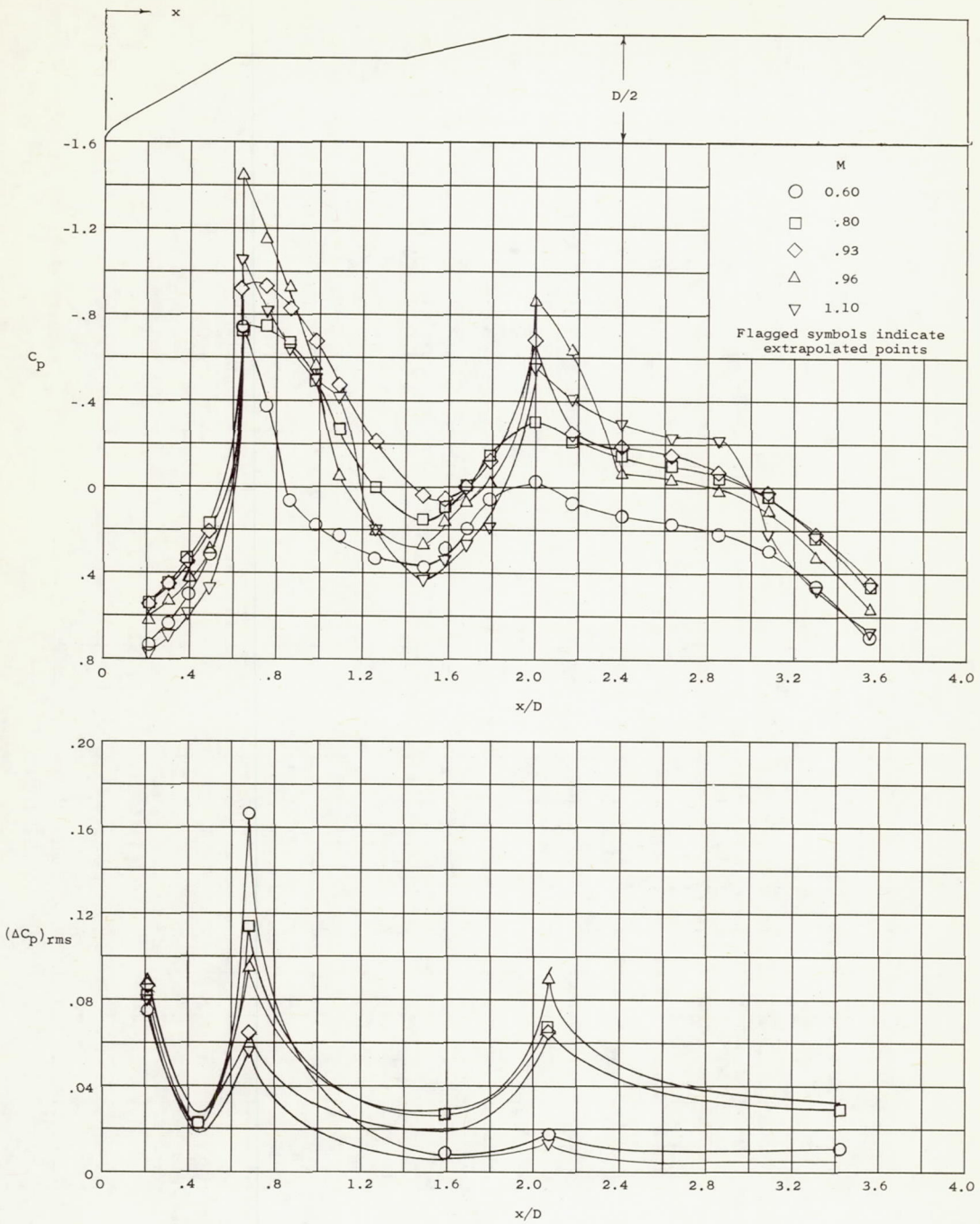

(c) $\alpha = 4^{\circ}$.

Figure 12.- Concluded.

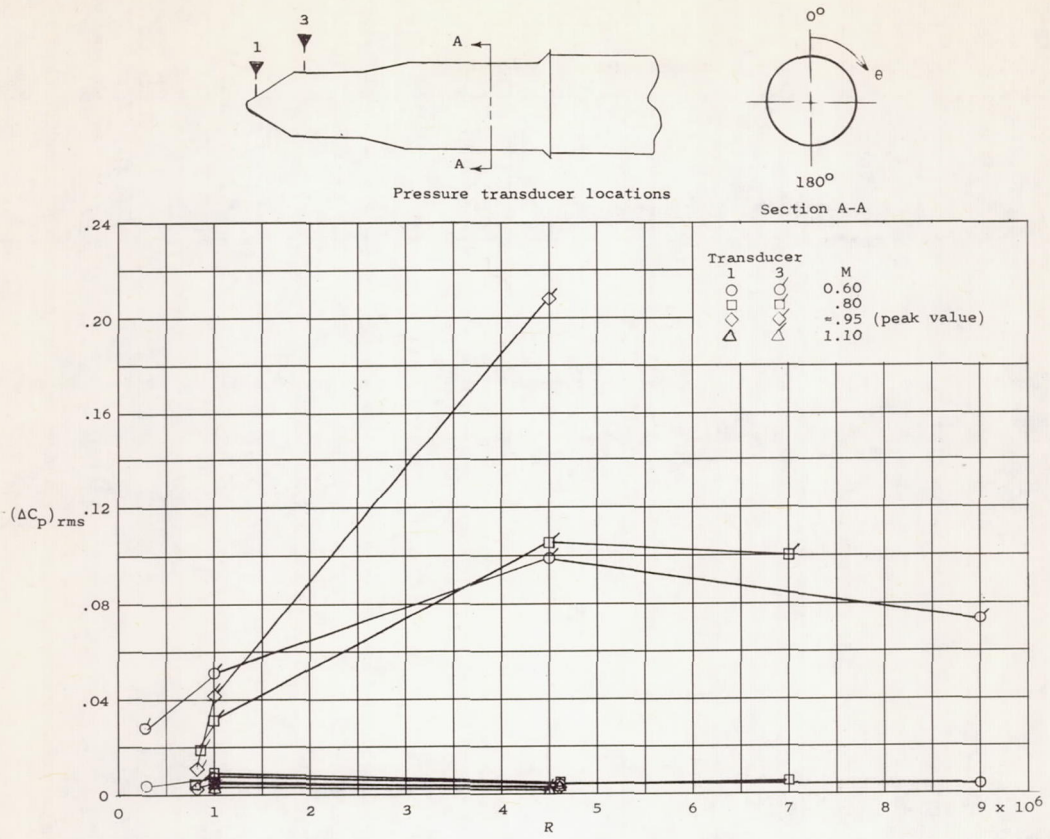

(a) Model without tower.

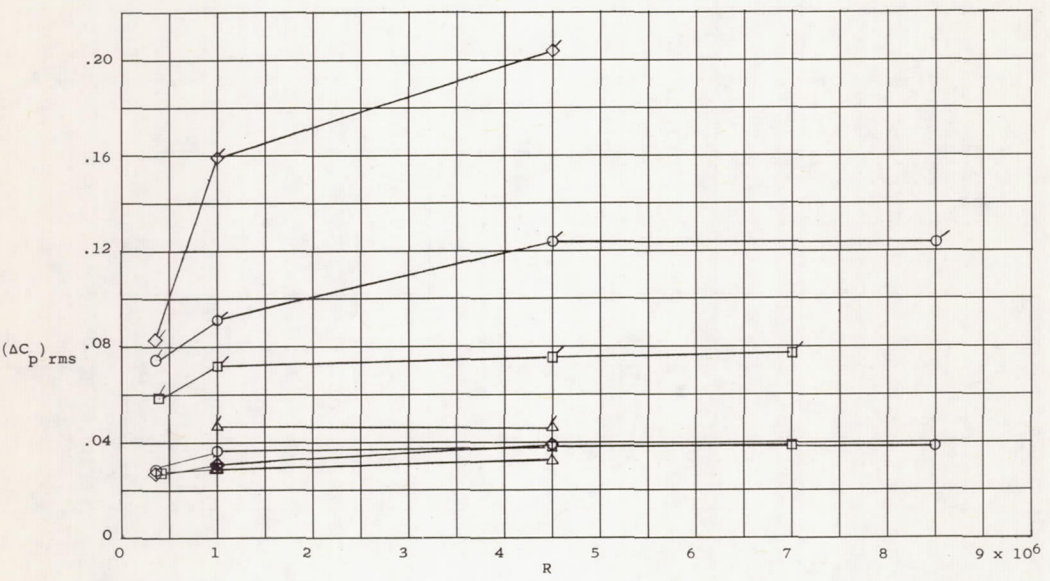

(b) Tower configuration 1.

Figure 13.- Variation of fluctuating pressure coefficients with Reynolds number at constant Mach numbers for two transducer locations at $\alpha = 0^\circ$.

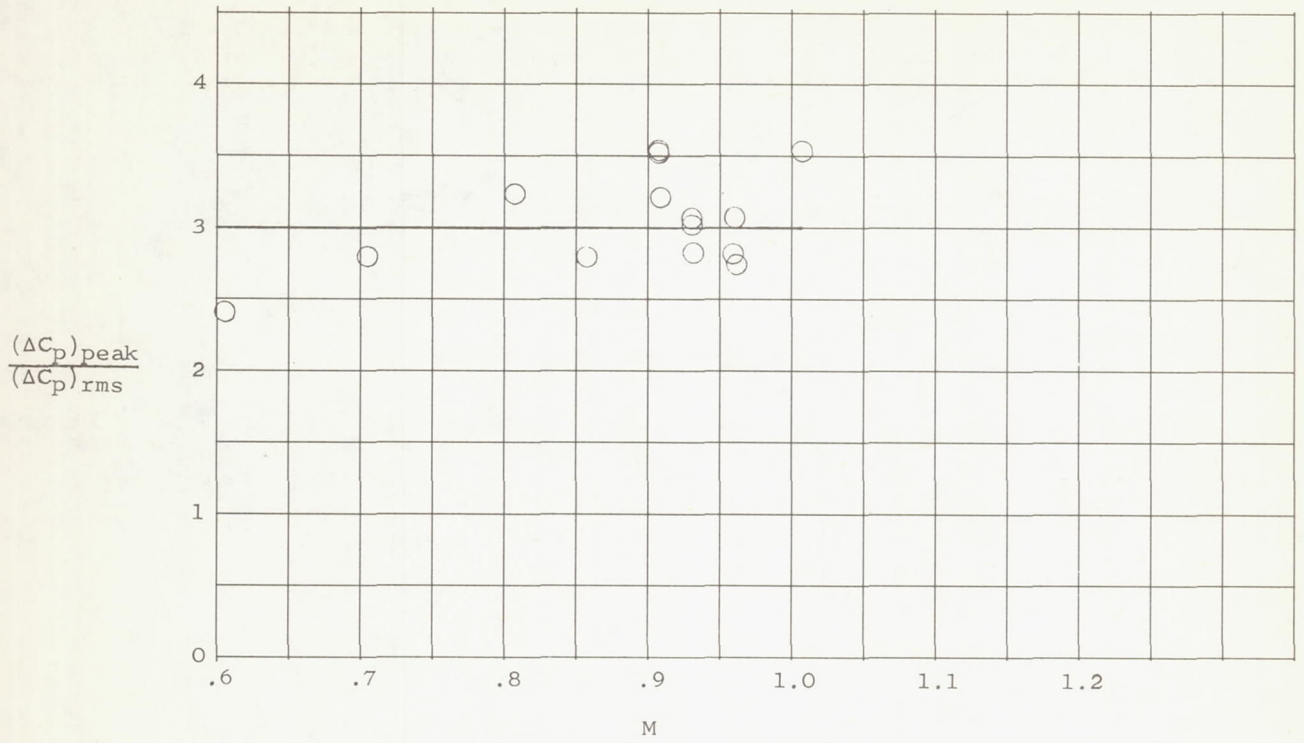

(a) 8-percent model without tower; transducer 1.

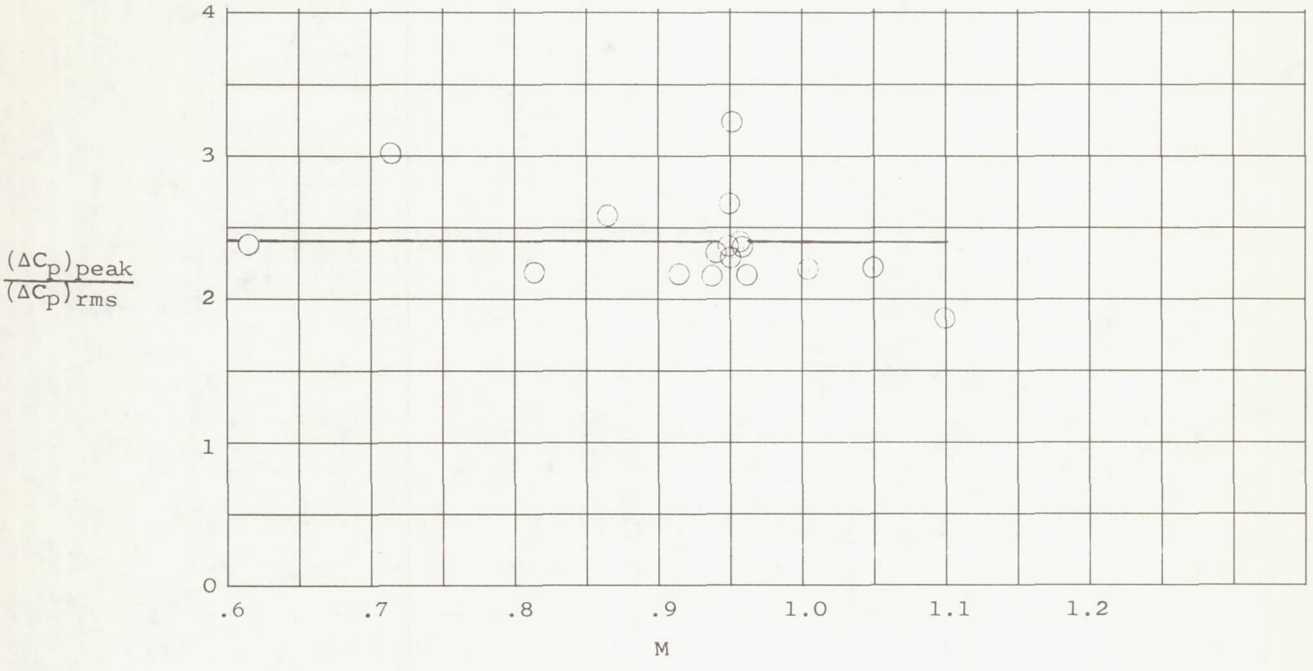

(b) 1.6-percent model with tower configuration 1; transducer 1.

Figure 14.- Typical ratios of the peak pressure fluctuations to root-mean-square pressure fluctuations for several data samples plotted as a function of Mach number.

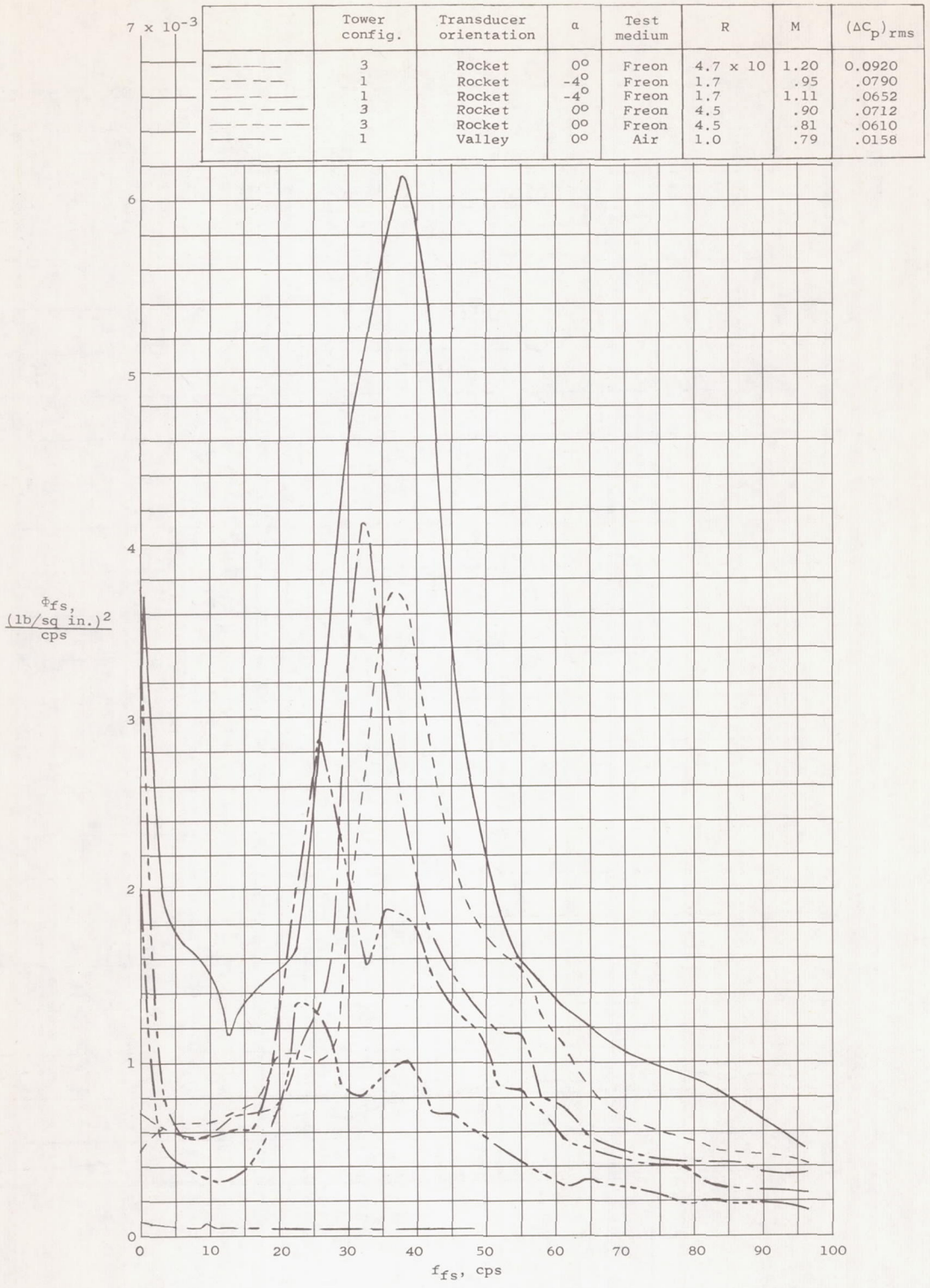

	Tower config.	Transducer orientation	α	Test medium	R	M	$(\Delta C_p)_{rms}$
———	3	Rocket	0°	Freon	4.7 x 10	1.20	0.0920
— — — —	1	Rocket	-4°	Freon	1.7	.95	.0790
— — — —	1	Rocket	-4°	Freon	1.7	1.11	.0652
———	3	Rocket	0°	Freon	4.5	.90	.0712
— — — —	3	Rocket	0°	Freon	4.5	.81	.0610
— — —	1	Valley	0°	Air	1.0	.79	.0158

(a) Power spectral densities of fluctuating pressures on nose of 8-percent model. Transducer 1.

Figure 15.- Power spectral densities of fluctuating pressures measured on model and scaled to full-size vehicle.

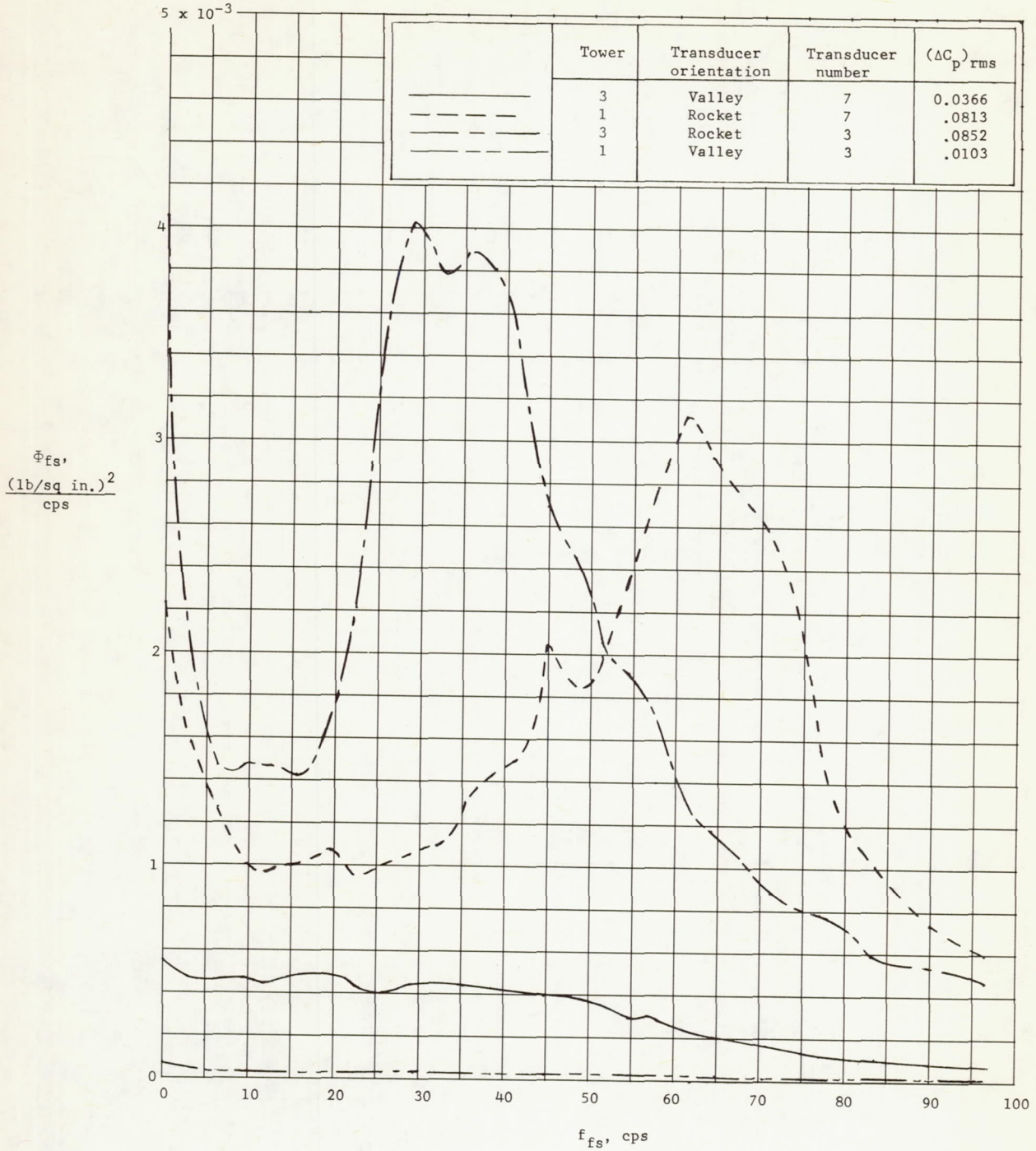

(b) Power spectral densities measured on first cone-cylinder shoulder of 8-percent model in Freon at supersonic Mach numbers. $M \approx 1.1$; $R \approx 4.5 \times 10^6$; $\alpha = 0^\circ$.

Figure 15.- Continued.

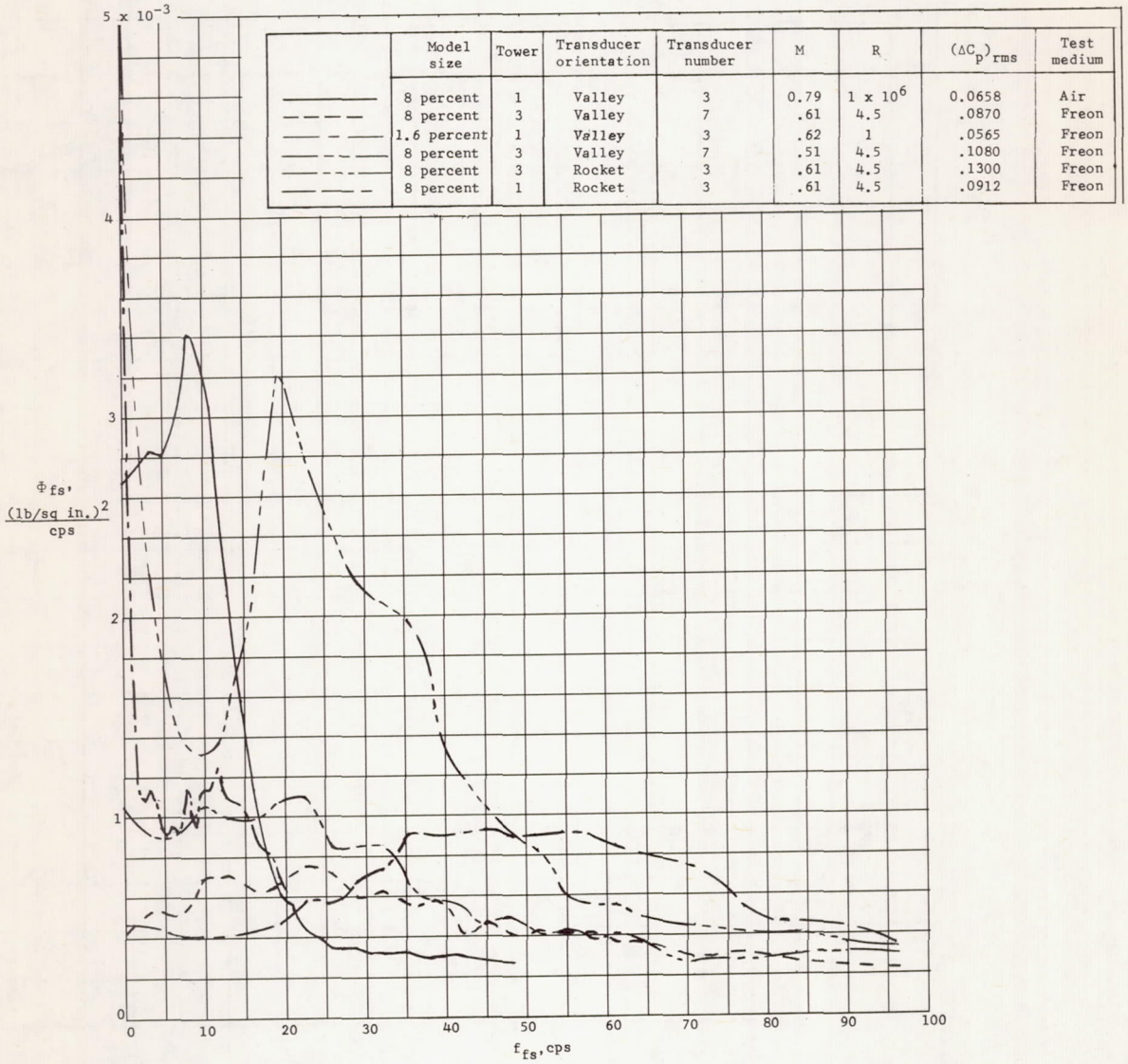

(c) Power spectral densities of fluctuating pressures on first cone-cylinder shoulder at subsonic Mach numbers. $\alpha = 0^{\circ}$.

Figure 15.- Continued.

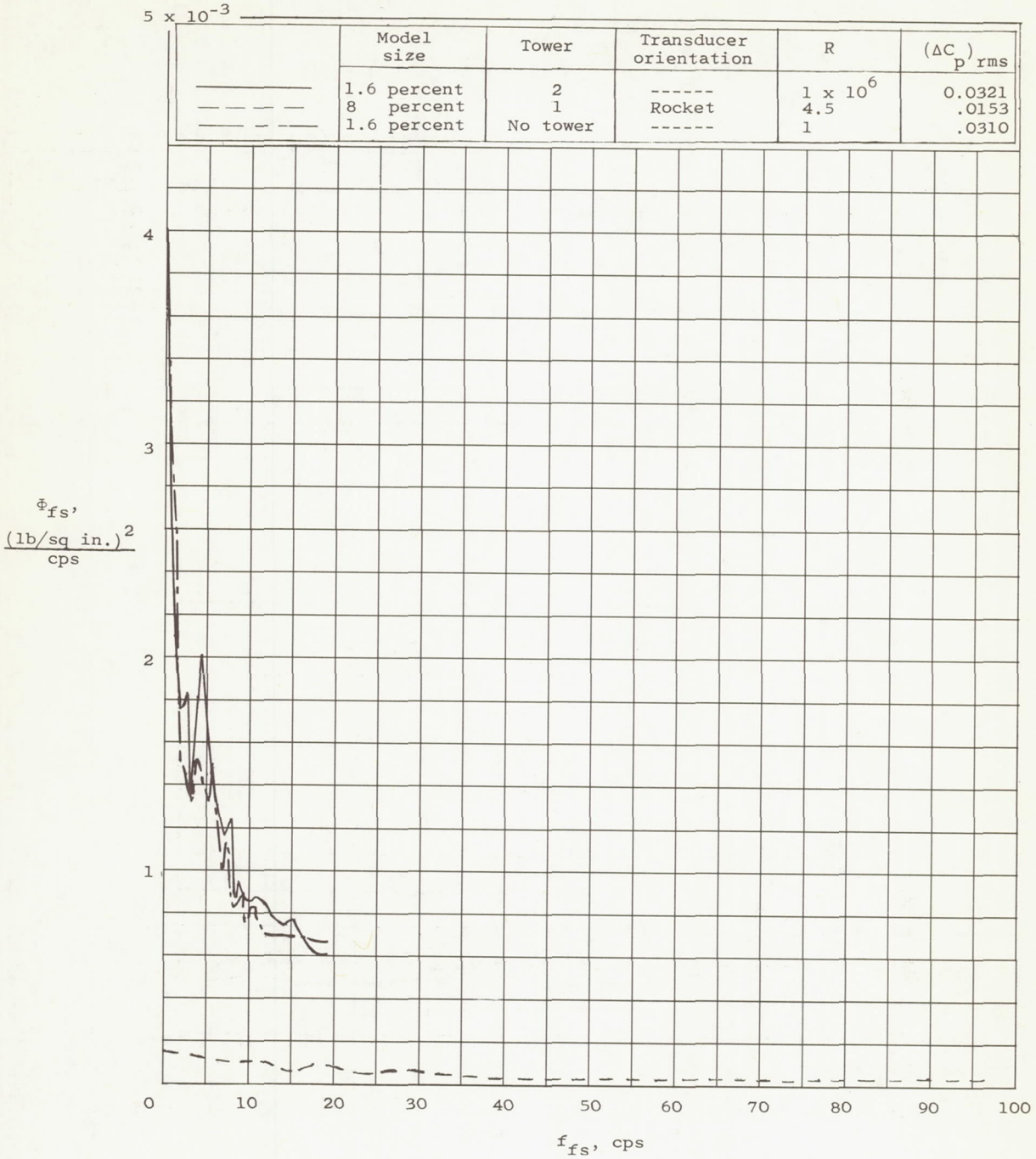

(d) Power spectral densities of fluctuating pressures on rear of second stage of multistage model in Freon at supersonic Mach numbers. Transducer 6; M = 1.1; $\alpha = 0^{\circ}$.

Figure 15.- Concluded.

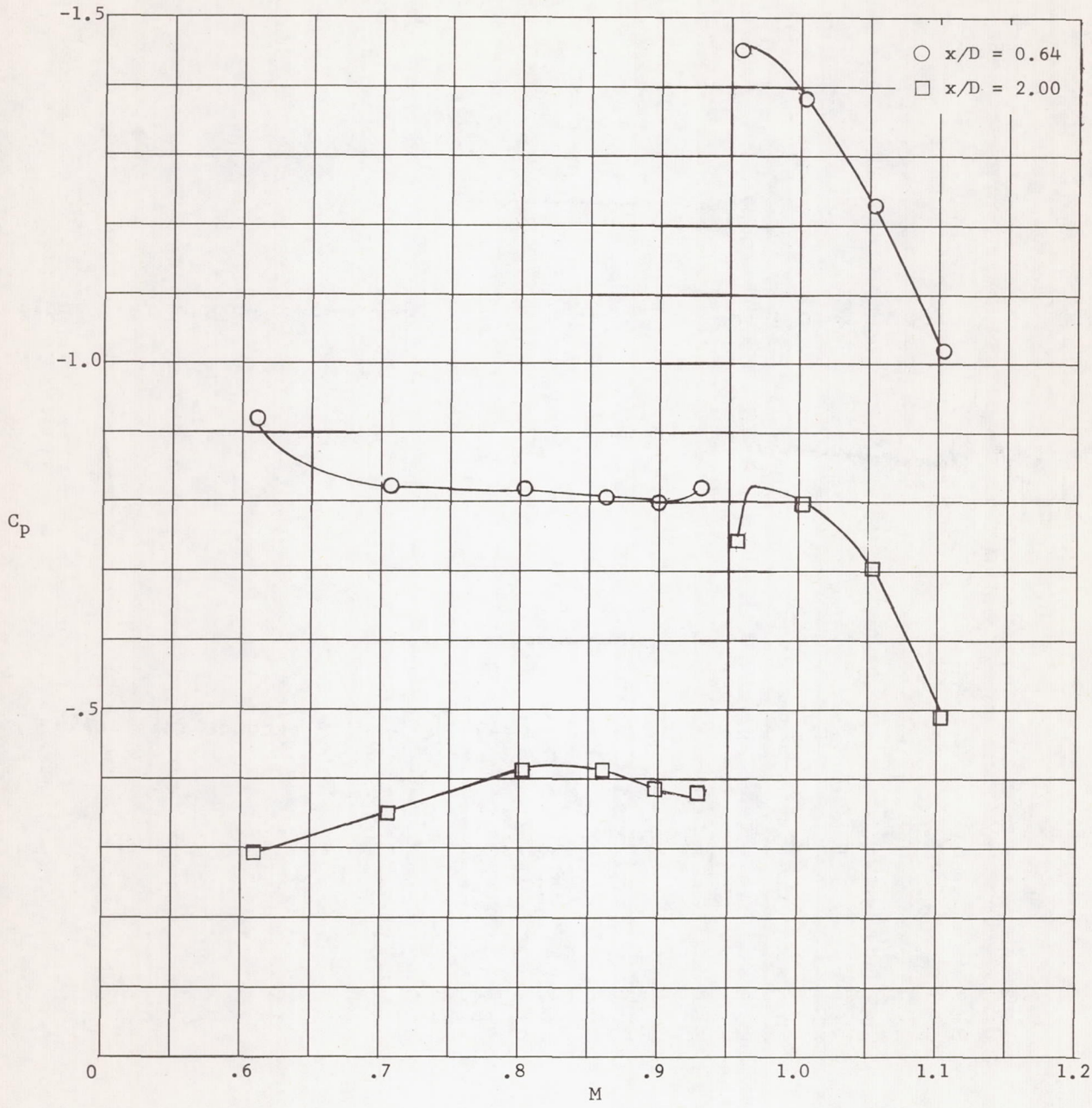

Figure 16.- Variation with Mach number of static pressure coefficients at first and second shoulders of 8-percent model with tower in Freon. Configuration 1; $\alpha = 0^{o}$; $R \approx 4.5 \times 10^{6}$.

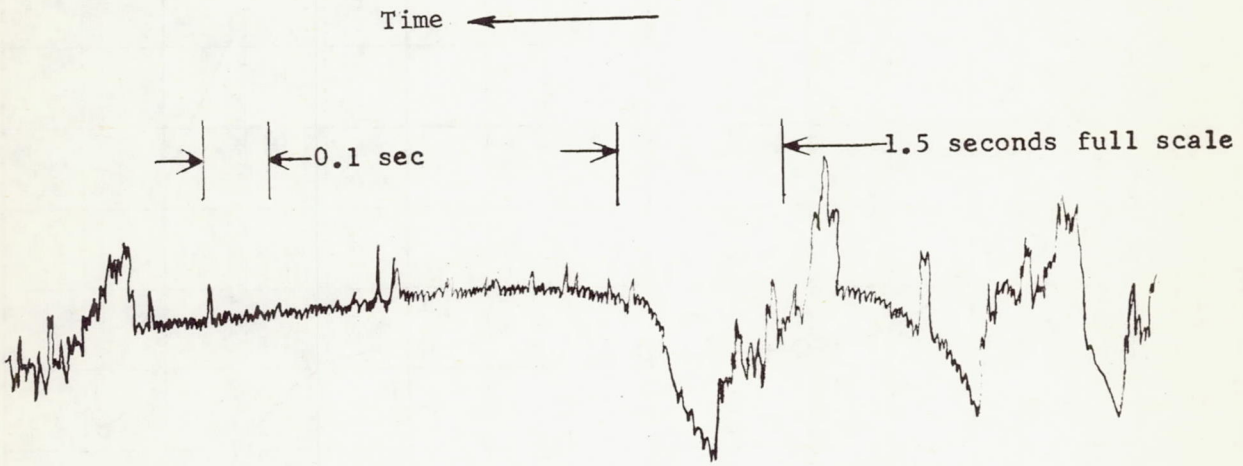

(a) 8-percent model in Freon.

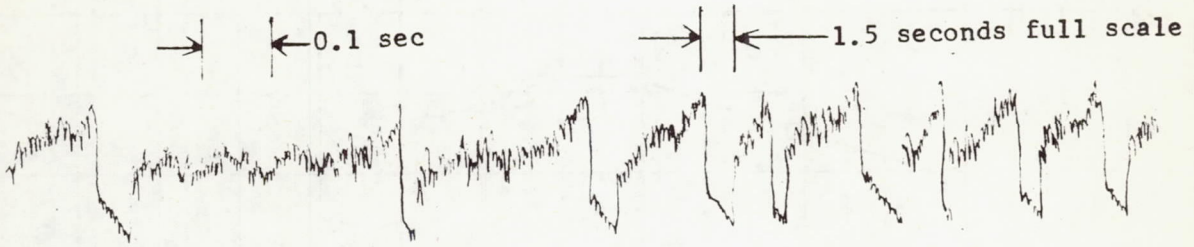

(b) 1.6-percent model in Freon.

Figure 17.- Tracings of typical oscillograph time histories of peak fluctuating pressures measured behind first shoulder. Transducer 3; $x/D = 0.68$ on rigid models. Tower configuration 1; $M = 0.95$; $R \approx 1.0 \times 10^6$; and $\alpha = 0^\circ$.

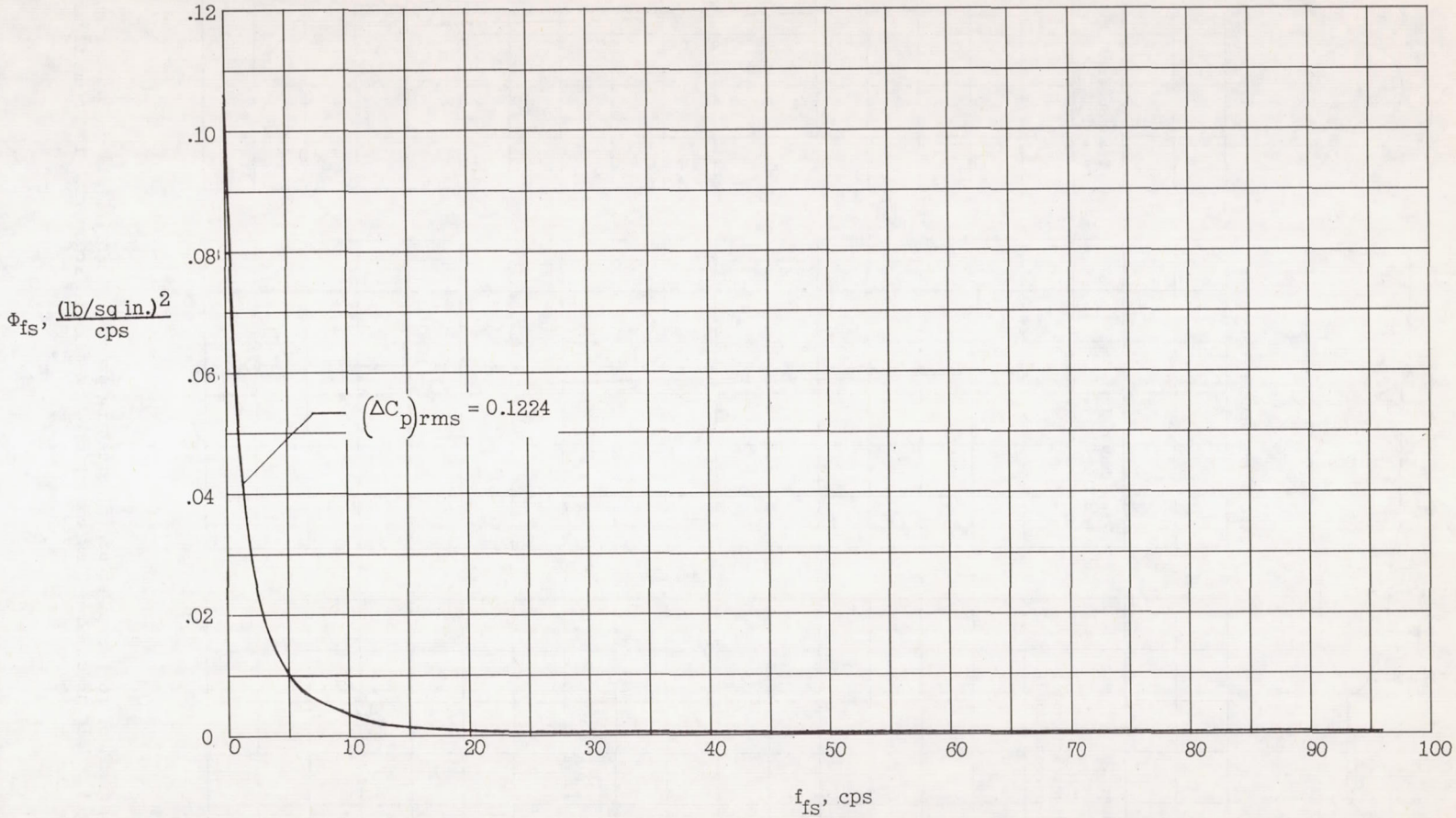

Figure 18.- Typical power spectral density of buffet pressures (corresponding to the peak in $(\Delta C_p)_{rms}$ data) measured at first shoulder of 8-percent model in Freon and scaled to full-size vehicle. Transducer 3; tower configuration 1; $R \approx 4.5 \times 10^6$; $M = 0.924$; and $\alpha = 0^o$.

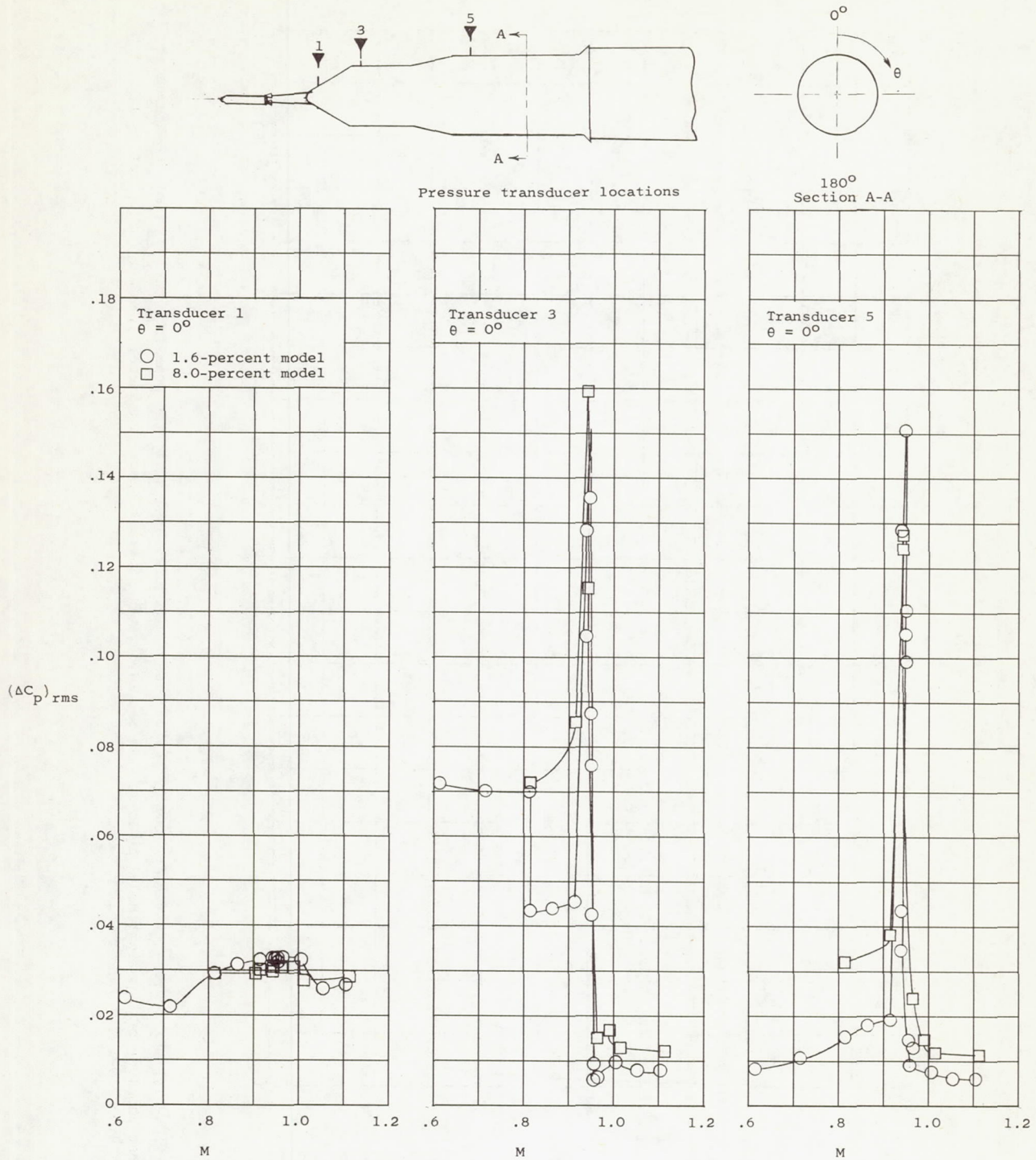

Figure 19.- Comparison of root-mean-square fluctuating pressure coefficients on 1.6-percent and 8-percent rigid models under same flow conditions. Models in Freon with tower configuration 1; $R \approx 1.0 \times 10^6$; and $\alpha = 0^\circ$.

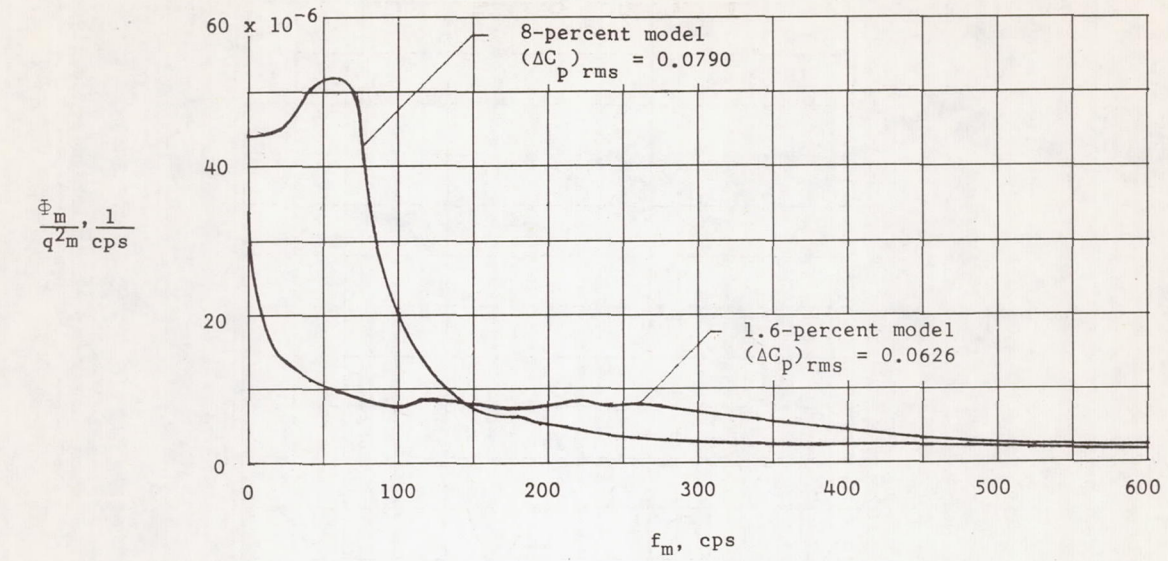

(a) Model power spectral density normalized by q_m^2.

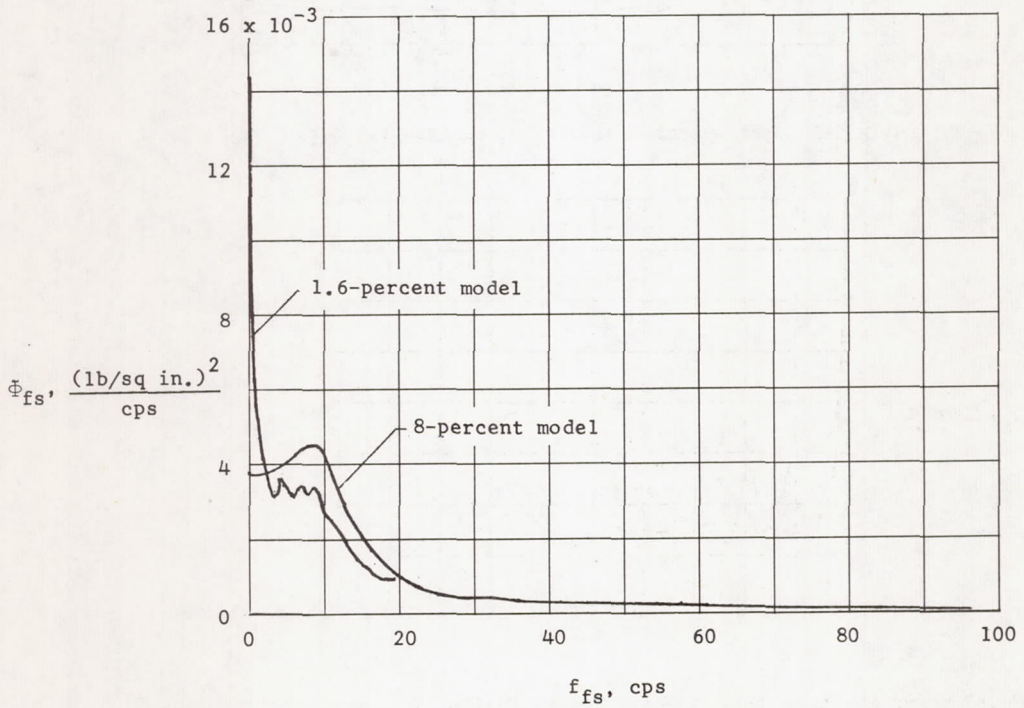

(b) Model power spectral density converted to full-scale power spectral density.

Figure 20.- Comparison of power spectra of buffet pressures at forward shoulder (transducer 3, x/D = 0.68) on 8-percent and 1.6-percent models with tower configuration 1 in Freon. $R \approx 1 \times 10^6$; M = 0.80; and $\alpha = 0^\circ$.

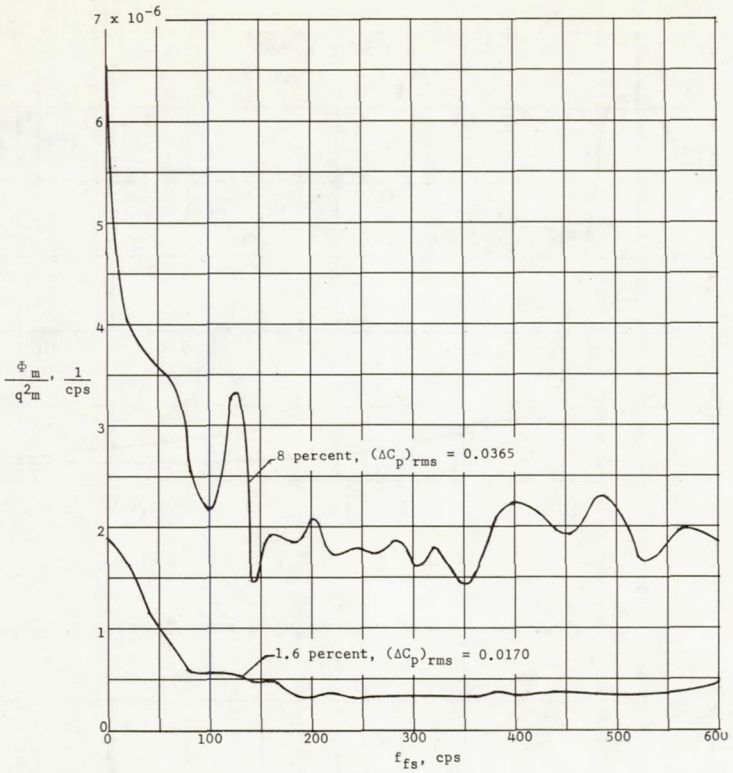

(a) Model power spectral density normalized by q_m^2.

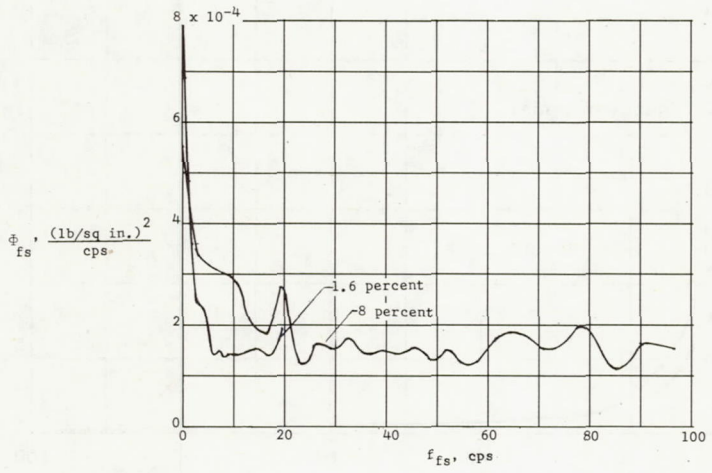

(b) Model power spectral density converted to full-scale power spectral density.

Figure 21.- Comparison of power spectra of buffet pressures on 8-percent and 1.6-percent models in Freon. Transducer 1; x/D = 0.21; tower configuration 1; $R \approx 1 \times 10^6$; M = 0.81; and $\alpha = 0^\circ$.

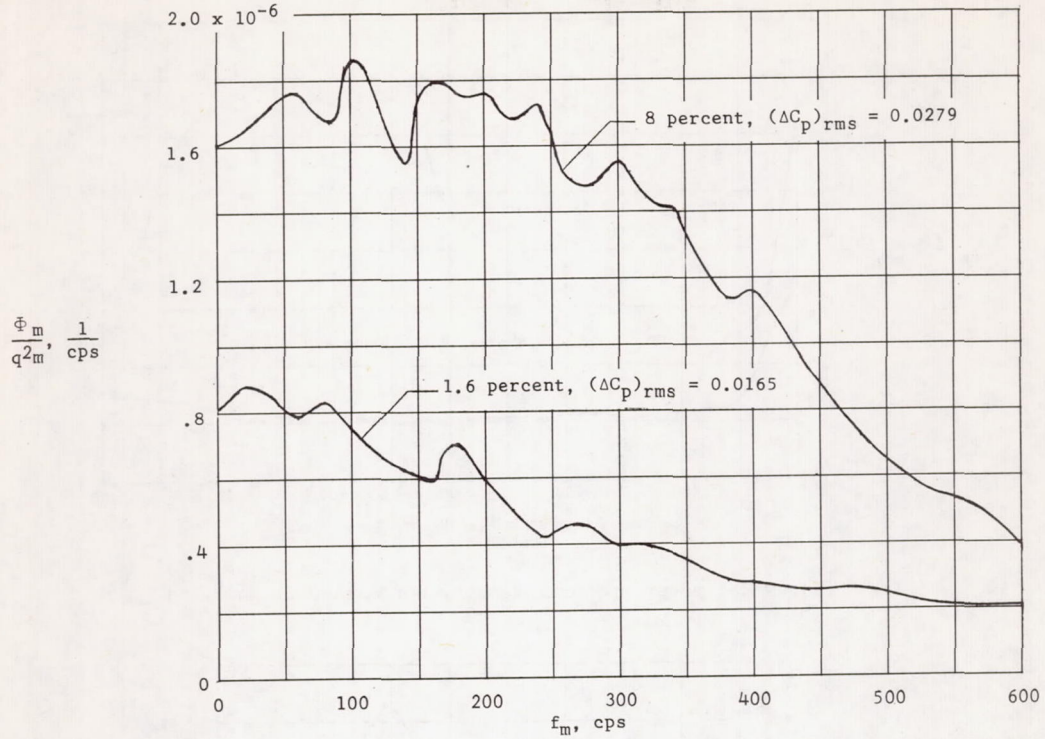

(a) Model power spectral density normalized by q_m^2.

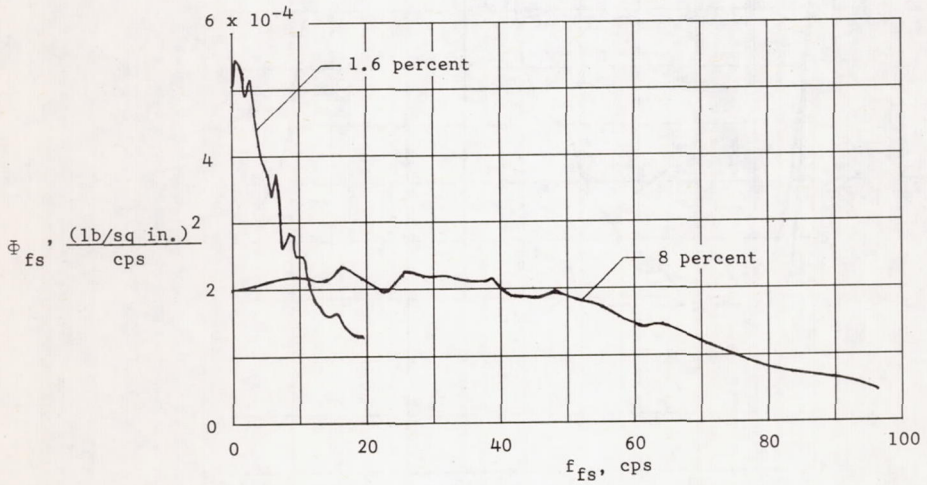

(b) Model power spectral density converted to full-scale power spectral density.

Figure 22.- Comparison of power spectra of buffet pressures on 8-percent and 1.6-percent models in Freon. Transducer 3; x/D = 0.68; tower configuration 2; $R \approx 1 \times 10^6$; M = 1.01; and $\alpha = 0^\circ$.

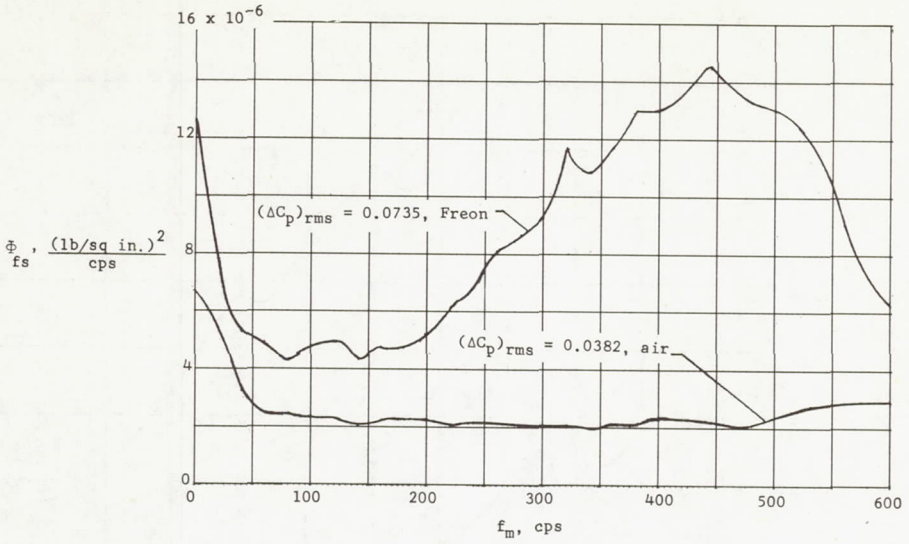

(a) Model power spectral density normalized by q_m^2.

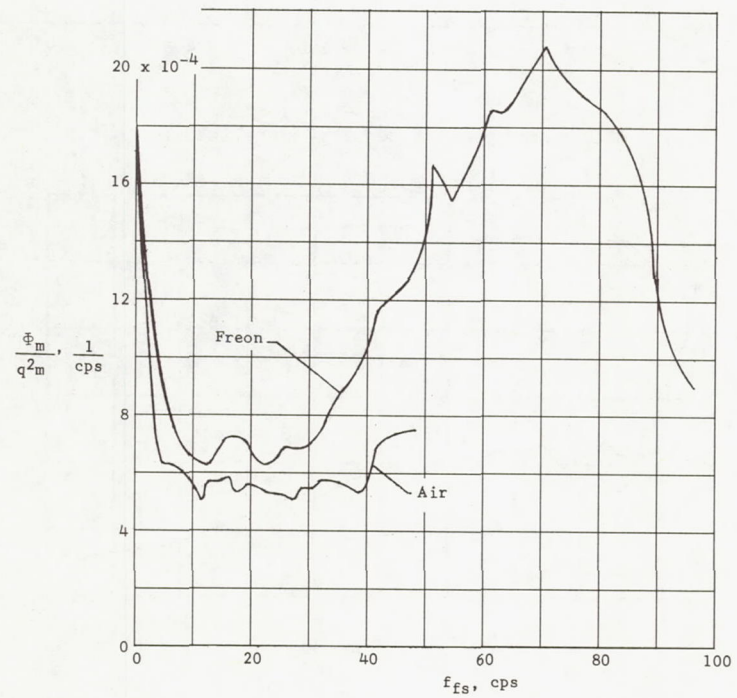

(b) Model power spectral density converted to full-scale power spectral density.

Figure 23.- Comparison of power spectra of supersonic buffet level at forward shoulder (x/D = 0.68) of 8-percent model in air and Freon. $R \approx 1.0 \times 10^6$; M = 1.05; and $\alpha = 0^\circ$.

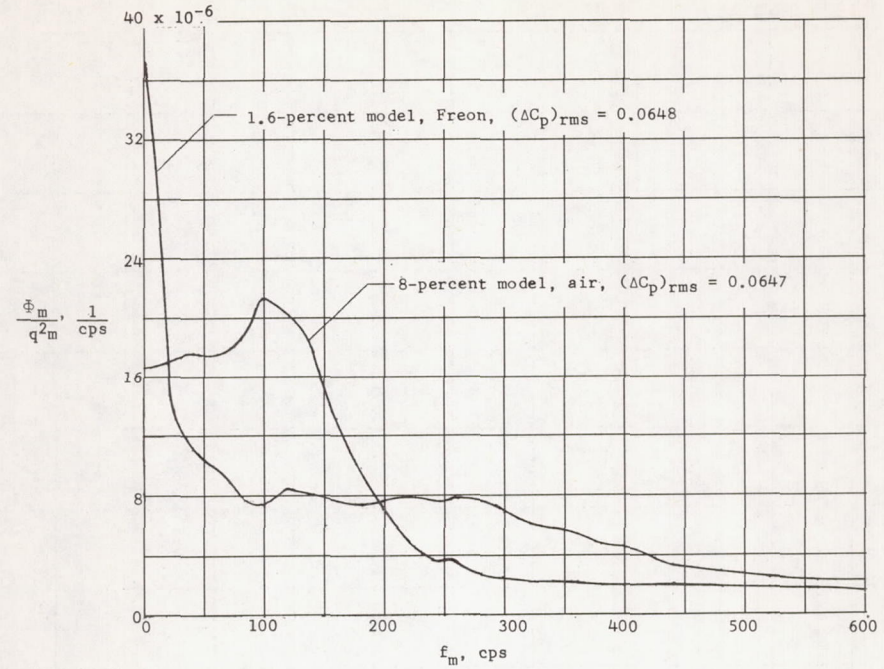

(a) Model power spectral density normalized by q_m^2.

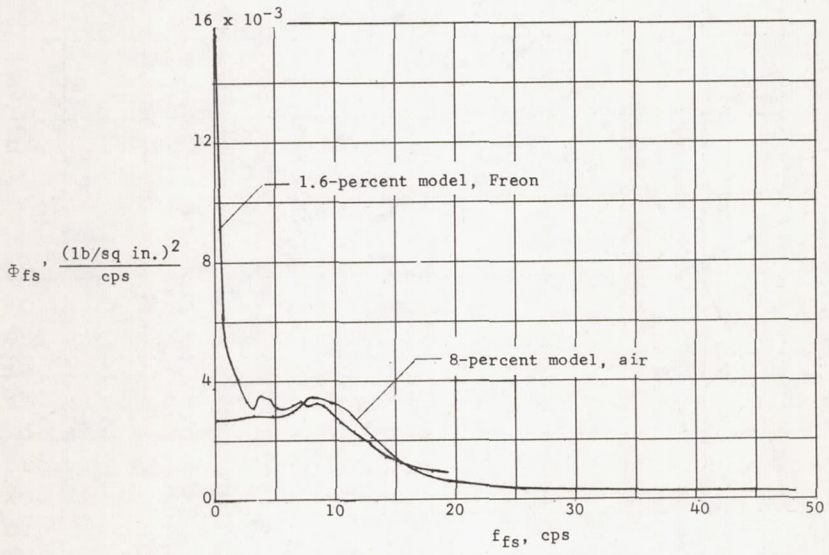

(b) Model power spectral density converted to full-scale power spectral density.

Figure 24.- Comparison of power spectra of subsonic buffet pressures on forward shoulder of 1.6-percent model in Freon with those of 8-percent model in air. Configuration 1; transducer 3; $M \approx 0.8$; $R \approx 1 \times 10^6$; and $\alpha = 0^\circ$.

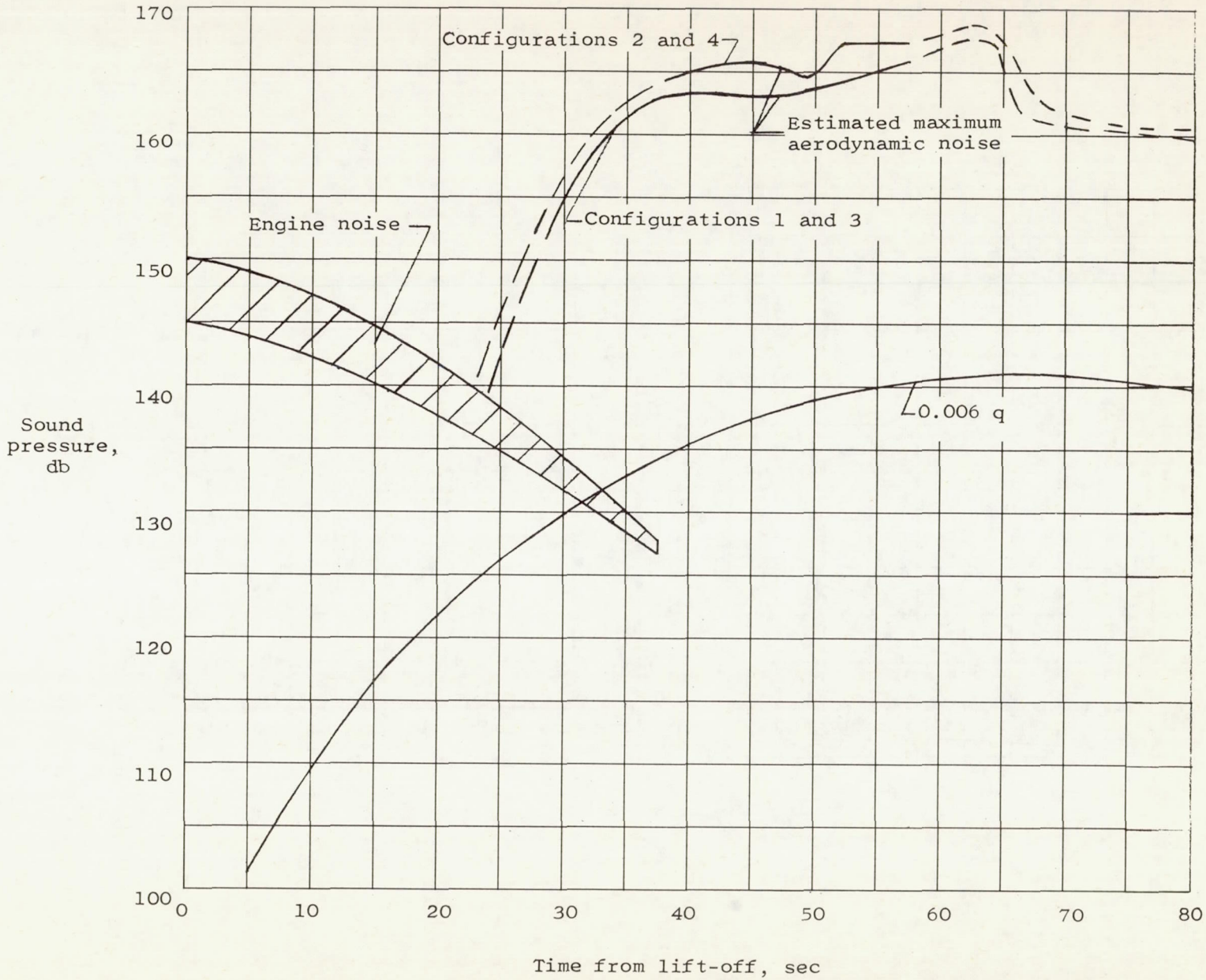

Figure 25.- Estimated external acoustic environment of large manned launch vehicle.